

PEOPLE'S DEMOCRATIC REPUBLIC OF ALGERIA
MINISTRY OF HIGHER EDUCATION AND SCIENTIFIC RESEARCH



UNIVERSITY OF SAAD DAHLAB OF BLIDA 1
FACULTY OF TECHNOLOGY
MECHANICAL ENGINEERING DEPARTMENT

Thesis for the Master's Degree in
Mechanical Engineering

Option: Energetics

Theme

**Spatial and temporal prediction of temperature distribution in a
naturally and mechanically ventilated compartment**

Realized by:

- SEMAN ABDERRAHMANE

Proposed and supervised by:

- Dr. M.ROUDANE

Co-promoter:

- Pr. A.BENAROUS

Academic year 2019/2020

Contents

List of figure.....	1
List of table.....	5
Nomenclature.....	7
Acknowledgment.....	9
Dedication.....	10
Abstract.....	11
General introduction	13
I Fire phenomena and correlative models for T	16
I.1 Introduction.....	17
I.2 General description of fire physics, effects on both human and structures.....	17
I.2.1 Definition of fire compartment.....	17
I.2.2 Flame regimes and their behavior in a room.....	18
I.2. 2.1 Surface de la base d'une flamme.....	18
I. 2.2.2 Flame height.....	18
I.2.3 Different phases of a confined fire.....	20
I.2.4 Heat transfer.....	21
I.2.4.1 Convection.....	22
I.2.4.2 Conduction	23
I.2.4.3 Radiation.....	23
I.2.5 Phases of fires in compartment.....	25
I.2.6 Development of a fire with sufficient oxygen supply.....	26
I.1.6.1 Phase 1: ignition of the fire.....	26
a- Pyrolysis.....	26

I.2.6.2 Phase 2 development phase.....	28
a- Gravitational current and neutral zone.....	29
I.2.6.3 Phase 3.....	30
a- Flashover.....	30
b- Rollover.....	31
I.2.6.4 Phase 4, the fully developed chamber fire.....	32
I.2.6.5 Phase 5extinction.....	33
I.2.7 The thermal effects of the fire on people.....	33
I.2.7.1 Burns.....	33
I.2.7.2 Effect of incident radiative heat flux.....	35
I.2.7.3 Temperature effect.....	37
I.3 Models for temperature distribution.....	37
I.3.1 Fire detection.....	37
I.3.2Descriptionof the problem.....	38
I.3.3 Radiant heat transfer to solid.....	39
I.3.3.1 Solid flame pattern.....	39
a- Solid one-zone flame pattern.....	40
I.3.4 Geometry of the flame.....	41
I.3.4.1 Calculation of the equivalent diameter.....	41
I.3.5 Fire scenario.....	41
I.3.5.1 Localized fires.....	41
I.3.5.2 Small Fires.....	42

I.3.5.3 Large Fires Impacting on the Ceiling.....	43
I.3.5.4 Definition of fire (HRR) fire event.....	43
I.3.5.5 Factors controlling energy release rates in enclosure fires.....	44
I.4 Plume models.....	45
I.4.1 HESKESTAD correlation	45
I.4.2 Wind effects.....	46
I.4.3 Maximum Temperature during the fire event.....	46
I.5 Ceiling -jet models.....	47
I.5.1 Plume and Ceiling jet fires.....	47
I.5.1.1 Ceiling jet fire.....	47
I.5.1.1.1 Ceiling jet temperature.....	48
I.5.1.1.2 Ceiling jet radiation.....	48
I.5.1.2 Plume fire.....	49
I.5.2 CORRELATIVEMODELS.....	51
I.5.2.1 Definition of correlative models.....	51
I.5.2.2 Alpert correlations.....	52
I.6 Conclusion.....	53
II- FDS software presentation.....	55
II.1 Introduction to FDS.....	56
II.2 Features of FDS.....	56
II.2.1 Basic Description of FDS.....	57
II.2.1.1 Type of Model.....	57

II.2.1.2 Intended Uses.....	58
II.2.1.3 Input Parameters.....	59
II.2.1.4 Output Quantities.....	60
II.3 Running FDS.....	62
II.3.1 Starting an FDS Calculation.....	62
II.4 Governing Equations and Numerics.....	63
II.4.1 Mass and Species Transport	63
II.4.2 Momentum Transport.....	63
II.4.3- I Energy Transport.....	64
II.4.4- Energy Transport.....	65
II.5 Large Eddy Simulation (LES).....	65
II.6 Conclusion.....	67
III- Calculation, results and discussions.....	68
III.1 Introduction.....	69
III.2 Calculations over the fire plume.....	69
III.2.1 Ideal Plume (model 1).....	71
III.2.2 Heskestad model (model 2).....	71
III.2.3 McCaffrey (model 3).....	71
III.2.4 Plume radius in the ceiling: $z = 2.9\text{m}$	72
III.3 Axial distribution of the temperature $\Delta T_{\text{ax}}(z)$	74
III.3.1 Comparison between the ideal and the Heskestad models.....	74
III.3.2 Calculating ΔT and $\Delta T/T_{\text{amb}}$ with different radlosses in the Heskestad model.....	75

III.4 Horizontal distribution of the temperature $\Delta T(r, z)$	77
III.4.1 Distribution of ΔT in the ideal model.....	78
III.4.1.1 calculating ΔT & $\Delta T/T_{amb}$ of the ideal model.....	79
III.4.2 Distribution of ΔT in the Heskestad model.....	80
III.4.2.1 ΔT & $\Delta T/T_{amb}$ values of the Heskestad model.....	80
III.4.3 Plume radius in both models.....	81
III.5 Calculations on the flow of the stratified fumes (Alpert 1979).....	86
III.6 Calculations on the flow of the stratified fumes (Alpert 2011).....	103
III.7 Alpert's Correlations - Ceiling Jets 1972 for "maximum" temperature.....	114
III.8 Alpert's Correlations - Ceiling Jets 2011for maximum temperature.....	120
III.9 Comparison between Alpert 1972 & Alpert 2011($z_0 = -0.3479378m$; $H_{pool} = 0.5m$).....	127
III.10 Conclusion.....	132
General conclusion.....	133
Bibliography.....	134

Annex

List of figures

FigureI.1: The three regimes of fire plume.....	18
FigureI.2: Schematic representation of the flame.....	20
FigureI.3: Diagram showing the different phases of fire development in function of tim.....	20
FigureI.4: Mechanism of heat transfer in the flame (Alpert, Ward).....	22
FigureI.5: Ignition of pyrolysis gases.....	27
FigureI.6: During the development phase.....	28
FigureI.7: Evolution of the gravitational current.....,	29
FigureI.8: The neutral zone at the interface of hot fumes and fresh air.....	30
FigureI.9: Evolution of a TV fire to flashover.....	31
FigureI.10: A simulation of a rollover in a German training container.....	32
FigureI.11: The combustion of gases outside the room.....,	32
FigureI.12: Burns on the human left hand.....	34
FigureI.13: Burns on the wrist.....	34
FigureI.14: The evolution of the temperature in a room during the intervention.....	38
FigureI.15: The heat transfer modes between the fire and the firefighter garment.....	39
FigureI.16: Schematic diagram for small localised fires.....	43
FigureI.17: Temperature near the ceiling from Heskestad correlation.....	47
FigureI.18: fire plume and ceiling jet.....	48
FigureI.19: The three zones of the axi-symmetric buoyant plume.....	49
FigureI.20: Schematic of plume and ceiling jet flow for an unconfined ceiling.....	50
FigureI.21: Ceiling jet flow beneath an unconfined ceiling.....	52
FigureII.1: Input parameters of the FDS.....	59
FigureII.2: FDS Output gotten by Smokeview.....	60
FigureII.3: FDS Output calculations made by fds5.....	62
FigureIII.1: Geometry of the compartment.....	69

FigureIII.2: Geometry of the unconfined fire plume.....	72
FigureIII.3: Axial diminution of the temperature as a function of the plume.....	73
FigureIII.4: Plume radius in both cases as a function of the vertical distance above fire source.....	76
FigureIII.5: Diagram of the excess of temperature as a function of the vertical distance above fire in the ideal model.....	77
FigureIII.6: Diagram of the excess of temperature as a function of the vertical distance above fire in the Heskestad model.....	78
FigureIII.7: Diagram of the excess of temperature as a function of the radial distance above fire in the ideal model.....	80
FigureIII.8: Diagram of the excess of temperature as a function of the radial distance above fire in the Heskestad model.....	86
FigureIII.9: Diagram of the excess temperature as a function of the radial distance ($z_0 = -0.3479378\text{m}$ and $H_{\text{pool}}=0$).....	88
FigureIII.10: Diagram of the excess temperature as a function of the radial distance ($z_0 = 0$ and $H=0$).....	89
FigureIII.11: Diagram of the excess temperature as a function of the radial distance ($z_0 = -0.3479378\text{m}$ and $H_{\text{pool}} = 0,5\text{m}$).....	91
FigureIII.12: Diagram of the excess temperature as a function of the radial distance ($z_0 = 0$ and $H_{\text{pool}} = 0,5\text{m}$).....	92
FigureIII.13: Diagram of the excess temperature as a function of the radial distance ($z_0 = 0$ and $H = 0$).....	94
FigureIII.14: Diagram of the excess temperature as a function of the radial distance ($z_0 = -0.3479378\text{m}$ and $H_{\text{pool}} = 0$).....	96
FigureIII.15: Diagram of the excess temperature as a function of the radial distance ($z_0 = 0$ and $H_{\text{pool}}= 0,5\text{m}$).....	99
FigureIII.16: Diagram of the excess temperature as a function of the radial distance ($z_0 = -0.3479378\text{m}$ and $H_{\text{pool}}= 0,5\text{m}$).....	101
FigureIII.17: Diagram of the excess temperature as a function the radial distance ($H_{\text{pool}} = 0$ and $z_0 = -0.3479378\text{m}$).....	104
FigureIII.18: Diagram of the excess temperature as a function the radial distance ($H_{\text{pool}} = 0.5\text{m}$ and $z_0 = -0.3479378\text{m}$).....	105
FigureIII.19: Diagram of the excess temperature as a function the radial distance ($H_{\text{pool}} = 0$ and $z_0 = -0.3479378\text{m}$).....	107

FigureIII.20: Diagram of the excess temperature as a function the radial distance ($H_{\text{pool}} = 0.5\text{m}$ and $z_0 = -0.3479378\text{m}$).....	108
FigureIII.21: Histogram showing the centerline maximum temperature for the Alpert 1972 model when $H_{\text{pool}} = 0$ and $H_{\text{pool}} = 0.5\text{m}$	115
FigureIII.22: Histogram showing the turning region size for the Alpert 1972 model when $H_{\text{pool}} = 0$ and $H_{\text{pool}} = 0.5\text{m}$	116
FigureIII.23: Histogram showing the maximum temperature depending on the maximum plume radius at the ceiling for the Alpert 1972 model when $H_{\text{pool}} = 0$ and $H_{\text{pool}} = 0.5\text{m}$	117
FigureIII.24: Histogram showing the maximum temperature at the door and the window for the Alpert 1972 model when $H_{\text{pool}} = 0$ and $H_{\text{pool}} = 0.5\text{m}$	118
FigureIII.25: Histogram showing the ratio between the turning region size and the maximum plume radius at the ceiling for the Alpert 1972 model when $H_{\text{pool}} = 0$ and $H_{\text{pool}} = 0.5\text{m}$	119
FigureIII.26: Histogram showing the centerline maximum temperature for the Alpert 2011 model when $H_{\text{pool}} = 0$ and $H_{\text{pool}} = 0.5\text{m}$	122
FigureIII.27: Histogram showing the turning region size for the Alpert 2011 model when $H_{\text{pool}} = 0$ and $H_{\text{pool}} = 0.5\text{m}$	123
FigureIII.28: Histogram showing the maximum temperature depending on the maximum plume radius at the ceiling for the Alpert 2011 model when $H_{\text{pool}} = 0$ and $H_{\text{pool}} = 0.5\text{m}$	124
FigureIII.29: Histogram showing the maximum temperature at the door and the window for the Alpert 2011 model when $H_{\text{pool}} = 0$ and $H_{\text{pool}} = 0.5\text{m}$	125
FigurIII.30: Histogram showing the ratio between the turning region size and the maximum plume radius at the ceiling for the Alpert 2011 model when $H_{\text{pool}} = 0$ and $H_{\text{pool}} = 0.5$	126
FigureIII.31: Histogram showing the centerline maximum temperature for both models of Alpert 1972 and Alpert 2011 when $H_{\text{pool}} = 0.5\text{m}$	127
FigureIII.32: Histogram showing the turning region size for both models of Alpert 1972 and Alpert 2011 when $H_{\text{pool}} = 0.5\text{m}$	128
FigureIII.33: Histogram showing the maximum temperature depending on the maximum plume radius at the ceiling for both models of Alpert 1972 and Alpert 2011 when $H_{\text{pool}} = 0.5\text{m}$	129
FigureIII.34: Histogram showing the maximum temperature at the door and the window for both models of Alpert 1972 and Alpert 2011 when $H_{\text{pool}} = 0.5\text{m}$	130
FigureIII.35: Histogram showing the ratio between the turning region size and the maximum plume radius at the ceiling for both models of Alpert 1972 and Alpert 2011 when $H_{\text{pool}} = 0.5\text{m}$	131

List of tables

TableI.1: Burns depending on the skin temperature.....	34
TableI.2: Effects of radiative heat flux on humans.....	35
TableI.3: Effects of radiative heat flux on structures.....	35
TableI.4: Effects of Temperature on Individuals - US Navy -.....	37
TableI.5: The heat flow rate generated from various sources	44
TableIII.1: plume radius $b(z)$ with the ideal and Heskestad models.....	73
TableIII.2: plume radius $b(z)$, excess of temperature and the tolerance of the temperature with the ideal model ($\alpha = 0.15$) and the Heskestad models ($Radloss = 0.20$).....	74
TableIII.3: excess of temperature and the tolerance of the temperature with different radlosses.....	75
TableIII.4: excess of temperature and the tolerance of the temperature at different plume heights with the ideal model.....	79
TableIII.5: excess of temperature and the tolerance (relative error) of the temperature at different plume heights with the Heskestad model.....	80
TableIII.6: the tolerance of the temperature and the plume radius with the ideal model.....	81
TableIII.7: the tolerance (relative error) of the temperature and the plume radius with the Heskestad model.....	82
TableIII.8: the tolerance (relative error) of the temperature with different values of α and radloss at $z = 0.5m$	82
TableIII.9: the tolerance (relative error) of the temperature with different values of α and radloss at $z = 1.5m$	83
TableIII.10: the tolerance (relative error) of the temperature with different values of α and radloss at $z = 2.8m$	83
TableIII.11: the tolerance (relative error) of the temperature with different values of α and radloss at $z = 2.9m$	84
TableIII.12: the tolerance (relative error) and the excess of the temperature in the Alpert 1972 case when $H_{pool} = 0$	87
TableIII.13: the tolerance (relative error) and the excess of the temperature in the Alpert 1972 case when $H_{pool} = 0.5m$	89
TableIII.14: the tolerance (relative error) and the excess of the temperature in the Alpert 1972 case when $H_{pool} = 0$ and $z_0 = 0$ with the new intervals.....	94

TableIII.15: the tolerance (relative error) and the excess of the temperature in the Alpert 1972 case when $H_{pool} = 0$ and $z_0 = -0.3479378m$ with the new intervals.....96

TableIII.16: the tolerance (relative error) and the excess of the temperature in the Alpert 1972 case when $H_{pool} = 0.5$ and $z_0 = 0$ with the new intervals.....99

TableIII.17: the tolerance (relative error) and the excess of the temperature in the Alpert 1972 case when $H_{pool} = 0.5m$ and $z_0 = -0.3479378m$ with the new intervals.....101

TableIII.18: the tolerance (relative error) and the excess of the temperature in the Alpert 2011 case when $H_{pool} = 0$ and $z_0 = -0.3479378m$104

TableIII.19: the tolerance (relative error) and the excess of the temperature in the Alpert 2011 case when $H_{pool} = 0.5$ and $z_0 = -0.3479378m$105

TableIII.20: the tolerance (relative error) and the excess of the temperature in the Alpert 2011 case when $H_{pool} = 0$ and $z_0 = -0.3479378m$ with the new intervals.....107

TableIII.21: the tolerance (relative error) and the excess of the temperature in the Alpert 2011 case when $H_{pool} = 0.5m$ and $z_0 = -0.3479378m$ with the new intervals.....109

TableIII.22: recapitulating table of the previous flame parameters.....112

NOMENCLATURE

t	Time [min]
r	Radial distance from the fire [m]
C_p	Specific heat at constant pressure [J/(kg K)]
D	Diameter of fire source [m]
H	Distance between the fire and the ceiling [m]
H_{pool}	Fire pool height [m]
H_{ceiling}	Ceiling height [m]
\dot{Q}	Heat flow rate [kW]
Q_{conv}	Convective heat [kW]
T_{max}	Maximum temperature [K]
T_{amb}	Ambient temperature [K]
z	Height along the flame axis [m]
z_0	Height of virtual source above burning item [m]
b	Plume radius [m]
b_{max}	Maximum plume radius [m]
T_0	Temperature at $t=0$ s [K]
ΔT	Radial excess of the plume temperature [K]
ΔT_{ax}	Axial excess of the plume temperature [K]
$T_{\text{centerline}}$	Centerline temperature [K]
g	Acceleration of the gravity [m/s^2]
a	Fire pool edge [m]
A_{fire}	Fire pool surface area [m^2]

D_{fire}	Fire pool diameter [m]
R_{fire}	Fire pool radius [m]
ρ	Density of the fume [$\text{kg}\cdot\text{m}^{-3}$]
η	Dimensionless constant parameter
K	Thermal conductivity [SI]
α	Ratio used for the ideal calculations
r_{cz}	Plume radius at the ceiling zone [m]
r_{turn_r}	Turning region size [m]
\dot{m}_b^m	Production rate of species by evaporating particles [g/s]
Y_α	Individual gaseous species
uu	Dyadic tensor
τ_{ij}	Stress tensor
S_{ij}	Symmetric rate-of-strain tensor
μ	Dynamic viscosity of the fluid
\dot{q}'''	Heat release rate per unit volume from a chemical reaction [kW/m^3]
\dot{q}''	Conductive and radiative heat fluxes [kW/m^2]
Δ	Length on the order of the size of a grid cell [m]
Pr_t	Turbulent Prandtl number
Sc_t	Turbulent Schmidt number
\bar{u}_i	Filtered velocity [m/s]
\bar{p}	Filtered pressure [bar]
μ	Molecular viscosity [$\text{kg}\cdot\text{m}^2\cdot\text{s}^{-1}$]

Acknowledgement

As a preamble to this brief, I thank ALLAH who helped me and gave me patience and courage during these Long years of study

I express my sincere thanks to our promoter and co-promoter, Dr ROUDANE MOHAMED and Pr BENAROUS ABDELLAH, for bringing the topic to us.

I would like to thank him for his invaluable help, his availability and his invaluable advice in the development of this work.

I would also like to thank the president and the members of the jury for the honor they do us in judging this work.

My thanks also go to all the teachers in the Mechanical Engineering department for following me through our university course

Finally, I thank all the people who contributed directly or indirectly to the good accomplishment of our work.

DEDICATION

✚ This research paper is dedicated to my dear **father**, who has been nicely my supporter until my research was fully finished, and my beloved **mother** who, for months past, has encouraged me attentively with her fullest and truest attention to accomplish my work with truthful self-confidence.

✚ To my brother **Mohamed** and my sisters **Meriem** and **Fatima Zohra**

✚ To all people who wished me the best for my studies and my career and to my closest friends **Habib, Ahmed** and **Happy** to whom I feel very comfortable to talk and with whom I've never regretted to spend my holy time.

ABDERRAHMANE

Abstract:

The present study is a numerical attempt for the prediction of the variation of the flame temperature inside a compartment. The study focuses on calculating the temperature of the fumes that varies at each point vertically and radially as if various thermocouples would be placed at the same point. A radiative and convective transfer modeling is considered for a 3D geometry compartment, equipped with a door, a window and subject to a localized fire, with stationary heat release rate (HRR) during a prescribed exposure time. Dealing with any fire phenomenon requires a fire simulator called Fire Dynamic Simulator (FDS) which aims to mesh the compartment then calculate the temperature at each node by performing a thermocouple role virtually. So with the new technology someone can study any phenomenon virtually without using classical methods by handling with the appropriate devices.

Key words: Fire engineering; Natural ventilation; Mechanical ventilation; Temperature-Time curve; Field models; Correlative models; Large eddy Simulations (LES), Fire Dynamic Simulator (FDS)

Résumé :

La présente étude est une tentative numérique de prédiction de la variation de la température de la flamme à l'intérieur d'un compartiment. L'étude se concentre sur le calcul de la température des fumées qui varie en chaque point verticalement et radialement comme si différents thermocouples s'y trouvaient. Une modélisation par transfert radiatif et convectif est envisagée pour un compartiment à géométrie 3D, équipé d'une porte, d'une fenêtre et soumis à un incendie localisé, avec un taux de dégagement de chaleur stationnaire (HRR) pendant un temps d'exposition prescrit. Faire face à tout phénomène d'incendie nécessite un simulateur d'incendie appelé Fire Dynamic Simulator (FDS) qui vise à mailler le compartiment puis à calculer la température à chaque nœud en jouant virtuellement le rôle d'un thermocouple. Ainsi, avec la nouvelle technologie, on peut étudier n'importe quel phénomène pratiquement sans suivre des méthodes classiques en utilisant les appareils appropriés.

Mots clés: Incendie; Ventilation naturelle; Ventilation mécanique; courbe de température temporelle; modèles du domaine; Modèles corrélatifs; Large eddy Simulations (LES), Fire Dynamic Simulator (FDS)

الملخص:

الدراسة الحالية هي محاولة عديدة للتنبؤ بتغير درجة حرارة اللهب داخل حجرة. تركز الدراسة على حساب درجة حرارة الأبخرة التي تختلف عند كل نقطة عمودياً و أفقياً كما لو كانت مزدوجات حرارية مختلفة موضوعة في نفس النقطة. يتم النظر في نمذجة النقل الإشعاعي والحمل الحراري لمقصورة هندسية ثلاثية الأبعاد، ومجهزة بباب و نافذة و خاضعة لحريق موضعي، مع معدل إطلاق حرارة ثابت « heat release rate » (HRR) خلال وقت التعرض المحدد. يتطلب التعامل مع أي ظاهرة حريق بواسطة جهاز محاكاة النار المسمى ب(FDS) Fire Dynamic Simulator (محاكاة ديناميكية النار) و الذي يهدف إلى تشبيك المقصورة ثم حساب درجة الحرارة في كل عقدة عن طريق أداء دور المزدوج الحراري تقريباً. لذلك مع التكنولوجيا الجديدة، يمكن لأي شخص دراسة أي ظاهرة تقريباً دون استخدام الأساليب التقليدية من خلال التعامل مع الأجهزة المناسبة.

الكلمات المفتاحية: هندسة النار؛ تهوية طبيعية؛ تهوية ميكانيكية؛ منحنى درجة الحرارة الزمنية؛ نماذج المجال؛ نماذج اللفظ المتلازم؛ . محاكاة إيدي الكبيرة (LES)؛ محاكاة ديناميكية النار (FDS)

General introduction

Fire was recognized from the moment of human consciousness. It was present at the creation of the Universe. It has been a part of us from the beginning. Reliance on fire for warmth, light, cooking and the engine of industry has faded from our daily lives of today, and therefore we have become insensitive to the behavior of fire. Mankind has invested much in the technology to maintain fire, but relatively little to prevent it. Of course, dramatic disastrous fires have been chronicled over recorded history, and they have taught more fear than complete lessons. Uncontrolled fire can devastate our assets and production sources.

It's known that in any close compartment the fire fume starts spreading vertically until it gets to the lower layer of the ceiling and then it changes the direction instantaneously towards the radial axis, our project highlights on that phenomenon and stands for the study of the variation of the smoke temperature, resulting from a combustion happening in a fire pool placed somewhere inside the room, vertically and radially. This study it will, therefore, help anybody, especially firemen, to know which place is the most bearable to stand at that someone should receive the least heat and then he would have a time range to intervene and interact with the fire without being hurt or suffocated.

The temperature of the hot gases due to the fire in a compartment is the major dynamic characteristics that must be taken in consideration in the studies of fire.

The main objective of our study is the estimation of the temperature variation along the two axes and at any point in an open, a semi-confined and a confined compartment during an ignition and at the time of a flashover, as well as at the fully developed fire plume and its effects on the fire-fighter garment, in the three possible states of the compartment, standing close to and far from the source of the fire by relying on numerical simulations carried out using FDS (Fire Dynamic Simulator) software being a part of CFD (Computational fluid Dynamic).

Simple calculation methods, based on the correlative models devoted to fire plumes and ceiling jets, are going to be used to compare results of the temperature near the ceiling. Theoretically, our study requires some fire equations that were established by Heskestad and Alpert to predict temperature histories for arbitrary combinations of ceiling clearance and fire-growth rate and to know the virtual plume origin. According to their researches, fire detectors should be located in a vertical distance below the ceiling of no more than 6 % of the ceiling height. To concretize their formulas we need to use the simulator program FDS allowing us to know more about excess of temperature distribution along the vertical and radial axis, so all we have to do is defining the geometry of the compartment and the fire pool as well, then introducing the physical properties (colour and texture of the walls, ambient temperature, heat release rate of the pool fire) and meshing our geometry so that each node represent the location of a thermocouple which gives the local temperature, next we set the timing in seconds, commonly it's 900s, and we execute the program. After some

days (depending on the meshing) we get to the whole results, afterwards we compare them with the formulas' results and then we start interpreting.

This thesis is made up of three chapters, a conclusion and an annex. After an introduction, a general description of the fire phenomenon is given in the first chapter in order to identify the thermal effects of fire on the human body and on the geometric structure of the chamber and temperature distribution models, the plume as well as the jet on the ceiling.

The second chapter is devoted to the presentation of the "Fire Dynamic Simulator" (FDS) calculation code as well as the resolution procedures followed by the LES (Large Eddy Simulation) simulator.

The third and final chapter presents the numerical resolution and the numerical study by the FDS code, with interpretations and comparisons with results contained in the reference case.

Finally the results we get will lead us to a general conclusion in which we will recapitulate the phenomenon and speak about how will future generation address any fire behavior with proper science in the midst of significant social and technological advances, especially among the developed countries by creating likely some new technological devices or garments, and just after we will show all the sources and references we were relying on and from which we were taking the information.

Chapter I:
**Fire phenomena and
correlative models for
the temperature**

Chapter I: Fire phenomena and correlative models for the temperature

I.1- Introduction

A fire plume is loosely described as a vertically rising column of gases resulting from flames. The term plume is generally used to describe the non-combustion region, which might dominate the flow away from the combustion source, especially if the source is small. A plume is principally buoyancy driven. This means flow has been induced into the plume due to an increase in temperature or consequent reduction in density. A plume is also likely to be turbulent rather than laminar. Anyone who has observed a rising streak of white smoke from a cigarette left in an ash tray should recall seeing the wavy laminar emitted streak of smoke break-up into a turbulent wider plume in less than 1 foot of height. Thus, any significant accidental fire will have an associated turbulent plume – even a smoldering fire. Near the fire we will have to deal with a combusting plume, but ‘far’ from the fire it might suffice to ignore the details of combustion entirely. Indeed, much about fire plumes is empirical, meaning that its results are based on experimental correlations. In other cases, the correlations can be somewhat ambiguous since they represent time- averaged properties, or length scales (e.g. plume width, flame height), that were not precisely or consistently defined. However, because fire plume results are grounded in measurement – not purely theory – they are practical and invaluable for design and hazard assessment.

One of the most important problems in fire protection is the rapid detection of fire in a room while the fire is sufficiently small to be easily controlled. Controllable fires generally exist for more than half a minute after ignition when flames are confined by inert barrier for air gaps to a distinct portion of the total available fuel.

I.2- General description of fire physics, effects on both human and structures

I.2.1- Definition of fire compartment

Space within a building, extending over one or several floors, which is enclosed by separating elements such that fire spread beyond the compartment is prevented during the relevant fire exposure. Fire compartment is a volume within a building which is completely surrounded with fire-resistant construction elements, which can be integrated right into the structure of the building. Fire compartments are not absolutely fire proof. Fire can work its way into or out of a fire compartment if it is intense enough, poorly managed, or not addressed quickly enough. Existing buildings can be retrofitted to create fire compartments.

Chapter I: Fire phenomena and correlative models for the temperature

Movable barriers can be installed, or people can remodel parts of a building to create a fire compartment. Also known as a fire zone, a fire compartment can also sometimes address the potential of flood damage, as the same materials which keep fire out can sometimes keep water at bay as well. The fire compartments can consist of rooms or groups of rooms. When a fire starts inside a compartment, the sealed nature of the area can partition the fire, preventing it from spreading to other areas.

I.2.2- Flame regimes and their behavior in a room

The flame can thus be assimilated to a surface separating fresh gas and gaseous combustion products (CO₂, H₂O, etc.) and soot resulting from incomplete combustion. It substantially corresponds to the luminous part of the combustion zone.

I.2. 2.1- Fire pool surface area

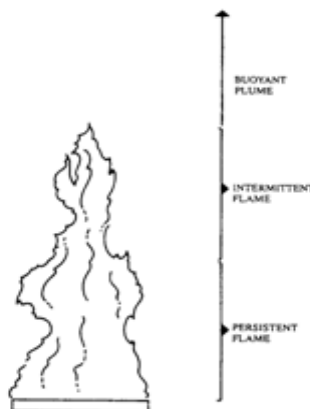
The equivalent diameter representative of the behavior of the flame, or the hydraulic diameter, is determined from the following expression:

$$D_h = 4 \frac{\text{surface area}}{\text{surface perimeter}} \quad (\text{I-1})$$

This formula does not apply to rectangular elongated basins.

I. 2.2.2- Flame height

The z axis, being vertical, is directed from bottom to top.



FigureI.1: The three regimes of fire plume [1]

Chapter I: Fire phenomena and correlative models for the temperature

In a simply way, unconfined fire plume comprises essentially three regimes which were distinguished by McCaffrey's works:

- 1- Persistent flame (flame is steady and present 100% of time) where heat is continually produced by flaming combustion (oxidation reaction) and has a magnitude of high temperature around 1000°C, commonly its height interval is calculated using the following equation[1]:

$$0.03 \dot{Q}^{2/5} < z < 0.08 \dot{Q}^{2/5} \quad (\text{I-2})$$

- 2- Intermittent flame (flame present < 100% of time) where combustion is irregular and chemical reactions and temperature are less important than in the persistent flame, its height interval is:

$$0.08 \dot{Q}^{2/5} < z < 0.20 \dot{Q}^{2/5} \quad (\text{I-3})$$

- 3- Buoyant (thermal) plume (no flame is ever present) where flaming combustion reactions do not occur, its height is:

$$0.20 \dot{Q}^{2/5} < z \quad (\text{I-4})$$

Where:

z: height above fire source (m)

\dot{Q} : heat release rate (kW)

D: fuel diameter (m).

Chapter I: Fire phenomena and correlative models for the temperature

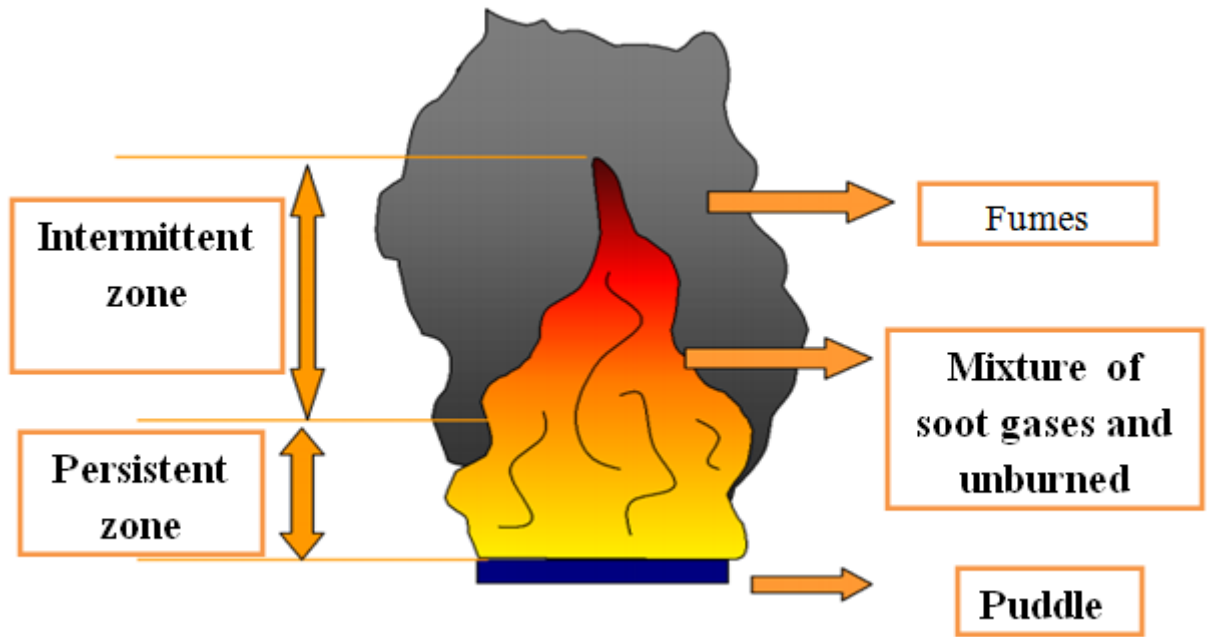


Figure I.2: Schematic representation of the flame [2].

I.2.3- Different phases of a confined fire

During its evolution, the fire goes through 3 phases:

- The growth of the fire during which it is located at its origin and its mean temperature is low.
- Total development, where the fire is fully developed.
- The extinction period, which is determined by a weakening phase of the fire (decay).

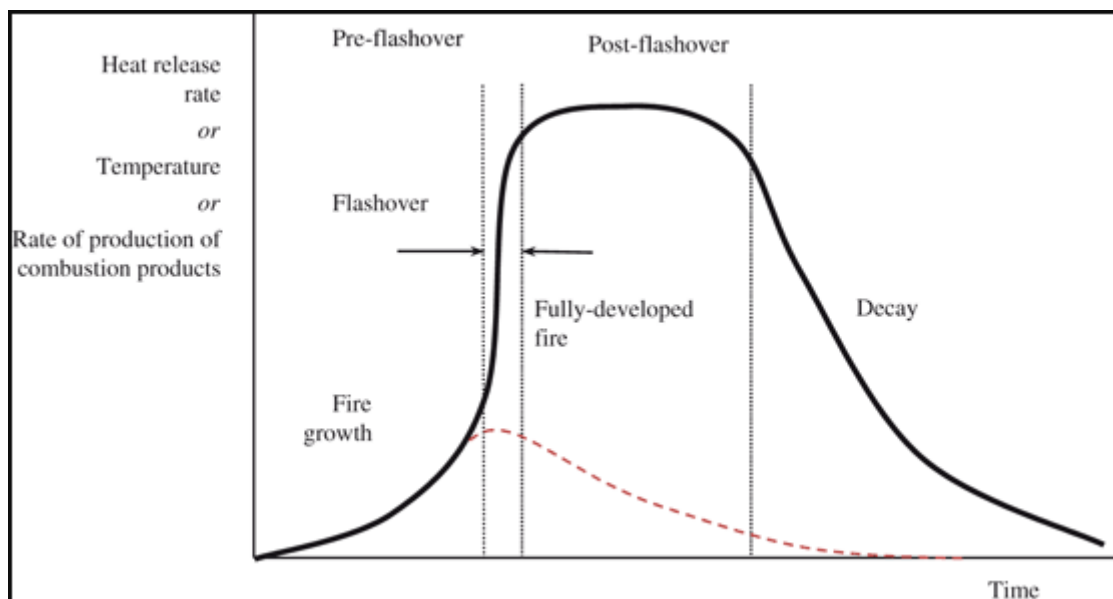


Figure I.3: Diagram showing the different phases of fire development in function of time

Chapter I: Fire phenomena and correlative models for the temperature

The phenomenon of transition from the initial phase of flame growth to the phase of full development is called "Flashover". This transition corresponds to a sudden generalized inflammation of the local.

I.2.4- Heat transfer

When combustion reactions are triggered, large amounts of heat are released. This is reflected in the notion of the calorific potential associated with a fuel, weighted by the combustion efficiency which defines the ratio between the quantity of heat theoretically available in the fire and that actually released. The amount of energy thus emitted in the form of heat is transferred in particular:

- Towards the external environment of the flame, which can thus cause the fire to spread.
- Towards the fuel, this energy retrocession maintains the emission of flammable vapors.

Three fundamental mechanisms of heat transfer from the flame coexist:

- Convection.
- conduction.
- radiation.

These three transfer modes, as well as the transport of incendiary brandons for solid product fires, contribute to the possible spread of a fire.

These different heat transfer mechanisms are represented schematically in the following figure:

Chapter I: Fire phenomena and correlative models for the temperature

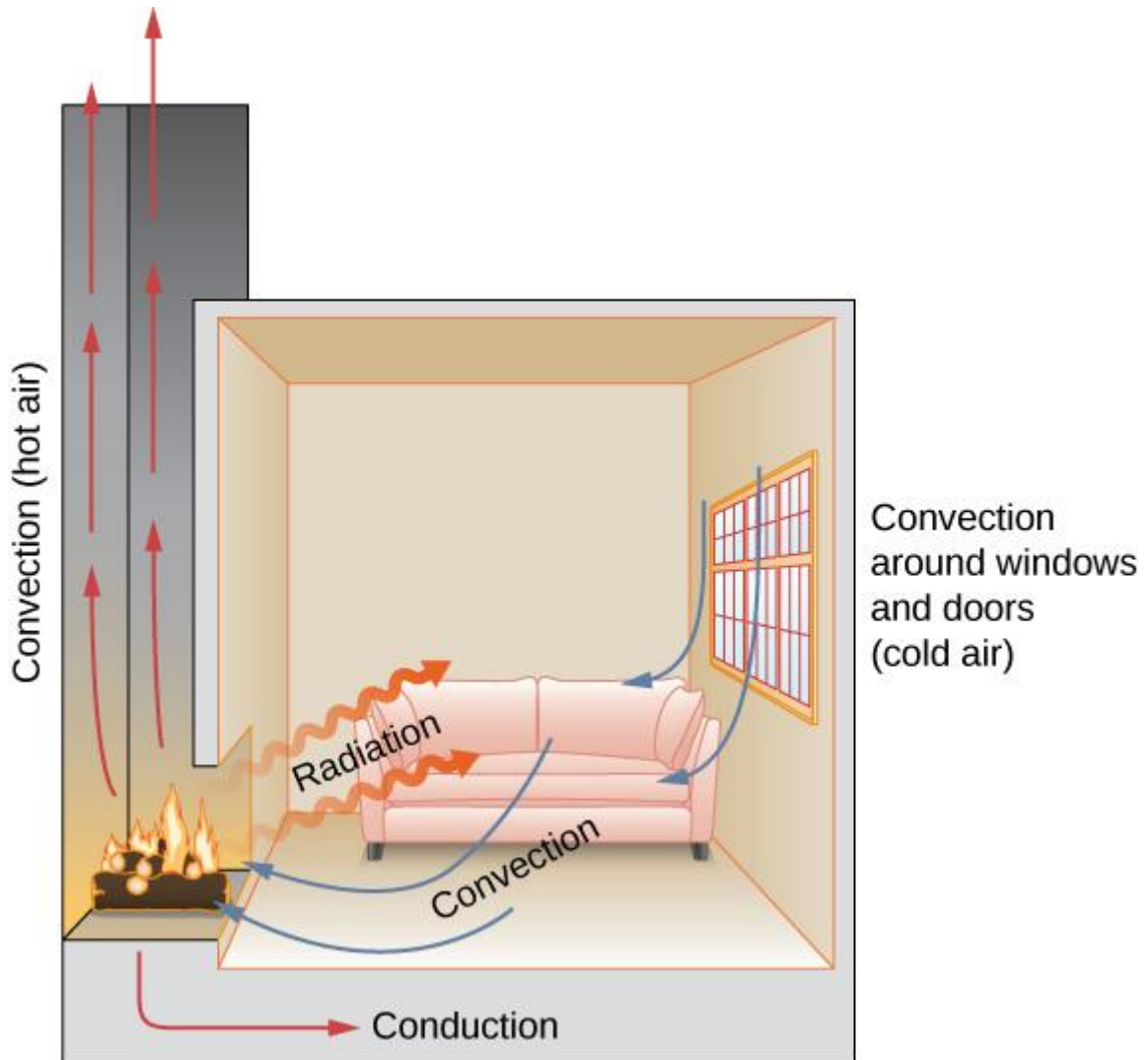


Figure I.4: Mechanism of heat transfer in the flame (Alpert, Ward)

I.2.4.1- Convection

Convection is the mode of heat transfer by the fluid present in the environment of the flame (eg air). This mechanism, involving mass motions of hot air, is mainly responsible for the vertical spread of the fire and the formation of the smoke plume.

Convection can be free or forced depending on what governs the motion of the fluid in question: density differences between hot gases and cold air, external mechanical action such as ventilation, or mechanical smoke extraction.

Chapter I: Fire phenomena and correlative models for the temperature

I.2.4.2- Conduction

Conduction is the way of heat transfer happening in the inside of the conductive body being in contact with a hot source by the transfer of calories. It may be viewed as the transfer of energy from the more energetic to the less energetic particles of a substance due to interactions between the particles and, by the way, higher temperatures are associated with higher molecular energies.

The physical mechanism of conduction is most easily explained by considering a gas in which there exists a temperature gradient assuming that there is no bulk, or macroscopic, motion. The gas may occupy the space between two surfaces that are maintained at different temperatures. We associate the temperature at any point with the energy of gas molecules in proximity to the point. This energy is related to the random translational motion, as well as to the internal rotational and vibrational motions, of the molecules.

In the presence of a temperature gradient, energy transfer by conduction must then occur in the direction of decreasing temperature. This would even be true in the absence of collisions.

I.2.4.3- Radiation

Thermal radiation is the isotropic mode of transfer of heat released by solid, liquid or gaseous bodies brought to high temperature. The transport of thermal energy is provided by electromagnetic waves. Thus requiring no material support, it is an almost immediate process of energy exchange between two distant bodies and capable of generating effects at great distances. This is the main vehicle for reaching potential human targets.

In terms of Physics, radiation is the result of an emission of electromagnetic vibrations, the wavelengths of which are approximately between 0.1 μ m and 100 μ m (visible range and fractions of ultraviolet and infrared).

The main energy quantities relating to an emitting surface are briefly presented below.

Considering a radiating surface, the energy emittance, M , is defined as the surface density of the energy flux emitted by the surface.

$$M = \frac{d\phi_{emis}}{ds} \quad (I.5)$$

Chapter I: Fire phenomena and correlative models for the temperature

In the case of a black body, the emittance is determined using Stefan-Boltzman's law, as varying in proportion to the fourth power of its absolute temperature, hence:

$$M = \sigma T^4 \quad (\text{I.6})$$

Where

σ : constant of Stefan-Boltzman ($5,67 \cdot 10^{-8} \text{ W/m}^2 \cdot \text{K}^4$)

T: absolute temperature (K)

A black body is defined as a theoretical opaque body that would absorb and emit, at a given temperature, all the radiations it would receive, whatever their wavelength and direction ($\forall \lambda$ and $\forall D$, $a = 1$).

It should be remembered here that a flame can be assimilated to a surface separating fresh gas and combustion products (CO_2 , H_2O , etc.), as well as soot brought to high temperature. Each of these components contributes to the emittance of the flame and the analogy with a uniform black body is therefore not immediate.

The emittance or emissive power of the flame, noted ϕ_0 , is then deducted by the following formula:

$$\phi_0 = \varepsilon \sigma (T_f^4 - T_a^4) \quad (\text{I.7})$$

Such as:

T_f : Flame temperature (K)

T_a : Surrounding temperature (K)

ε : Flame emissivity

The emissivity of the flame is a dimensionless number, less than or equal to 1, which indicates the ability of the flame to behave like a black body. It is thus worth 1 for a black body. Emissivity depends mainly on the soot content in the flame and on the composition of gases capable of absorbing external radiation, mainly molecules with non-zero dipole moment such as carbon dioxide and water vapor.

For hydrocarbons generating a lot of soot, the emissivity can be considered as unit when the diameter of the fire is greater than a few meters. The flame then behaves like a black body.

Chapter I: Fire phenomena and correlative models for the temperature

In addition, most authors note that the fumes from combustion, the production of which increases with the diameter of the fire, tend to cover more or less completely the surface of the flame and thus play the role of a screen absorbing part of the flame radiation emitted by the “open” flame. This screening effect tends to decrease the average emissivity of the flame.

I.2.5- Phases of fires in compartment

The fire in compartment is characterized by four principal phases. The first phase is the fire development which is the evolution of the size of the fire from a small incipient fire. If there is no action to stop the fire, it will have the maximum size. In this situation, the fire size will be controlled by the amount of existing fuel or by the amount of ventilation.

The second phase is the flashover which is usually obvious to the observer of fire growth. When an object begins to burn in a compartment, gives rise to the appearance of a fire plume of hot gases and smoke. By natural convection rises to the ceiling, where it begins to spread horizontally, forming a layer. An unconfined flame tends to follow the initial growth period, a law in which the heat release rate is proportional to the square of time. Thus the layer next to the ceiling increases temperature and thickness because the plume continues to transport mass and energy from the burning material. The temperature increase of that layer makes the emission of radiation, being primarily directed downward, higher and higher. This radiation focuses on the existing objects in the compartment is partially absorbed and increases the temperature of these objects, which continue to produce volatile combustibles. When the upper layer reaches of 600°C order, the incident radiation is sufficient to ignite these released volatile combustibles, bringing simultaneously all objects under fire. This incident radiation has an estimation value of 20kW/m² at ground level [3].

The third phase corresponds to the full development of the fire, which is affected by:

- size and shape of the enclosure
- amount, distribution and type of fuel in the enclosure
- amount, distribution and form of ventilation of the enclosure
- form and type of construction materials comprising the roof (or ceiling), walls and floor of the enclosure.

The fourth phase corresponds to the cool down of the fire, and depends on the fire brigade intervention or the limitation on fuel or oxygen.

Chapter I: Fire phenomena and correlative models for the temperature

I.2.6- Development of a fire with sufficient oxygen supply

I.2.6.1- Phase 1: ignition of the fire

During initiation, the fire cannot have a great influence on the heat, visibility and toxicity of the atmosphere. It can still be fought with small extinguishing means and without a breathing apparatus.

For a fire to take place, enough energy (heat), fuel and oxygen are needed. Once a fire starts, its development depends on the type of fuel and its location in the room. The fire is under fuel control. If the air in the room contains enough oxygen to sustain the fire, then it is called a controlled carburetion fire.

The velocity at which a fire spreads at this stage depends on various factors:

- The oxygen concentration;
- The type of fuel: easily flammable or not;
- The mixture between fuel and oxidizer; a block of wood will ignite less easily than wood chips;
- The temperature in the room: when the temperature is high, the amount of pyrolysis gas formed is greater and the ignition temperature of these gases will be reached faster;
- The location of the fire in the room: a fire spreads more quickly vertically by contact with flames and by convection. On the other hand, a fire spreads much less quickly laterally and downwards.

a- Pyrolysis:

In a class A (flammable solids) fire, the flames formed after ignition always come from pyrolysis gases.

Chapter I: Fire phenomena and correlative models for the temperature

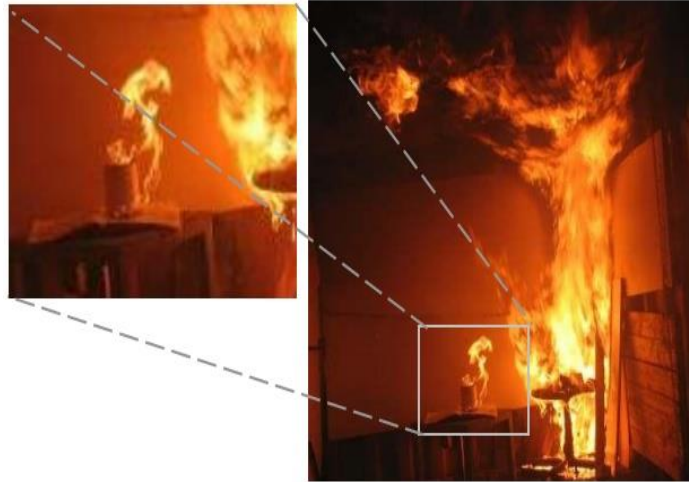


Figure I.5: Ignition of pyrolysis gases [4].

Chapter I: Fire phenomena and correlative models for the temperature

Pyrolysis can be initiated by all forms of heat transfer. A newspaper or paper placed on a table, located a few meters from a burning chair, will receive by radiation the heat necessary to emit pyrolysis gases and even ignite.

I.2.6.2- Phase 2: development phase

The phase between the initiation of the fire and the flashover is the development phase. The cigarette, forgotten in the armchair, can induce the formation of pyrolysis gases and ignite the cushion. Not all pyrolysis gases are consumed by the flames. They rise, together with the combustion gases rich in unburnt residues, towards the ceiling.

At this time, the fire is still under fuel control (controlled carburation fire). If the fuel is removed, the fire will go out. Surrounding materials cannot accumulate enough heat to sustain the fire.

As the hot gases reach the ceiling, they disperse horizontally. These hot gases mix with the cool air in the room and the overall room temperature rises.



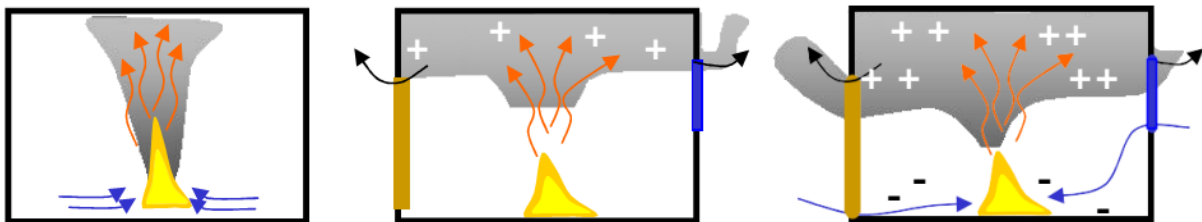
Figure I.6: During the development phase [5].

Chapter I: Fire phenomena and correlative models for the temperature

a- Gravitational current and neutral zone:

In the room, the color of the smoke layer, which at the start of the fire was rather light due to the pyrolysis gases, is becoming darker and darker. It is incomplete combustion that releases carbon particles into the smoke and increases the optical density of that smoke (which is proportional to the concentration of the combustion gases). Once the flames hit the ceiling, the volume and temperature in the smoke layer increases dramatically.

The smoke layer hits the horizontal boundary, i.e. the ceiling of the room, and searches for a path to the outside. An overpressure is created which tries to pulsate the smoke through the interstices and openings in the upper part of the room. At the base of the room, the pressure is lower and cool air is drawn into the fireplace (FigureI.7). This draft is very visible near open doors or windows.



FigureI.7: Evolution of the gravitational current [5].

There is therefore a motion of air towards the base of the fire (under pressure) and a movement of the very hot combustion elements towards the outside of the room (overpressure). The scientific term is gravitational current, because it is about hot and light gases and cold and heavier gases. Between the two zones (overpressure and under pressure) is the neutral zone. At this height of the neutral zone, there is no pressure difference. It is located just below the smoke layer FigureI.8.

Chapter I: Fire phenomena and correlative models for the temperature

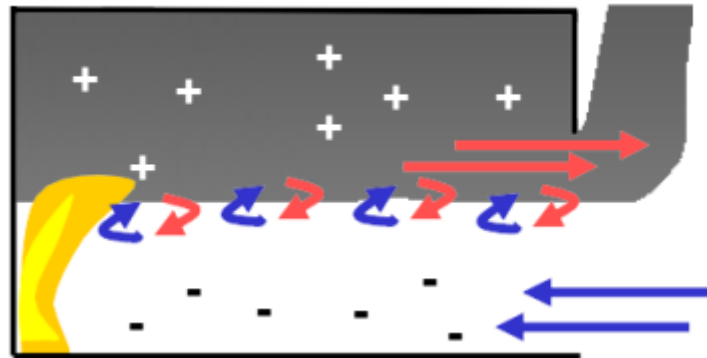


Figure I.8: The neutral zone at the interface of hot fumes and fresh air [5].

I.2.6.3- Phase 3:

a- flashover

The fire continues to develop and some flames are seen to begin to follow the smoke up to the neutral zone. However, the flames always remain more or less connected to the place where the fire started. These flames increase the heat radiation in the room and the pyrolysis of nearby objects takes place faster and faster. The flames fail to consume the large quantity of combustions at the height of the ever increasing ceiling. The temperature of these flue gases and the fresh air is sufficient to fuel the fire. Under these conditions, a flashover may occur.

The definition of a flashover is the point at which the temperature throughout the room reaches 600°C or the point where $15\text{-}20\text{KW} / \text{m}^2$ of radiant heat is measured at ground level.

The chance of survival for those in the room is nil, and from an economic point of view, the rescue of property is no longer possible. The survival time for a firefighter in full response gear, under real flashover conditions, is 8 to 10 seconds maximum. A firefighter who penetrates more than 1.5 meters in a room, without hydraulic means, has no chance of survival during a flashover.

Chapter I: Fire phenomena and correlative models for the temperature



FigureI.9: Evolution of a TV fire to flashover [6].

b- Rollover:

Many objects, which were in the vicinity of the fire, gave off pyrolysis gases under the influence of thermal radiation and by the incomplete combustion of the fire. The height of the neutral zone descends more and more. The concentration of combustion gases in the smoke layer intensifies from the ceiling downwards. At sufficient concentration, sudden inflammation may occur.

Ignition of combustion gases near the neutral zone, by direct contact with flames or embers, gives rise to the formation of slowly moving flame rollers. In the field, these flame rollers are almost always invisible to the responders. However, the team on the inside will feel them well. This is the roll-over, the ultimate precursor to the flash-over. The roll-over triggers a real chain reaction.

It is the roll-over that increases the temperature from 800 ° C up to 1000 ° C throughout the smoke layer. The combustion gases, which are too rich in fuel, will exceed their self-ignition thresholds. The heat radiation from the smoke layer to other flammable materials in the room increases dramatically.

Chapter I: Fire phenomena and correlative models for the temperature



FigureI.10: A simulation of a rollover in a German training container [7].

I.2.6.4- Phase 4, the fully developed chamber fire

During the first two phases, ie initiation and development, the fire is a controlled carburetion fire. After the flashover, it evolves into a controlled ventilation fire. The flammable pyrolysis gases, from the first two phases and partially burned during the flashover, are present in such large quantities in the room that there is not enough oxygen in the room by their combustion. The combustion of these pyrolysis gases will take place outside the room, at the level of the windows and doors (FigureI.11).



FigureI.11: The combustion of gases outside the room [8].

Chapter I: Fire phenomena and correlative models for the temperature

Temperatures in the room reach 700 ° C to 900 ° C. The duration of phase 4 depends on the presence in the room in sufficient quantity of combustion gases and of materials giving off pyrolysis gases.

I.2.6.5- Phase 5: extinction

When the fire is limited to one compartment and when the fuel in that compartment is consumed, the temperature will drop. The smoke layer in the room increases and the flames outside the windows and doors will start to disappear. In this space, air circulation may again be possible.

I.2.7- The thermal effects of the fire on people

The thermal effects of fire on people have three main origins:

- An overflow of thermoregulation which generates an increase in body temperature. Like fever, this elevation causes headaches and can lead to death above 42C °. since heat removal by thermoregulation is based on the principle of evaporation of sweat, ambient humidity is essential;
- Impairment of the respiratory tract, characterized by dryness or burns at different levels: throat, trachea and bronchi, pulmonary alveoli;
- A direct effect on the skin which can be of radiative origin (incident radiative flux), without skin contact with the fumes, or linked to convection and tissue contact with the fumes. This is the effect that interests us in this project.

These attacks can be characterized by two quantities: the incident heat flow and the temperature of the fumes.

I.2.7.1- Burns:

Burns occur at the skin temperatures listed in Table (I.1). These temperatures are considerably lower than the temperatures inside a burning room. Some sources still mention lower temperatures. It is important to note that burns are always a function of time and temperature. As soon as you feel something, you have to act, either move to decrease the compression or leave the room.

Chapter I: Fire phenomena and correlative models for the temperature

TableI.1: Burns depending on the skin temperature [5].

Skin temperature	Burn
48°C	1 st degree
55°C	2 nd degree
>55°C	3 rd degree
62°C	Insensitive
72°C	Immidiata destruction of the skin



FigureI.12: Burns on the human left hand



FigureI.13: Burns on the wrists [5].

Chapter I: Fire phenomena and correlative models for the temperature

I.2.7.2- Effect of incident radiative heat flux

The radiative heat flux contributes to the risks for people and contributes significantly to the development of fire. With the temperature, it presents risks to people; the heat flow causes direct burns to the skin depending on the exposure. The different effects on humans and on structures depending on heat flow are presented in the following two tables:

TableI.2: Effects of radiative heat flux on humans [9].

Heat flux	Effects on humans
2 ,5 kW/m ²	Limit of tenacity of the skin in 30 minutes.
3 kW/m ²	Irreversible effects on humans (area of significant dangers for human life).
5 kW/m ²	Lethal effects on humans (area of serious danger to human life) (blisters in 30 seconds).
8 kW/m ²	Significant lethal effects on humans (area of very serious danger to human life).
9,5 kW/m ²	Pain thresholding 6 seconds.
90 kW/m ²	Immediate tissue destruction.

TableI.3: Effects of radiative heat flux on structures [9].

Heat flux	Effects on the structures
1 kW/m ²	Solar radiation in tropical areas.
5 kW/m ²	Destruction of significant windows.
8 kW/m ²	Domino effects (threshold from which the domino effects must be examined and the start of spontaneous combustion of the wood).

Chapter I: Fire phenomena and correlative models for the temperature

16 kW/m ²	Prolonged exposure threshold for structures Very serious damage to structures, excluding concrete structures.
20 kW/m ²	Holds concrete for several hours. Very serious damage to concrete structures.
200 kW/m ²	Concrete ruin in a few tens of minutes.

Three sources of radiative heat flux are to be considered in the fire:

- The direct heat flow emitted by the fireplace. It spreads in a straight line from this focus. It is the most intense in terms of flow, but it is localized and people are not necessarily subject to its action during an extended period of the evacuation. The effect is usually on the face and upper limbs. In the case of a fully developed fire, this heat flux can carry over long distances and generate "domino" effects. this is why it is particularly treated in the monitoring of the remote consequences of highly developed fires (collateral damage, possibility of intervention);
- The heat flux from smoke is linked to its emissivity and temperature. In a stratified system, the entire surface under the fumes receives from them a radiative flux which is a function of the fourth power of the flue gas temperature. She assimilates the smoke to a gray body, even black. In this case, the effect can be considerable for people being evacuated, even at great distances from the home. The effect is usually directed towards the top of the head and the shoulders;
- The heat flow from the walls. A thermally thin wall can heat up and transmit flux by radiation without having a fume passage. This is the case in the case of fires in ships with unprotected metal partitions (outside the cantons), or for example for those present after a fire has been extinguished. The walls then behave like a gray body and return the accumulated heat in the form of radiation, according to Stefan-Boltzmann's law.

Chapter I: Fire phenomena and correlative models for the temperature

I.2.7.3- Temperature effect

Temperature can have different physio-pathological effects on humans. In particular, short exposure to high temperatures causes direct effects such as burns to the dermis or the respiratory system, while more moderate exposure may only cause hyperthermia. A table of increasing temperature, physio-pathological effect and tenability time has been established by the US [10]. Navy and is presented below:

TableI.4: Effects of Temperature on Individuals - US Navy - [10].

Temperature	Incapacitation	Lethality
90°C	35 minutes	60 minutes
150°C	5 minutes	30 minutes
190°C	Immédiate	15 minutes
200°C	Irreversible damage to the respiratory tract	
340°C	Instant death	

I.3- Models for temperature distribution

I.3.1- Fire detection

Reliable fire detection is an essential part of the fire protection program in nuclear power plants (NPPs), it relates to both fire control or extinguishment and safe evacuation of occupants. Most of the devices associated with fire detection and suppression are typically located near the ceiling surfaces. In the event of a fire, hot gases in the fire plume rise directly above the burning fuel and impinge upon the ceiling. The ceiling surface causes the flow to turn and move horizontally beneath the ceiling to other areas of the building located at some distance from the fire. The response of detection devices (heat/smoke detectors) and sprinklers installed below the ceiling submerged in this hot flow of combustion products provides the basis for the building's active fire protection measures. Smoke and heat detectors are best suited for fire detection in confined spaces, where rapid heat generation can be expected in the event of a fire. Smoke and heat detectors have been installed extensively in most NPPs.

Chapter I: Fire phenomena and correlative models for the temperature

Generally, such detectors are installed as part of a building-wide alarm system, which typically alarms in the main control room. The purpose of such systems is to provide early warning to building occupants, and rapid notification of the fire brigade. Some detection devices will also perform the function of automatically actuating suppression systems and interfacing with other building systems such as heating, ventilation, and air-conditioning (HVAC)

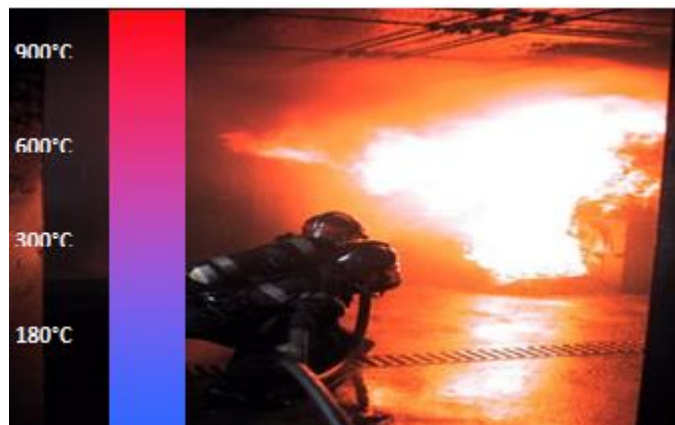


Figure I.14: The evolution of the temperature in a room during the intervention [5].

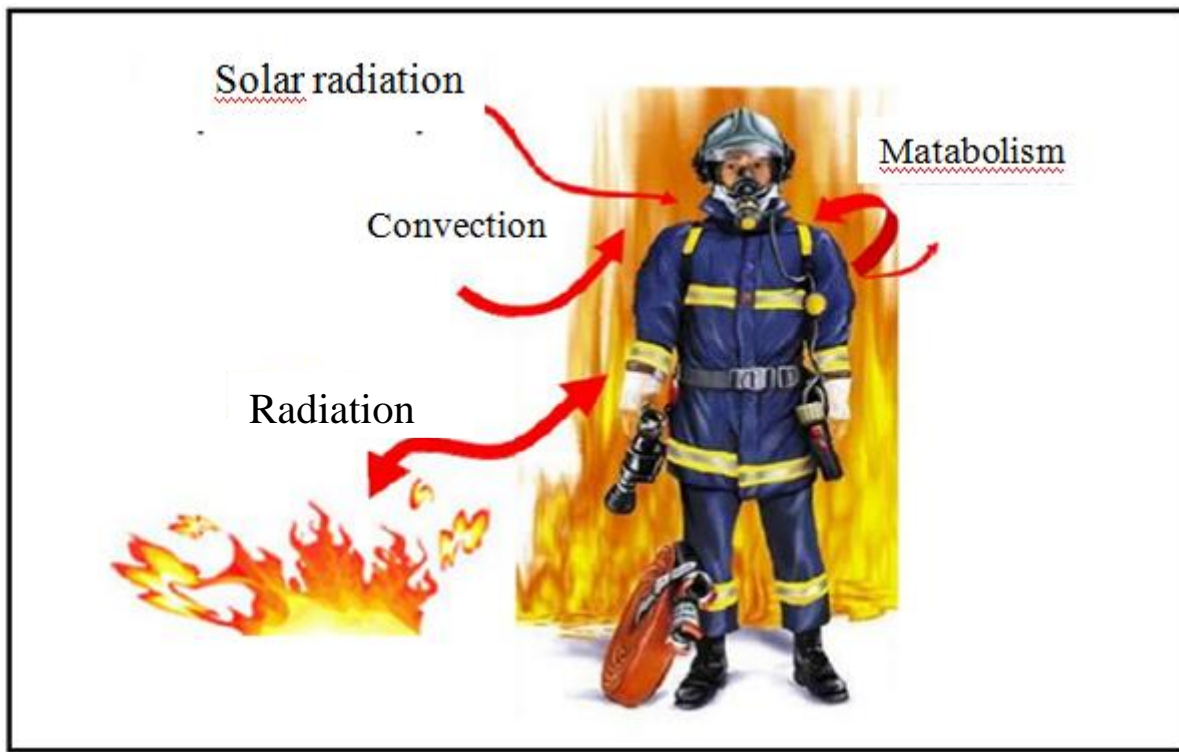
I.3.2- Description of the problem

The consequences of a fire in a point located near the fire in a confined space, or even semi-confined (local), are estimated from the heat flux received (radiation, convection) by this point.

The flux radiated by the flame is directly related to the heat of combustion of the burning material and corresponds to the fraction of the heat given off by the flame in radiative form.

The heat given off by the fire heats the surrounding air and creates an upward current of warm air; inert gases (nitrogen, argon...), an oxidizing gas (oxygen) and combustion products (smoke). As it rises, this current of warm air causes a current of cool air to feed the base of the fire. The difference in density between hot air and cold air causes convection movements, that is, air movements caused by temperature differences.

Chapter I: Fire phenomena and correlative models for the temperature



FigureI.15: The heat transfer modes between the fire and the firefighter garment [11].

I.3.3- Radiant heat transfer to solid

I.3.3.1- Solid flame pattern

In the solid flame model, the flame is assimilated to an outer surface of an opaque volume of simple geometry (parallelepiped for our work). This model is based in particular on the following assumptions:

- 1- the visible surface of the flame emits thermal radiation towards the target while the non-visible part does not;
- 2- the flame is assimilated to the outer surface of a simple geometric volume (parallelepiped). The base of this volume then corresponds to the base of the fire and its height for which the flame is visible 50% of the time.

Chapter I: Fire phenomena and correlative models for the temperature

a- Solid one-zone flame pattern

For the one-zone model, the flame is assumed to radiate uniformly over its entire surface, which amounts to considering a flame temperature and a homogeneous composition over the entire height of the flame.

The radiative heat flux density received by an element external to the flame will be calculated by the following equation:

$$q_{inc,rad} = \Phi_0 F \tau \alpha \quad (I.8)$$

Where

$q_{inc,rad}$: Density of radiative heat flux received by an external element (kW/m²);

F: Factor of view between the external element and the flame;

τ : Atmospheric attenuation coefficient;

α : Coefficient of absorption of the external element;

Φ_0 : Emissive power of the flame (kW/m²).

In reality, any non-black body receiving radiation reflects some of it.

The application of the solid flame model requires the definition of a number of parameters, necessary to estimate the radiative heat flux density received by a target from the radiation emitted by the flame.

Three important data must be determined:

- The geometry of the flame involved in the calculation of the view factor. This factor ultimately reflects the solid angle at which the target perceives the flame.
- The emissive power of the flame, ie the power radiated per unit of flame area.
- The atmospheric attenuation coefficient, which is the fraction of radiation absorbed by the atmosphere

Chapter I: Fire phenomena and correlative models for the temperature

I.3.4- Geometry of the flame

The flame is assimilated to a volume of simple geometry (in our case, a volume of a rectangular parallelepiped) with variable or homogeneous properties (in particular in terms of parameters such as the geometry and the emissivity of the flame).

To characterize the geometry of the flame, it is essential to determine, among other things:

- The surface of the base of the flame;
- Its height H;
- If necessary, effects due to the action of the wind.

I.3.4.1- Calculation of the equivalent diameter

For a non-circular pit fire, the equivalent diameter, D_{eq} , can be estimated by the following formula:

$$D_{eq} = \frac{4.A}{P} \quad (I.9)$$

Where:

D_{eq} : fire pool diameter (m);

A: fire pool surface area (m²);

P: fire pool perimeter (m).

I.3.5- Fire scenario

I.3.5.1- Localized fires

Depending on the height of the fire flame, relative to the ceiling of the compartment, a localized fire can be defined as either a small fire (or open-air fire) or a large fire impacting on the ceiling. For a small fire, a design formula is given to calculate the temperature in the flame along the vertical axis. For a bigger fire, some simple steps have been developed to calculate the heat flux received by the surfaces exposed to the fire at the ceiling level. The limitations of this approach include:

Chapter I: Fire phenomena and correlative models for the temperature

- The diameter of fire $D \leq 10$ m
- The heat release rate of the fire $Q \leq 50$ MW.

In a localized fire, there is an accumulation of combustion products in a layer beneath the ceiling (upper layer), with a horizontal interface between this hot layer and the lower layer where the temperature of the gases remains much colder. This situation is well represented by a two-zone model, useful for all pre-flashover conditions. Besides calculating the evolution of gas temperature, these models are used in order to know the smoke propagation in buildings and to estimate the life safety as a function of smoke layer height, toxic gases concentration, radiative flux and optical density. The thermal action on horizontal elements located above the fire also depends on their distance from the fire.

I.3.5.2- Small Fires

In a localized fire the highest temperature is at the axis of the vertical flame, decreasing towards the edge of the flame. The flame axis temperature changes with height. It is roughly constant in the continuous flame region and represents the mean flame temperature. The temperature decreases sharply above the flames as an increasing amount of fresh air enters into the fire compartment. EN 1991-1-2 [12] provides a design formula to calculate the temperature in the plume of a small localized fire, based on the fire model developed by Heskestad [13]. It can be applied to open- air fires as well. Considering a localized fire as shown in Figure16, the flame height L_f of the fire is provided by:

$$L_f = -1.02 D + 0.0148 \dot{Q}^{2/5} \quad (\text{I.10})$$

Where:

D: the diameter of the fire (m)

Q: heat release rate of the fire (W)

H: distance between the fire source and the ceiling (m).

This model allows determining the temperatures along the vertical axis of the flame. However, in a real structural scenario, a column and respective flame are likely to be positioned side by side. Therefore, the temperature estimated by the first model is unlikely to

Chapter I: Fire phenomena and correlative models for the temperature

be the boundary temperature of a column subjected to a localized fire. Moreover, an estimation of gas temperatures in the vicinity of the column is a prerequisite to assessing the convective heat flux.

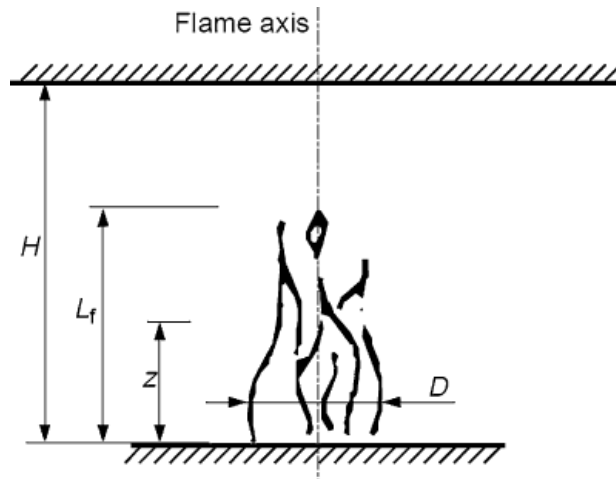


Figure I.16: Schematic diagram for small localized fires [14].

The flame lengths L_f of a localized fire (see Figure I.16) is given by Eq (I.10) where L_f represents the flame lengths fire [m], D represents the diameter of the fire [m] and Q is the rate of heat release [W]:

The virtual origin z_0 [m] of the axis is given by Eq (I.11) [13]:

$$z_0 = -1.02 D + 0.00524 \dot{Q}^{2/5} \quad (\text{I.11})$$

I.3.5.3- Large Fires Impacting on the Ceiling

When a localized fire becomes large enough, with $L_f > H$, the fire's flames will impact on the ceiling of the compartment. The ceiling surface will cause the flame to turn and move horizontally beneath the ceiling.

I.3.5.4- Definition of fire (HRR) fire event

Energy release rate (often termed heat release rate or HRR) is measured in W, kW, or MW. Table 1 gives some characteristic values of energy released by various burning fuel packages and heat output from different sources.

Chapter I: Fire phenomena and correlative models for the temperature

TableI.5: The heat flow rate generated from various sources [15].

Source	Heat flow rate
A burning cigarette	5 W
A typical light bulb	60 W
A human being at normal exertion.	100 W
A burning waste paper basket.	100 kW
A burning 1m ² pool of gasoline.	2.5 MW
Burning wood pallets, stacked to the height of 3 m.	7 MW
Burning polystyrene jars, in cartons, 2 m, 4.9 m high.	30–40 MW
Output from a typical reactor at a Nuclear Power Plant.	500–1000 MW

TableI.5 indicates that for many design purposes the design fire energy output could be in the range 100 kW to 50 MW.

I.3.5.5- Factors controlling energy release rates in enclosure fires

The rate at which energy is released in a fire depends mainly on the type, quantity, and orientation of fuel and on the effects that an enclosure may have on the energy release rate.

The energy release rate will vary with time. Such measurements are often termed “free burn” tests, indicating that the items are burning without any effects of the enclosure in which the fire takes place [15].

Chapter I: Fire phenomena and correlative models for the temperature

I.4- Plume models

I.4.1- HESKESTAD correlation [2]

It's a relatively recent correlation (1983). It has the most important domain of validity whether, in terms of product or type of fire.

Heskestad suggests a simplified formula providing a rational approximation of this correlation for the most common fuels under classical and typical atmospheric conditions.

Virtual origin (best fit from experiments) [13]:

$$z_0 = -1.02D + 0.083\dot{Q}^{2/5} \quad (\text{I.12})$$

Mean flame height:

$$H = -1.02D + 0.235\dot{Q}^{2/5} \quad (\text{I.13})$$

Radius of the Plume:

$$b(z) = 0.12 * (T_0/T_{\text{amb}})^{1/2} * (z-z_0) \quad (\text{I.14})$$

Where:

H: flame height (m)

D: fuel diameter (m)

\dot{Q} : heat released by the fuel (kW)

z_0 : virtual origin (m)

T_0 and T_{amb} : temperature at t_0 and the ambient temperature respectively (K)

Heskestad has presented the bulk of the theory regarding flows within a primary channel. His paper also presents correlations for the temperature and velocity of the ceiling jet, within this channel, which is initially axi-symmetric until it is intercepted by the beams. At this point a transition region begins until the flow converges to a two dimensional, channel flow. Upon intersection of the ceiling jet with the beams, a portion of the gases escape under the beam and into adjacent channels. The remainder of the gases flow within the channel in opposite

Chapter I: Fire phenomena and correlative models for the temperature

directions. However, if the beams are sufficiently deep, large d/H , the leakage under the beams becomes small, and all of the fire gases are restricted to the primary channel.

Temperature, gas velocity and optical density were measured at various locations along the ceiling. In addition, several commercially available smoke and heat detectors were grouped together and located at several positions along the test ceiling. The response of these detectors was recorded.

A set of functional relationships for the temperature and velocity of ceiling jet gases has been proposed by Heskestad. The expressions relate fire size, fire growth rate, height above the fire, radial distance from the fire, gas temperature and gas velocity for the general class of fires called power-law fires.

For most ceiling jet models, it is necessary to know the height of the ceiling above the virtual origin of the plume (focal point of the fire plume).

I.4.2- Wind effects

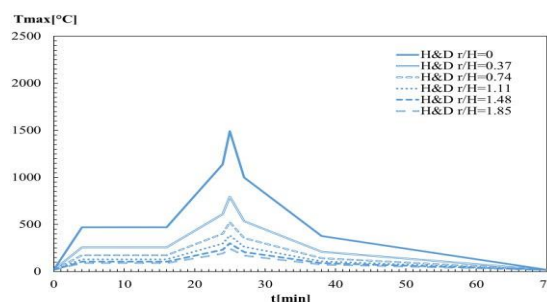
Schematically, the effects associated with the wind action on the behaviour of the flame are:

- The inclination of the flame from the vertical axis;
- The modification of the mean height of the flame (according to the wind velocities);
- The widening of the base of the flame in the direction of the wind.

It's clear the estimation of these phenomena is complex given in particular the intermittent nature of the wind at the local scale. As part of this work, we didn't take into account the impact of the wind.

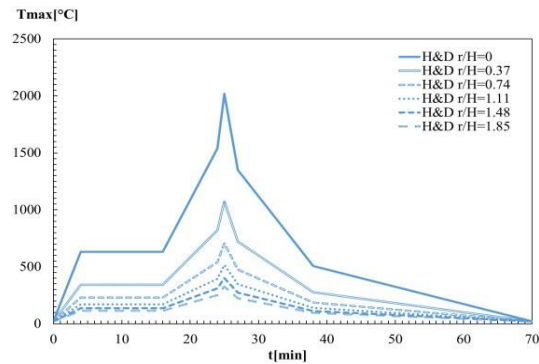
I.4.3- Maximum Temperature during the fire event

The results of the maximum temperature obtained from the simple correlative model of Heskestad are shown in Figure I.17



Chapter I: Fire phenomena and correlative models for the temperature

Class1



Class2

Figure I.17: Temperature near the ceiling from Heskestad correlation.

I.5- Ceiling -jet models

I.5.1- Plume and Ceiling jet fires

I.5.1.1- Ceiling jet fire

The ceiling jet is created when there is an impingement between a buoyant plume and flat unobstructed ceiling where the hot gases spreads radially under the ceiling, see Figure 18.

Ceiling jet fire can also be defined as the rapid flow of gas in a surface layer below the ceiling surface that is driven by the buoyancy of hot combustion products.

Chapter I: Fire phenomena and correlative models for the temperature

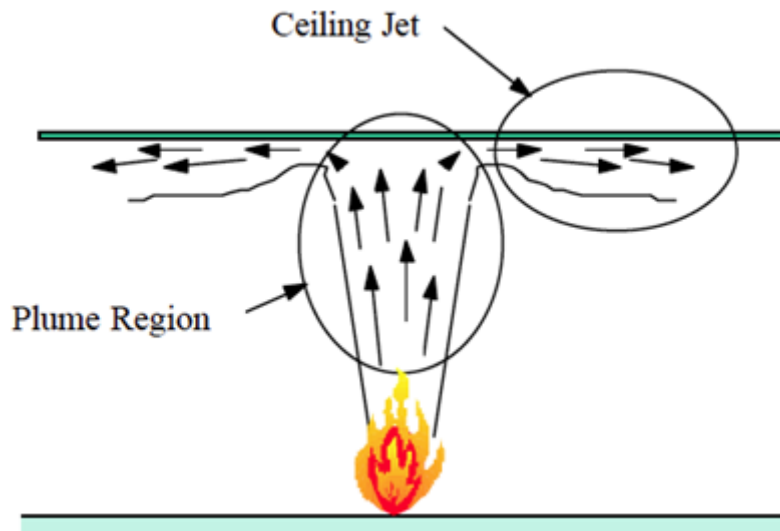


Figure I.18: fire plume and ceiling jet [16].

I.5.1.1.1- Ceiling jet temperature

Li et al. [20, 21] have theoretically and experimentally investigated the maximum ceiling gas temperature and its corresponding position in tunnel fires and robust equations have been proposed for both low and high ventilations. However, how the flame temperature varies with distance in the vicinity of the fire has not yet been fully explored. While correlating, all the temperature distribution curves, there is a “virtual origin” along the ceiling [17]. The horizontal distance at the ceiling between the fire source and virtual origin needs to be clearly determined.

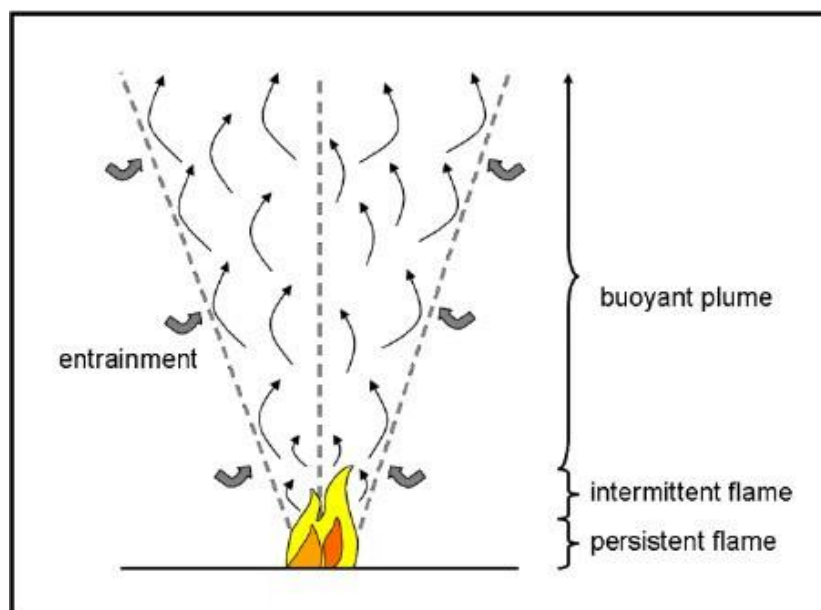
I.5.1.1.2- Ceiling jet radiation

There is a strong correlation [18] between the ceiling gas temperature and the heat flux at the floor level in the far-field of the fire. However, the radiation directly from the flame to the objects at floor level or at a certain height in the vicinity of the fire needs to be thoroughly investigated, since the fire spread to the neighboring objects or vehicles mainly results from this radiation.

Chapter I: Fire phenomena and correlative models for the temperature

I.5.1.2- Plume fire

The fire plume is usually divided into three regions ‘persistent flame’ zone at the flame base, ‘intermittent flame’ zone following, and ‘buoyant plume’ in the highest region see FigureI.19. The persistent zone has chemical reactions and air entrainment taking place and thus is the most interesting regarding flame establishment, stabilization, and mass formation. In this first zone, where the chemical reactions and heat release occur, the flame appears nearly laminar with a light blue colour. The heat release induces a large increase in the gas velocity and temperature in this region. The characteristics of flame in this zone are generated by the following basic mechanism as heat transfer, radiative and convective. In the intermittent zone, the flame turns into yellow colour with the maximum temperature shifting toward the burner axis. Air entrainment in these two zones pushes the flame inward, forming a characteristic ‘neck’ at the top of which intermittent, large eddy structures are formed, see FigureI.19. In the plume zone, velocities and temperatures decrease with height [19].



FigureI.19: The three zones of the axi-symmetric buoyant plume [20].

The unconfined point-source plume configuration has been used by previous researchers to establish plume theory. This theory provides solutions for the temperature profile, velocity profile and entrainment for thermal plumes at various elevations above the source [16]. Based

Chapter I: Fire phenomena and correlative models for the temperature

on point source theory, the behaviour of the fire plume is independent of the details of the heat source including the fuel source and source geometry. The turbulent flow above a point source of heat is analyzed in terms of the total mass, momentum and energy integrated across the plume cross section assuming that the entrainment velocity is proportional to the centerline plume velocity.

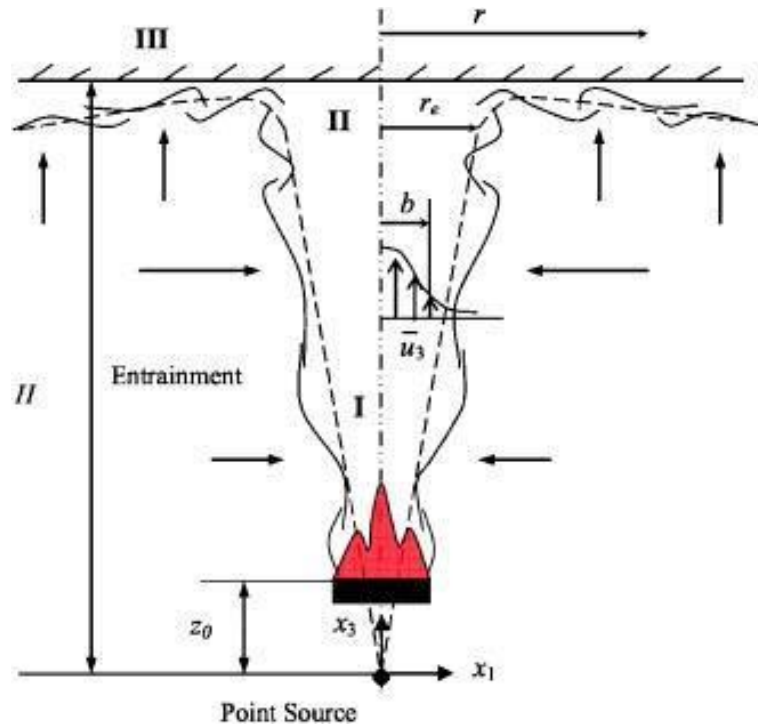


Figure I.20: Schematic of plume and ceiling jet flow for an unconfined ceiling [21]

I: Plume Region; II: Turning Region; III: Ceiling Jet Region.

Once the plume impinges on a ceiling, it turns to form a radially expanding ceiling jet. The flow behaviour becomes more complicated compared with the fire plume. Due to the viscous interactions with ceiling, there is a competition between turbulent mixing and stable stratification along the ceiling. Most notably, Alpert [21] performed an analytical and experimental study developing the theory and associated scaling laws for fire induced ceiling jets. His analysis successfully predicted the maximum temperature distributions in the ceiling jets and is widely used in hazard analysis. Based on his analysis, he provided relationships for dimensionless ceiling layer thickness, velocity, and temperature, which compares favourably with measurements. In fact, his analysis revealed that these flow quantities are relatively

Chapter I: Fire phenomena and correlative models for the temperature

insensitive to geometric scale. Alpert suggested that credible small scale fire experiments could be conducted at ceiling heights down to 0.6 m.

I.5.2- CORRELATIVEMODELS

I.5.2.1- Definition of correlative models

Correlations to estimate temperatures and velocities in the hot gases beneath a ceiling in a fire, a so-called ceiling jet, have existed for at least four decades. These types of correlations are often used in fire safety engineering in order to get an estimate of sprinkler and/or heat detector activation in enclosure fires. Such correlations can also be used to estimate damage if a ceiling material will ignite or if structures will be affected. A ceiling jet is created when a buoyancy driven plume impinges on a flat unobstructed ceiling and the hot gases spreads radially under the ceiling, see Figure I.21. As the ceiling jet moves radially from the outward, air will be entrained and the temperature cools down due to entrainment of cold air and heat losses to the ceiling. If the ceiling jet is unconfined it will have a maximum thickness, distance to where the excess of gas temperature drops to $1/e$ of $(1/2.72)$ the maximum excess temperature, of about 5-13% of the total room height and the maximum temperature will be at a distance of 1% of the room height below the ceiling. In a normal compartment fire, this type of unconfined ceiling jet will only exist in the earliest stages of fire development before the hot gases will accumulate in the compartment.

Chapter I: Fire phenomena and correlative models for the temperature

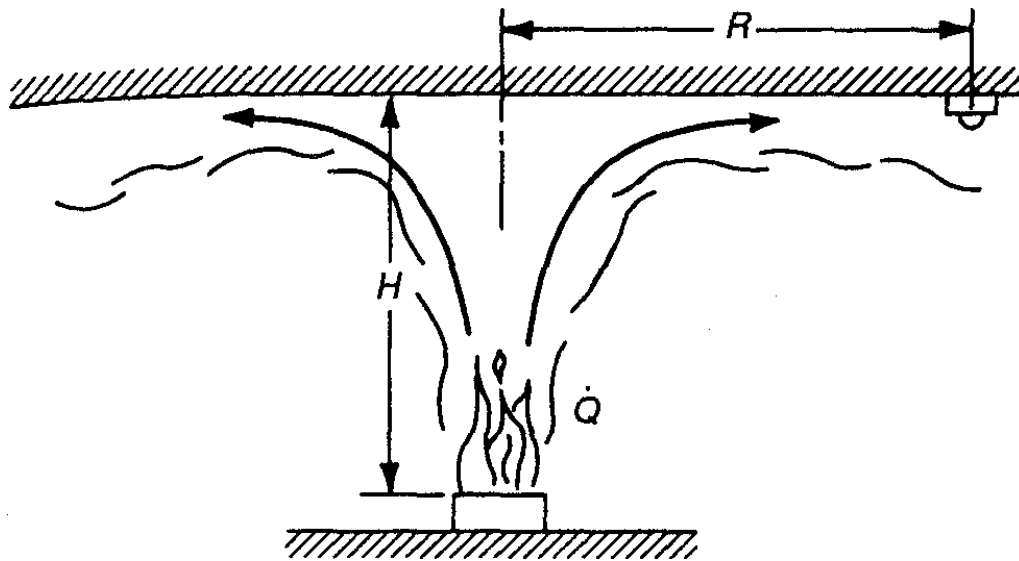


Figure I.21: Ceiling jet flow beneath an unconfined ceiling [22].

The main parameters of the fire induce ceiling jet are represented. For our case, it is assumed that this fire is equivalent to a pool fire with an elevation surface H_{pool} equivalent to 0.5 m above the ground and a remaining distance H up to the ceiling equals 2.4 m, we will deal with these values in the last chapter.

I.5.2.2- Alpert correlations

Alpert assumed an axi-symmetric fire induced flow beneath a flat, horizontal ceiling that was unobstructed by walls and the ceiling jet was divided into two regions. Thus there are two sets of correlations, for the maximum excess temperature (T_{max}) and maximum velocity (u_{max}), presented. In our work we highlight only on T_{max} with which the first one is valid in the turning region where the plume impinges the ceiling ($r/H \leq 0.18$ Eq I.15), while the second set is valid in the far field ($r/H > 0.18$ Eq I.16) and depends on the radial distance from the plume centerline.

The correlations developed by Alpert [23] for determining maximum ceiling jet temperatures and velocities in S.I. Units are:

$$\text{For } r \leq 0.18 H \quad T_{\text{max}} - T_{\infty} = 16.9 \dot{Q}^{2/3} (H - z_0)^{-5/3} \quad (\text{I.15})$$

Chapter I: Fire phenomena and correlative models for the temperature

$$\text{For } r > 0.18 H \quad T_{\max} - T_{\infty} = 5.38 \left(\frac{\dot{Q}}{r} \right)^{\frac{2}{3}} (H - z_0)^{-1} \quad (\text{I.16})$$

Where:

H: ceiling height,

r: radial distance from the plume centerline

\dot{Q} : heat release rate of the fire.

Alpert also conducted a numerical study of ceiling jets. It was, among other things, studied how heat transfer to the ceiling affects the ceiling jet and it was seen that there was no large effect on the ceiling jet temperature and thickness within a radial distance of less than 1 ceiling height ($r/H < 1$). However, at distances of 3 to 5 ceiling heights, the effects were significant [24]. These correlations are divided into two zones, one part applies to the region of impingement where the upward flow of gas in the plume turns to flow out beneath the ceiling horizontally. The correlations are based on measurements collected during test burns of fuel arrays of wood and plastic pallets, cardboard boxes, plastic materials in cardboard boxes, and liquid fuels with energy release rates ranging from 668 kW to 98 MW under ceiling heights from 4.6 to 15.5 m.

I.6- Conclusion

Correlative results are usually derived from experimental results and the numerical models are used to solve differential equations.

The confrontation between correlative, two zones and CFD models can improve the knowledge state on the ceiling-jets and probably helps the fire engineers to enhance the performance of the fire protection devices.

Our fire modelling capabilities are frequently used to support fire cause and origin investigations. In this capacity, Exponent uses the most widely used tools in fire modelling the (CFD).

Chapter I: Fire phenomena and correlative models for the temperature

In case of fire, flames and fumes emit some of the energy released by the combustion reaction in the form of electromagnetic radiations (radiative heat flux) and part of energy as convective heat flux.

Several mathematical models exist for estimating the consequences of a fire depending on the exposure time, the development space of the fire, the type and the geometry of the fireplace and the distance between the observer and the source of the fire.

Chapter II:
FDS software
presentation

Chapter II: FDS software presentation

II.1- Introduction to FDS

The Fire Dynamics Simulator is the newest and most versatile of the fire models developed by NIST. The Fire Dynamics Simulator has been used for many types of problems, like sprinkler activation in warehouse fires, tenability in residential fires, and smoke concentration in outdoor pool fires.

The NIST Fire Dynamics Simulator consists of two programs - FDS and Smokeview. The NIST Fire Dynamics Simulator predicts smoke and/or air flow movement caused by fire, wind, ventilation systems etc. Smokeview visualizes the predictions generated by FDS.

FDS, a computational fluid dynamics (CFD) model, solves a form of the Navier-Stokes equations appropriate for low-speed, thermally-driven flows of smoke and hot gases generated in a fire. FDS has integrated sub models that calculate many fire related phenomena such as radiative and convective heat transfer, sprinkler activation and sprinkler sprays, mixture fraction combustion model, and many others.

II.2- Features of FDS

Hydrodynamic Model FDS solves numerically a form of the Navier-Stokes equations appropriate for low speed, thermally-driven flow with an emphasis on smoke and heat transport from fires. The core algorithm is an explicit predictor-corrector scheme, second order accurate in space and time. Turbulence is treated by means of the Smagorinsky form of Large Eddy Simulation (LES). It is possible to perform a Direct Numerical Simulation (DNS) if the underlying numerical mesh is fine enough. LES is the default mode of operation.

Combustion Model For most applications, FDS uses a single step chemical reaction whose products are tracked via a two-parameter mixture fraction model. The mixture fraction is a conserved scalar quantity that represents the mass fraction of one or more components of the gas at a given point in the flow field. By default, two components of the mixture fraction are explicitly computed. The first is the mass fraction of unburned fuel and the second is the mass fraction of burned fuel (i.e. the mass of the combustion products that originated as fuel). A two-step chemical reaction with a three-parameter mixture fraction decomposition can also be used with the first step being oxidation of fuel to carbon monoxide and the second step the oxidation of carbon monoxide to carbon dioxide. The three mixture fraction components for

Chapter II: FDS software presentation

the two step reaction are unburned fuel, mass of fuel that has completed the first reaction step, and the mass of fuel that has completed the second reaction step. The mass fractions of all of the major reactants and products can be derived from the mixture fraction parameters by means of “state relations.” Lastly, a multiple-step finite rate model is also available.

Radiation Transport Radiative heat transfer is included in the model via the solution of the radiation transport equation for a gray gas, and in some limited cases using a wide band model. The equation is solved using a technique similar to finite volume methods for convective transport, thus the name given to it is the Finite Volume Method (FVM).

Geometry FDS approximates the governing equations on a rectilinear mesh. Rectangular obstructions are forced to conform with the underlying mesh.

It is possible to prescribe more than one rectangular mesh to handle cases where the computational domain is not easily embedded within a single mesh.

Parallel Processing It is possible to run an FDS calculation on more than one computer using the Message Passing Interface (MPI).

II.2.1- Basic Description of FDS

II.2.1.1- Type of Model

FDS is a Computational Fluid Dynamics (CFD) model of fire-driven fluid flow which was publicly released in February 2000 as a first version. The model solves numerically a form of the Navier-Stokes equations appropriate for low-speed, thermally-driven flow with an emphasis on smoke and heat transport from fires. The partial derivatives of the conservation equations of mass, momentum and energy are approximated as finite differences, and the solution is updated in time on a three-dimensional, rectilinear grid. Thermal radiation is computed using a finite volume technique on the same grid as the flow solver. Lagrangian particles are used to simulate smoke movement, sprinkler discharge, and fuel sprays.

Smokeview is a companion program to FDS that produces images and animations of the results. In recent years, its developer, Glenn Forney, has added to Smokeview the ability to visualize fire and smoke in a fairly realistic way. In a sense, Smokeview now is, via its three-dimensional renderings, an integral part of the physical model, as it allows one to assess the

Chapter II: FDS software presentation

visibility within a fire compartment in ways that ordinary scientific visualization software cannot.

II.2.1.2- Intended Uses

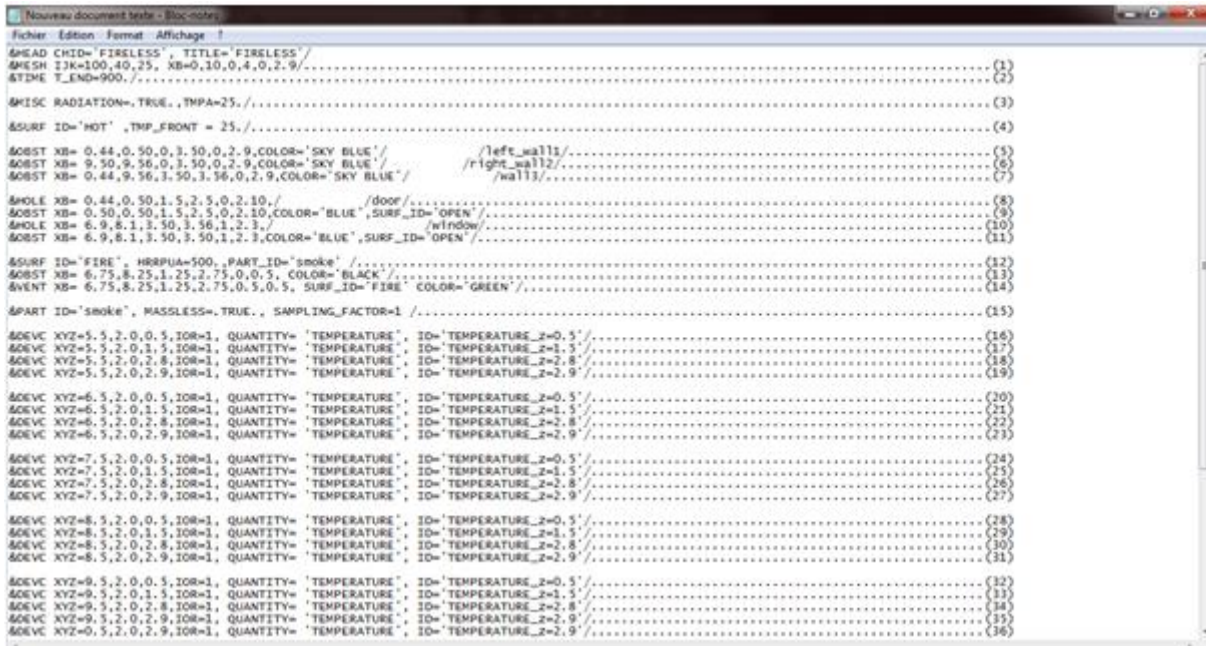
Throughout its development, FDS has been aimed at solving practical fire problems in fire protection engineering, while at the same time providing a tool to study fundamental fire dynamics and combustion. FDS can be used to model the following phenomena:

- Low speed transport of heat and combustion products from fire
- Radiative and convective heat transfer between the gas and solid surfaces
- Pyrolysis
- Flame spread and fire growth
- Sprinkler, heat detector, and smoke detector activation
- Sprinkler sprays and suppression by water

Although FDS was designed specifically for fire simulations, it can be used for other low-speed fluid flow simulations that do not necessarily include fire or thermal effects. To date, about half of the applications of the model have been for design of smoke control systems and sprinkler/detector activation studies. The other half consists of residential and industrial fire reconstructions.

Chapter II: FDS software presentation

II.2.1.3- Input Parameters



```
Fichier Edition Format Affichage ?
&HEAD CHID='FIRELESS', TITLE='FIRELESS' /..... (1)
&MESH IJK=100,40,25, XB=0,10,0,4,0,2,9 /..... (2)
&TIME T_END=900 /..... (3)
&MISC RADIATION=.TRUE., TMPA=25 /..... (4)
&SURF ID='HOT', TMP_FRONT = 25 /..... (5)
&SOBST XB= 0.44,0.50,0.3,50,0,2,9,COLOR='SKY BLUE' /..... (6)
&SOBST XB= 9.50,9.50,0.3,50,0,2,9,COLOR='SKY BLUE' /..... (7)
&SOBST XB= 0.44,9.50,3.50,3.56,0,2,9,COLOR='SKY BLUE' /..... (8)
&HOLE XB= 0.44,0.50,1.5,2.5,0,2,10 /..... (9)
&HOLE XB= 0.50,0.50,1.5,2.5,0,2,10,COLOR='BLUE',SURF_ID='OPEN' /..... (10)
&HOLE XB= 6.9,6.1,1.50,3.56,1,2,3 /..... (11)
&SOBST XB= 6.9,6.1,3.50,3.50,1,2,3,COLOR='BLUE',SURF_ID='OPEN' /..... (12)
&SURF ID='FIRE', HRRPUA=500, PART_ID='smoke' /..... (13)
&EVENT XB= 6.75,8.25,1.25,2.75,0,0,5, COLOR='BLACK' /..... (14)
&EVENT XB= 6.75,8.25,1.25,2.75,0,5,0,5, SURF_ID='FIRE' COLOR='GREEN' /..... (15)
&PART ID='smoke', MASSLESS=.TRUE., SAMPLING_FACTOR=1 /..... (16)
&CEVC XYZ=5.5,2,0,0.5,IOR=1, QUANTITY='TEMPERATURE', ID='TEMPERATURE_2=0.5' /..... (17)
&CEVC XYZ=5.5,2,0,1.5,IOR=1, QUANTITY='TEMPERATURE', ID='TEMPERATURE_2=1.5' /..... (18)
&CEVC XYZ=5.5,2,0,2.8,IOR=1, QUANTITY='TEMPERATURE', ID='TEMPERATURE_2=2.8' /..... (19)
&CEVC XYZ=5.5,2,0,2.9,IOR=1, QUANTITY='TEMPERATURE', ID='TEMPERATURE_2=2.9' /..... (20)
&CEVC XYZ=6.5,2,0,0.5,IOR=1, QUANTITY='TEMPERATURE', ID='TEMPERATURE_2=0.5' /..... (21)
&CEVC XYZ=6.5,2,0,1.5,IOR=1, QUANTITY='TEMPERATURE', ID='TEMPERATURE_2=1.5' /..... (22)
&CEVC XYZ=6.5,2,0,2.8,IOR=1, QUANTITY='TEMPERATURE', ID='TEMPERATURE_2=2.8' /..... (23)
&CEVC XYZ=6.5,2,0,2.9,IOR=1, QUANTITY='TEMPERATURE', ID='TEMPERATURE_2=2.9' /..... (24)
&CEVC XYZ=7.5,2,0,0.5,IOR=1, QUANTITY='TEMPERATURE', ID='TEMPERATURE_2=0.5' /..... (25)
&CEVC XYZ=7.5,2,0,1.5,IOR=1, QUANTITY='TEMPERATURE', ID='TEMPERATURE_2=1.5' /..... (26)
&CEVC XYZ=7.5,2,0,2.8,IOR=1, QUANTITY='TEMPERATURE', ID='TEMPERATURE_2=2.8' /..... (27)
&CEVC XYZ=7.5,2,0,2.9,IOR=1, QUANTITY='TEMPERATURE', ID='TEMPERATURE_2=2.9' /..... (28)
&CEVC XYZ=8.5,2,0,0.5,IOR=1, QUANTITY='TEMPERATURE', ID='TEMPERATURE_2=0.5' /..... (29)
&CEVC XYZ=8.5,2,0,1.5,IOR=1, QUANTITY='TEMPERATURE', ID='TEMPERATURE_2=1.5' /..... (30)
&CEVC XYZ=8.5,2,0,2.8,IOR=1, QUANTITY='TEMPERATURE', ID='TEMPERATURE_2=2.8' /..... (31)
&CEVC XYZ=8.5,2,0,2.9,IOR=1, QUANTITY='TEMPERATURE', ID='TEMPERATURE_2=2.9' /..... (32)
&CEVC XYZ=9.5,2,0,0.5,IOR=1, QUANTITY='TEMPERATURE', ID='TEMPERATURE_2=0.5' /..... (33)
&CEVC XYZ=9.5,2,0,1.5,IOR=1, QUANTITY='TEMPERATURE', ID='TEMPERATURE_2=1.5' /..... (34)
&CEVC XYZ=9.5,2,0,2.8,IOR=1, QUANTITY='TEMPERATURE', ID='TEMPERATURE_2=2.8' /..... (35)
&CEVC XYZ=9.5,2,0,2.9,IOR=1, QUANTITY='TEMPERATURE', ID='TEMPERATURE_2=2.9' /..... (36)
&CEVC XYZ=0,5,2,0,2,9,IOR=1, QUANTITY='TEMPERATURE', ID='TEMPERATURE_2=2.9' /..... (36)
```

Figure II.1: Input parameters of the FDS

All of the input parameters required by FDS to describe a particular scenario are conveyed via a single text file created by the user. The file contains information about the numerical grid, ambient environment, building geometry, material properties, combustion kinetics, and desired output quantities. The numerical grid consists of one or more rectilinear meshes with (usually) uniform cells. All geometric features of the scenario must conform to this numerical grid. Objects being smaller than a single grid cell are either approximated as a single cell, or rejected. The building geometry is input as a series of rectangular blocks.

Boundary conditions are applied to solid surfaces as rectangular patches. Materials are defined by their thermal conductivity, specific heat, density, thickness, and burning behavior.

Any simulation of a real fire scenario involves specifying material properties for the walls, floor, ceiling, and furnishings. FDS treats all of these objects as multi-layered solids, thus the physical parameters for many real objects can only be viewed as approximations to the actual properties. Describing these materials in the input file is the single most challenging task for the user. Thermal properties such as conductivity, specific heat, density, and thickness can be found in various handbooks, or in manufacturer literature, or from bench-scale measurements.

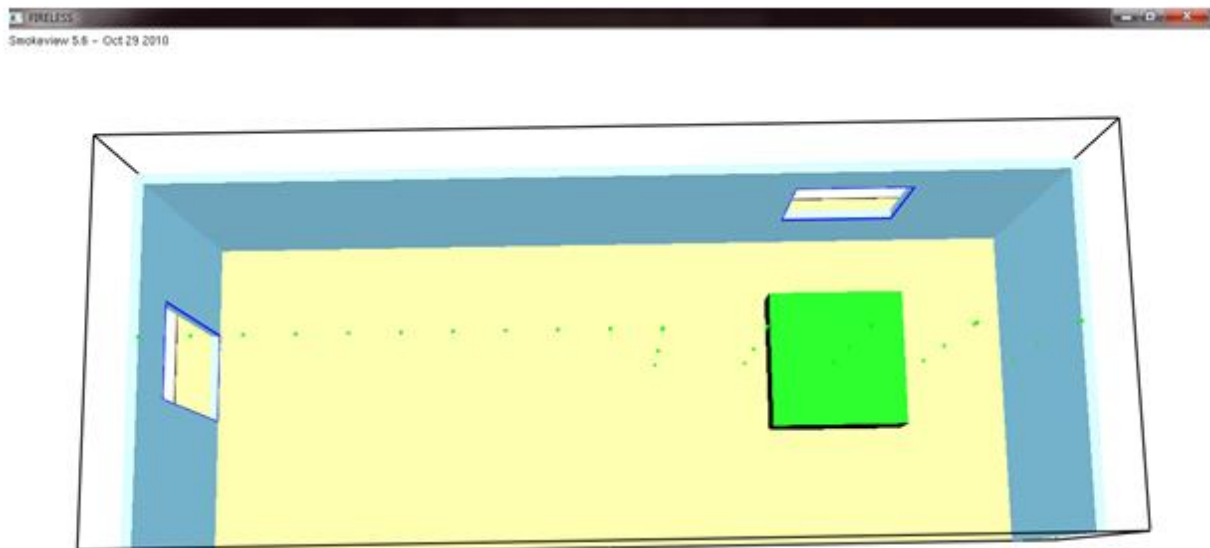
Chapter II: FDS software presentation

The burning behavior of materials at different heat fluxes is more difficult to describe, and the properties more difficult to obtain.

A significant part of the FDS input file directs the code to output various quantities in various ways.

Much like in an actual experiment, the user must decide before the calculation begins what information to save. There is no way to recover information after the calculation is over if it was not requested at the start.

II.2.1.4- Output Quantities



FigureII.2: FDS Output gotten by Smokeview

FDS computes the temperature, density, pressure, velocity and chemical composition within each numerical grid cell at each discrete time step. There are typically hundreds of thousands to millions of grid cells and thousands to hundreds of thousands of time steps. In addition, FDS computes at solid surfaces the temperature, heat flux, mass loss rate, and various other quantities. The user must carefully select what data to save, much like one would do in designing an actual experiment. Even though only a small fraction of the computed information can be saved, the output typically consists of fairly large data files. Typical output quantities for the gas phase include:

- Gas temperature

Chapter II: FDS software presentation

- Gas velocity
- Gas species concentration (water vapor, CO₂, CO, N₂)
- Smoke concentration and visibility estimates
- Pressure
- Heat release rate per unit volume
- Mixture fraction (or air/fuel ratio)
- Gas density
- Water droplet mass per unit volume

On solid surfaces, FDS predicts additional quantities associated with the energy balance between gas and solid phase, including

- Surface and interior temperature
- Heat flux, both radiative and convective
- Burning rate
- Water droplet mass per unit area

Global quantities recorded by the program include:

- Total Heat Release Rate (HRR)
- Sprinkler and detector activation times
- Mass and energy fluxes through openings or solids

Time histories of various quantities at a single point in space or global quantities like the fire's heat release rate (HRR) are saved in simple, comma-delimited text files that can be plotted using a spreadsheet program.

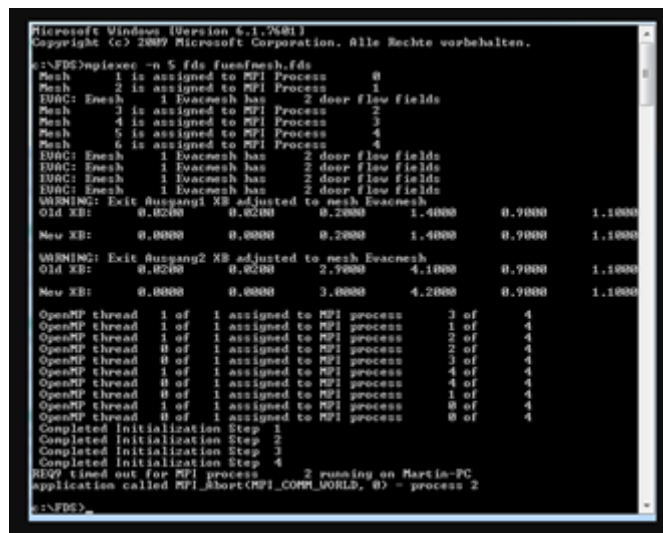
Chapter II: FDS software presentation

However, most field or surface data are visualized with Smokeview. FDS and Smokeview are used in concert to model and visualize fire phenomena. Smokeview performs this visualization by presenting animated tracer particle flow, animated contour slices of computed gas variables and animated surface data. Smokeview also presents contours and vector plots of static data anywhere within a scene at a fixed time.

II.3- Running FDS

The primary requirement for any calculation is an FDS input file. You start with an existing data file, run it as is, and then make the appropriate changes to the input file for the desired scenario. Sample input files are included as part of the standard installation.

II.3.1- Starting an FDS Calculation



```
Microsoft Windows [Version 6.1.7601]
Copyright (c) 2009 Microsoft Corporation. Alle Rechte vorbehalten.

c:\FDS>mpifexec -n 5 fds fuemfmesh.fds
Mesh 1 is assigned to MPI Process 0
Mesh 2 is assigned to MPI Process 1
EJRC: Emesh 1 Evmesh has 2 door flow fields
Mesh 3 is assigned to MPI Process 2
Mesh 4 is assigned to MPI Process 3
Mesh 5 is assigned to MPI Process 4
Mesh 6 is assigned to MPI Process 4
EJRC: Emesh 1 Evmesh has 2 door flow fields
EJRC: Emesh 1 Evmesh has 2 door flow fields
EJRC: Emesh 1 Evmesh has 2 door flow fields
EJRC: Emesh 1 Evmesh has 2 door flow fields
WARNING: Exit fuzgang1 XB adjusted to mesh Evmesh
Old XB: 0.0200 0.0200 0.2000 1.4000 0.9000 1.1000
New XB: 0.0000 0.0000 0.2000 1.4000 0.9000 1.1000
WARNING: Exit fuzgang2 XB adjusted to mesh Evmesh
Old XB: 0.0200 0.0200 2.9000 4.1000 0.9000 1.1000
New XB: 0.0000 0.0000 3.0000 4.2000 0.9000 1.1000
OpenMP thread 1 of 1 assigned to MPI process 3 of 4
OpenMP thread 1 of 1 assigned to MPI process 1 of 4
OpenMP thread 1 of 1 assigned to MPI process 2 of 4
OpenMP thread 0 of 1 assigned to MPI process 2 of 4
OpenMP thread 0 of 1 assigned to MPI process 3 of 4
OpenMP thread 1 of 1 assigned to MPI process 4 of 4
OpenMP thread 0 of 1 assigned to MPI process 4 of 4
OpenMP thread 0 of 1 assigned to MPI process 1 of 4
OpenMP thread 1 of 1 assigned to MPI process 0 of 4
OpenMP thread 0 of 1 assigned to MPI process 0 of 4
Completed Initialization Step 1
Completed Initialization Step 2
Completed Initialization Step 3
Completed Initialization Step 4
BSP timed out for MPI process 2 running on Martin-PC
application called MPI_Abort(MPI_COMM_WORLD, 0) - process 2

c:\FDS>
```

Figure II.3: FDS Output calculations made by fds5

It is assumed that FDS is being run from the command prompt. It can be run on a single computer, using only one CPU, or it can be run on multiple computers and use multiple CPUs. For any operating system, there are two FDS executable files. The single CPU Windows executable is called `fds5.exe`. The parallel executable is called `fds5_mpi.exe`. The letters “mpi” in the filename denote Message Passing Interface

Note that the input files for both single and parallel versions of FDS are the same. In fact, it is recommended that before embarking on parallel processing, one should run one’s input file in serial mode to ensure that it is properly set up.

Chapter II: FDS software presentation

II.4- Governing Equations and Numerics

This section introduces the basic conservation equations for mass, momentum and energy for a Newtonian fluid. Note that this is a set of partial differential equations consisting of six equations for six unknowns, all functions of three spatial dimensions and time: the density ρ , the three components of velocity $\mathbf{u} = [u;v;w]^T$, the temperature T , and the pressure

II.4.1- Mass and Species Transport

Mass conservation can be expressed either in terms of the density, ρ ,

$$\frac{\partial \rho}{\partial t} + \nabla \cdot \rho \mathbf{u} = \dot{m}_b^m \quad (\text{II.1})$$

or in terms of the individual gaseous species, Y_α :

$$\frac{\partial}{\partial t} \rho Y_\alpha + \nabla \cdot \rho Y_\alpha \mathbf{u} = \nabla \cdot \rho D_\alpha \nabla Y_\alpha + \dot{m}_\alpha^m + \dot{m}_{b,\alpha}^m \quad (\text{II.2})$$

$\dot{m}_b^m = \sum_\alpha \dot{m}_{b,\alpha}^m$: production rate of species by evaporating droplets or particles. Summing these equations over all species yields the original mass conservation equation because $\sum Y_\alpha = 1$ and $\sum \dot{m}_\alpha^m = 0$ and $\sum \dot{m}_{b,\alpha}^m = \dot{m}_b^m$, by definition, and because it is assumed that $\sum \rho D_\alpha \nabla Y_\alpha = 0$. This last assertion is not true, in general. However, transport equations are solved for total mass and all but one of the species, implying that the diffusion coefficient of the implicit species is chosen so that the sum of all the diffusive fluxes is zero.

II.4.2- Momentum Transport

The momentum equation in conservative form is written:

$$\frac{\partial}{\partial t} (\rho \mathbf{u}) + \nabla \cdot \rho \mathbf{u} \mathbf{u} + \nabla p = \rho \mathbf{g} + \mathbf{f}_b + \nabla \cdot \boldsymbol{\delta}_{ij} \quad (\text{II.3})$$

$\mathbf{u}\mathbf{u}$: dyadic tensor. In matrix notation, with $\mathbf{u} = [u,v,w]^T$, the dyadic is given by the tensor product of the vectors \mathbf{u} and \mathbf{u}^T .

$\nabla \cdot \rho \mathbf{u}\mathbf{u}$: vector formed by applying the vector operator $\nabla = \left(\frac{\partial}{\partial x}, \frac{\partial}{\partial y}, \frac{\partial}{\partial z} \right)$ to the tensor.

The force term \mathbf{f}_b in the momentum equation represents external forces such as the drag exerted by liquid droplets. The stress tensor τ_{ij} is defined:

Chapter II: FDS software presentation

$$\tau_{ij} = \mu \left(2 S_{ij} - \frac{2}{3} \delta_{ij} (\nabla \cdot \mathbf{u}) \right) \quad ; \quad \delta_{ij} = \begin{cases} 1 & i = j \\ 0 & i \neq j \end{cases} \quad ; \quad S_{ij} = \frac{1}{2} \left(\frac{\partial u_i}{\partial x_j} + \frac{\partial u_j}{\partial x_i} \right) \quad i, j = 1, 2, 3 \quad (\text{II.4})$$

S_{ij} : symmetric rate-of-strain tensor, written using conventional tensor notation.

μ : dynamic viscosity of the fluid.

The overall computation can either be treated as a Direct Numerical Simulation (DNS), in which the dissipative terms are computed directly, or as a Large Eddy Simulation (LES), in which the large-scale eddies are computed directly and the subgrid-scale dissipative processes are modeled. The numerical algorithm is designed so that LES becomes DNS as the grid is refined. Most applications of FDS are LES. For example, in simulating the flow of smoke through a large, multi-room enclosure, it is not possible to resolve the combustion and transport processes directly. However, for small-scale combustion experiments, it is possible to compute the transport and combustion processes directly.

For the purpose of outlining the solution procedure below, it is sufficient to consider the momentum equation written as:

$$\frac{\partial \mathbf{u}}{\partial t} + \mathbf{F} + \nabla \cdot \mathbf{H} = 0 \quad (\text{II.5})$$

and the pressure equation as

$$\nabla^2 H = - \frac{\partial}{\partial t} (\nabla \cdot \mathbf{u}) - \nabla \cdot \mathbf{F} \quad (\text{II.6})$$

which is obtained by taking the divergence of the momentum equation.

II.4.3- Energy Transport

The energy conservation equation is written in terms of the sensible enthalpy, h_s :

$$\frac{\partial}{\partial t} (\rho h_s) + \nabla \cdot \rho h_s \mathbf{u} = \frac{Dp}{Dt} \dot{q}^m + \dot{q}_b^m - \nabla \cdot \dot{q}'' + \varepsilon \quad (\text{II.7})$$

The sensible enthalpy is a function of the temperature:

$$h_s = \sum_{\alpha} Y_{\alpha} h_{s,\alpha} \quad ; \quad h_{s,\alpha}(T) = \int_{T_0}^T c_{p,\alpha}(T') dT' \quad (\text{II.8})$$

Chapter II: FDS software presentation

Note the use of the material derivative, $D(\cdot)/Dt = \partial(\cdot)/\partial t + \mathbf{u} \cdot \nabla(\cdot)$. The term \dot{q}''' is the heat release rate per unit volume from a chemical reaction. The term \dot{q}_b'''' is the energy transferred to the evaporating droplets.

\dot{q}'' : conductive and radiative heat fluxes:

$$\dot{q}'' = -k \nabla T - \sum h_{s,a} \rho D_\alpha \nabla Y_\alpha + \dot{q}_r'''' \quad (\text{II.9})$$

k: thermal conductivity.

II.4.4- Equation of State

$$p = \frac{\rho R T}{\bar{W}} \quad (\text{II.10})$$

An approximate form of the Navier-Stokes [56] equations appropriate for low Mach number applications is used in the model. The approximation involves the filtering out of acoustic waves while allowing for large variations in temperature and density. This gives the equations an elliptic character, consistent with low speed, thermal convective processes. In practice, this means that the spatially resolved pressure, $p(x,y,z)$, is replaced by an “average” or “background” pressure, $\bar{p}_m(z; t)$, that is only a function of time and height above the ground.

$$\bar{p}_m(z, t) = \rho T R \sum_\alpha Y_\alpha / W_\alpha \quad (\text{II.11})$$

Taking the material derivative of the background pressure and substituting the result into the energy conservation equation yields an expression for the velocity divergence, $\nabla \cdot \mathbf{u}$, that is an important term in the numerical algorithm because it effectively eliminates the need to solve a transport equation for the specific enthalpy. The source terms from the energy conservation equation are incorporated into the divergence, which appears in the mass transport equations. The temperature is found from the density and background pressure via the equation of state.

II.5- Large Eddy Simulation (LES)

Large eddy simulations (LES) was introduced by Smagorinsky, in the early 1970s, and it has become one of the most promising and successful methodology for simulating turbulent flows with the improvement of computing power, (LES) have advanced considerably, and their application is transitioning from the academic environment to industry. Therefore, it is now in

Chapter II: FDS software presentation

widespread use in the academic community and is an option available in most commercial flow-solvers and feasible to simulate complex engineering flows using LES. However, apart from the computing power, significant challenges still remain for LES to reach a level of maturity that brings this approach to the mainstream of engineering and industrial computations.

Almost all practical engineering and the vast majority of naturally occurring flows are turbulent and hence the focus of research in computational fluid dynamics (CFD) is devoted to flows in which turbulence plays a dominant role. Although the exact physical nature of turbulence has not been fully understood, it can be modelled to a sufficient degree of accuracy in numerical simulations.

Statistical theories of turbulence have provided understanding of the scaling laws in various flow regimes, and experiments have given insights on the statistics and structure of turbulent flows. A significant contribution to this progress is the development of numerical solution techniques for turbulent flows, in which the dynamics of some or all of the turbulent eddies are captured by the simulation. We shall refer to them as ‘eddy-resolving’ methods; they include direct numerical simulations (DNS), which is very expensive computationally and at present it can be applied only to low Reynolds number flows over simple geometry, and large eddy simulations (LES). While in DNS, all the turbulent motions are resolved accurately (i.e. the grid is finer than the smallest turbulent eddy), in LES only the contribution of the large, energy-carrying structures to momentum and energy transfer is computed exactly, and the effect of the small scales of turbulence is modelled.

Eddy-resolving techniques have made available data that had never been measurable previously: multi-point, unobtrusive measurements of velocity, velocity gradients, pressure, passive scalars, etc. Databases obtained from simulations have provided new insights on the physics of turbulent flows. As prediction and control of turbulence becomes increasingly important, the need for accurate models has become more critical, and eddy-resolving simulations are used to make inroads into these problems.

LES is more accurate than the RANS approach since the large eddies contain most of the turbulent energy and are responsible for most of the momentum transfer and turbulent mixing, and LES captures these eddies in full detail directly whereas they are modelled in the RANS

Chapter II: FDS software presentation

approach. Furthermore the small scales tend to be more isotropic and homogeneous than the large ones. Therefore, currently LES is the most viable/promising numerical tool for simulating realistic turbulent/transitional flows.

II.6- Conclusion

Since the 1960s researches have obtained great advances in the field of LES with demonstration of its capabilities in calculations of complex turbulent flows and its superiority over RANS in numerous cases. Nowadays, thanks to the rapid progress of information analysis systems and various simulation codes, LES has become a very powerful and popular tool in simulating turbulent flow, and has been widely used for not only turbulent flow analysis but also for combustion, aeroacoustics and many other areas. It has also been demonstrated that it is feasible to perform LES of complex engineering flows such as a realistic full annular gas turbine combustor.

With its huge amounts of flow information included in 3D unsteady flow field, LES will be undoubtedly the main tool for engineering fluid analysis within a couple of decades since DNS will still be far too expensive. In the future, LES is likely to become used for a broader range of flow problems and for more complex problems including more multi-disciplinary applications. For the foreseeable future it is very unlikely that LES will replace RANS completely and become a design tool used by design engineers without extensive years of LES experiences.

Chapter III:

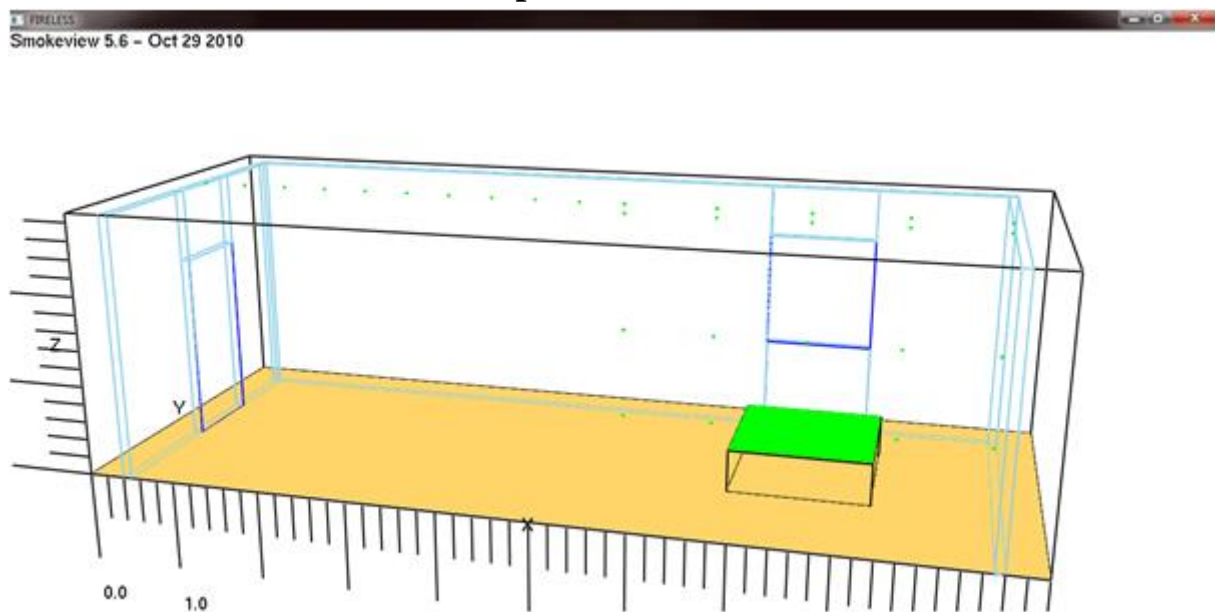
Calculation, results and discussions

Chapter III: Calculation, results and discussions

III.1- Introduction

We saw in the previous chapter, the tool for numerical calculation of fire dynamics FDS, and its conformity for the calculation of the fire phenomenon in various geometries. The aim of this chapter is to illustrate the numerical approach to estimate the temperature varying vertically and then radially in an enclosed space, taking into consideration the different correlations of Heskestad and Alpert. Therefore, this chapter is made up of six parts. In the first part, we are interested in calculating the height of the flame as well as that of the three regions of the plume. The second part of this chapter is devoted to the calculation of the radius of the plume at the ceiling. The third part, dedicated for the calculations of the temperature variation along the vertical axis and then along the horizontal axis on the ceiling. The fourth and fifth parts, in which we will focus on the temperature variation in the turning region zone of the smoke. Finally the last part of this chapter is dedicated to making histograms which summarize all the results we have had.

III.2- Calculations over the fire plume



FigureIII.1: Geometry of the compartment

Our calculation and simulation parts of the study take in consideration a compartment which is a set of a room plus an external fictitious domain which lets the fume evacuating outwards the room. The room consists of a door, a window and the fire pool such as, the door is opposite to the fire pool through the x axis and the window is opposite to the fire pool through the y axis. We are going to use the following data taken form “Fortran” to calculate the

Chapter III: Calculation, results and discussions

variation of the temperature vertically and radially. Here we have the parameters of the flame and the air that we need in our work:

$T_{amb} = 298.15K$; $g = 9.81m/s^2$; $c_{pair} = 1000 J.kg^{-1}.K^{-1}$; $\rho_{amb} = 1.184727 kg.m^{-3}$; radiative loss rate = 20% - 40% (we take in our work 25%).

$H_{pool} = 0.5m$; $H_{ceiling} = 2.90m$; the fire pool is a square having an edge of $a = 1.5m$ so $A_{fire} = 1.5*1.5 = 2.25m^2$; $D_{fire} = 1.692998m$; $Q^* = 0.2727987$ and $R_{fire} = 0.846499m$; $\dot{Q} = 1125kW$ [26]; $t = 15min$ [26].

We aim to make approximate calculations on the temperature of the plume fire over the flame source (pool fire). For the geometry of the unconfined fire plume see figure I.1 by scrolling to the very top of the first chapter

According to All_Correlations [1] data:

- Persistent flame zone is:

$$0.03*\dot{Q}^{2/5} < z < 0.08*\dot{Q}^{2/5} \quad (III.1)$$

→ $0.498m < z < 1.329m$

- Intermittent flame zone is:

$$0.08*\dot{Q}^{2/5} < z < 0.2*\dot{Q}^{2/5} \quad (III.2)$$

→ $1.329m < z < 3.32m$

- Buoyant flame zone is:

$$0.20*\dot{Q}^{2/5} < z \quad (III.3)$$

→ $3.32m < z$

- Flame average height:

$$l = 0.235*\dot{Q}^{2/5} - 1.02*D \quad (III.4)$$

→ $l = 2.1773m$

- Punctual source height (virtual height):

$$z_0 = 0.083*\dot{Q}^{2/5} - 1.02*D \quad (III.5)$$

→ $z_0 = -0.3479378m$

$$Q_{conv} = (1-radloss)*\dot{Q} \quad [1]$$

$$0.2 < radloss < 0.4 \rightarrow -0.4 < -radloss < -0.2 \rightarrow 0.6 < 1-radloss < 0.8 \rightarrow 675 < (1-radloss)*\dot{Q} < 900 \rightarrow 675 kW < Q_{conv} < 900 kW$$

If radloss is equal to:

- $0.20 \rightarrow Q_{conv} = 900kW$

- $0.25 \rightarrow Q_{conv} = 843.75kW$

- $0.30 \rightarrow Q_{conv} = 787.50kW$

- $0.35 \rightarrow Q_{conv} = 731.25kW$

- $0.40 \rightarrow Q_{conv} = 675kW$

Chapter III: Calculation, results and discussions

III.2.1- Ideal Plume (model 1) [13]

- 1- Plume radius: (with $\alpha = 0.15$)

$$b(z) = \frac{6}{5} * \alpha * z \quad (III.6)$$

We have: $0 < z < 3.32 \rightarrow b(0) = 0$ and $b(3.32) = 0.5976$ m, then $0 < b(z) < 0.5976$

- 2- Plume temperature rise: $\Delta T_{ax}(z) = 5.0 * [T_{amb}/(g * c_p^2 * \rho_{amb}^2)]^{1/3} * \dot{Q}^{2/3} * z^{-5/3} \rightarrow \Delta T_{ax}(z) = 15.07 * z^{-5/3}$

III.2.2- Heskestad model (model 2) [13]

- 1- Plume radius:

$$b(z) = 0.12 * (T_0/T_{amb})^{1/2} * (z-z_0) \quad (III.7)$$

$$T_0 = \Delta T(0) + T_{amb} = 131.6035 + 298 = 429.6035K.$$

In our work, we take z between -0.3479378m and 3.32m then:

$$-0.3479378 < z < 3.32 \rightarrow 0 < z-z_0 < 3.6679378 \rightarrow 0 < (T_0/T_{amb})^{1/2} * (z-z_0) < 4.4040 \rightarrow 0 < 0.12 * (T_0/T_{amb})^{1/2} * (z-z_0) < 0.5285 \rightarrow 0 < b(z) < 0.5285m \text{ (with radloss} = 25\%)$$

- 2- Axial temperature:

$$T_{ax} = \Delta T(z) + T_{amb} \quad ;$$

$$\Delta T_{ax}(z) = 9.1 * [T_{amb}/(g * c_p^2 * \rho_{amb}^2)]^{1/3} * \dot{Q}_c^{2/3} * (z-z_0)^{-5/3} \quad (III.8)$$

$$\Delta T_{ax}(z) = 22.64 * (z+0.3479378)^{-5/3}$$

- 3- Radial temperature:

$$\Delta T(r, z) = \Delta T_{ax}(z) e^{[-(1.2r)^2/b^2]} \quad (III.9)$$

III.2.3- McCaffrey (model 3) [25]

- 1- Axial temperature:

$$\Delta T_{ax}(z) = [K/(0.9 * \sqrt{(2 * g)})]^2 * (z/\dot{Q}^{2/5})^{2\eta-1} * T_{amb} \quad (III.10)$$

- a- Continuous region:

$$z/\dot{Q}^{2/5} < 0.08 ; \eta = 1/2 ; K = 6.8 \rightarrow (z/\dot{Q}^{2/5})^{2\eta-1} < 1 \rightarrow [K/(0.9 * \sqrt{(2 * g)})]^2 * (z/\dot{Q}^{2/5})^{2\eta-1} < 2.91 \rightarrow [K/(0.9 * \sqrt{(2 * g)})]^2 * (z/\dot{Q}^{2/5})^{2\eta-1} * T_{amb} < 857$$

$$\rightarrow [K/(0.9 * \sqrt{(2 * g)})]^2 * (z/\dot{Q}^{2/5})^{2\eta-1} * T_{amb} < 857$$

Therefore, $\Delta T_{ax}(z) < 857$ K

- b- Intermittent region:

$$0.08 < z/\dot{Q}^{2/5} < 0.2 ; \eta = 0 ; K = 1.9 \rightarrow 5 < (z/\dot{Q}^{2/5})^{2\eta-1} < 12.5 \rightarrow 335$$

$$< [K/(0.9 * \sqrt{(2 * g)})]^2 * z^{2\eta-1} * T_{amb} < 857$$

As a result, 335 K $< \Delta T_{ax}(z) < 857$ K

- c- Plume region:

$$0.2 < z/\dot{Q}^{2/5} ; \eta = -1/3 ; K = 1.1 \rightarrow (z/\dot{Q}^{2/5})^{2\eta-1} < 14.62$$

$$\rightarrow [K/(0.9 * \sqrt{(2 * g)})]^2 * z^{2\eta-1} * T_{amb} < 335$$

Hence, $\Delta T_{ax}(z) < 335$ K

Chapter III: Calculation, results and discussions

Note: the second model (Heskestad) is the only model with which the equation of the radial temperature exists

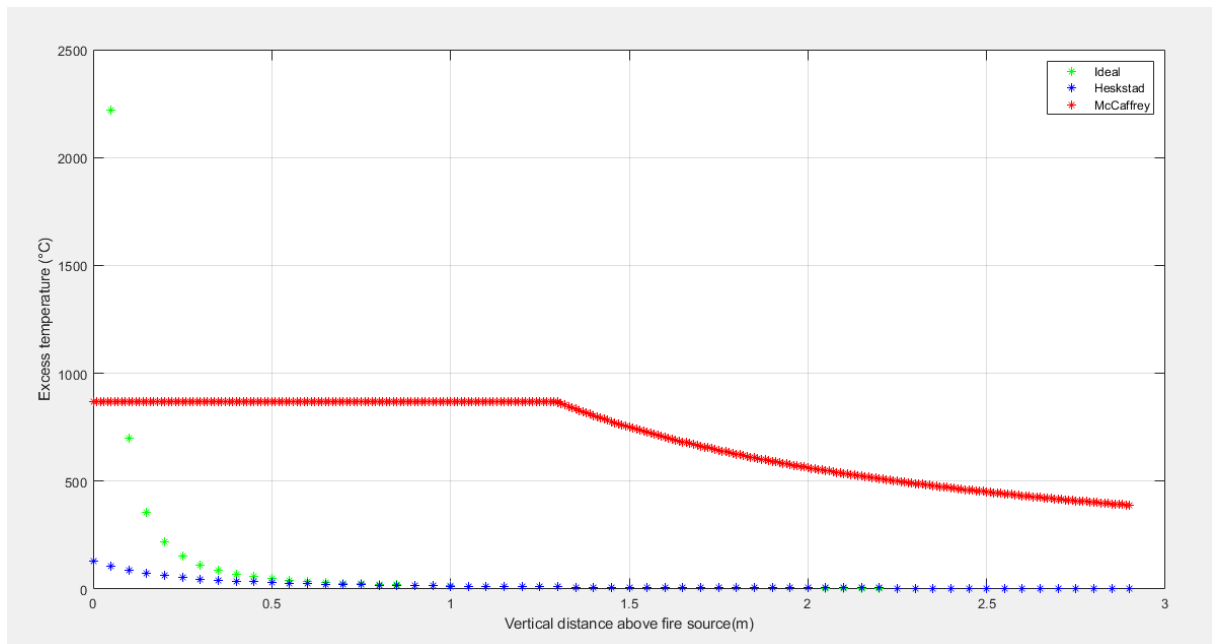


Figure III.2: Axial diminution of the temperature as a function of the plume

The higher we go, the less the excess of the temperature becomes, and that happens in the three models, but its variation range differs from one model to the other such as:

- In the ideal model it decreases from a high value of the excess of the temperature until it starts tending to zero at $z \approx 1\text{m}$
- In the Heskestad model it starts with an excess of the temperature ΔT being equal to 131.5K then it keeps decreasing until it starts tending to zero at $z \approx 1.5\text{m}$
- In the McCaffrey model the excess of the temperature ΔT remains constant and being equal to 857K from $z = 0$ to around $z = 1.3\text{m}$ then it starts decreasing until $\Delta T = 335\text{K}$ at $z = 2.9\text{m}$ (at the ceiling)

III.2.4- Plume radius in the ceiling: $z=2.9\text{m}$

- 1- **Heskestad model**[13]: $b(z) = 0.12 * (T_0/T_{\text{amb}})^{1/2} * (z-z_0)$, such as : $T_0 = \Delta T_{\text{ax}}(0) + T_{\text{amb}}$
 $\Delta T_{\text{ax}}(z) = 9.1 * [T_{\text{amb}} / (g * c_p^2 * \rho_{\text{amb}}^2)]^{1/3} * \dot{Q}_c^{2/3} * (z-z_0)^{-5/3}$
 - If $z_0 = -0.3479378\text{m}$:
 - a- **Radloss = 0** $\rightarrow T_0 = 159.3982 + 298.15 = 457.5482\text{K}$ and $b(z = 2.9) = 0.12 * (457.5482/298.15)^{1/2} * (2.9 + 0.3479378) = \mathbf{0.4828\text{m}}$
 - b- **Radloss = 0.20** $\rightarrow T_0 = 137.3894 + 298.15 = 435.5394\text{K}$ and $b(z = 2.9) = 0.12 * (435.5394/298.15)^{1/2} * (2.9 + 0.3479378) = \mathbf{0.4711\text{m}}$

Chapter III: Calculation, results and discussions

c- **Radloss = 0.30** → $T_0 = 125.6875 + 298.15 = 423.8375\text{K}$ and $b(z = 2.9) = 0.12 * (423.8375/298.15)^{1/2} * (2.9 + 0.3479378) = \mathbf{0.4647\text{m}}$

d- **Radloss = 0.40** → $T_0 = 113.4125 + 298.15 = 411.5625\text{K}$ and $b(z = 2.9) = 0.12 * (411.5625/298.15)^{1/2} * (2.9 + 0.3479378) = \mathbf{0.4579\text{m}}$

2- **Ideal model** : $b(z) = (6/5) * \alpha * z \rightarrow b(2.9) = 3.48 * \alpha$

A	0.10	0.15	0.20	0.25	0.30	0.35
b (z=2.9) (m)	0.348	0.522	0.696	0.870	1.044	1.218

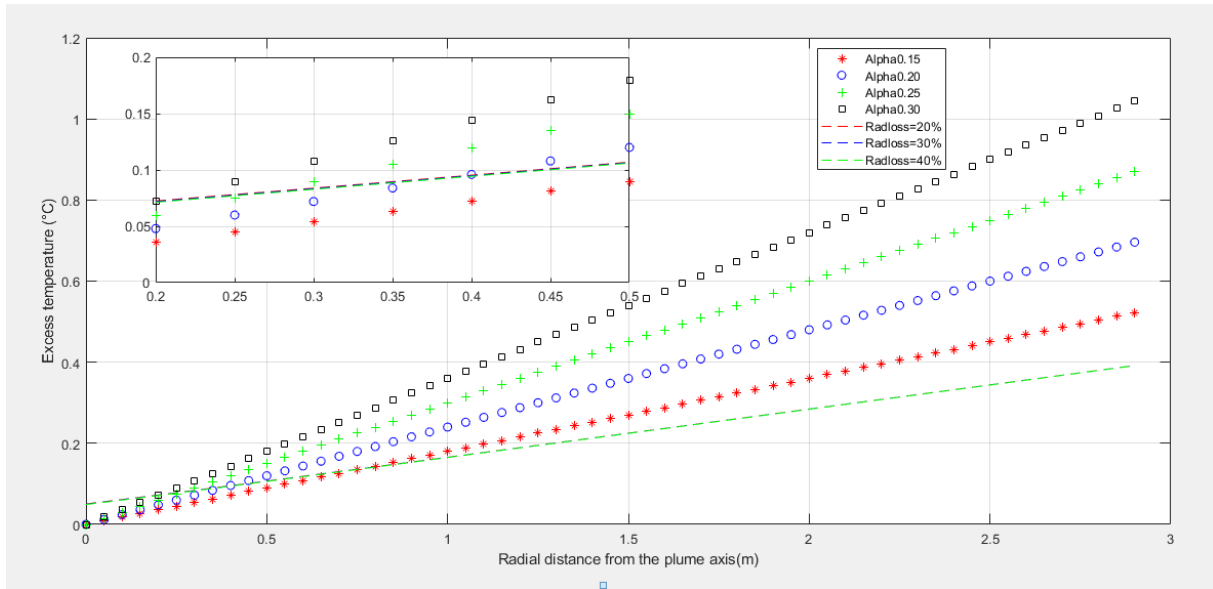


Figure III.3: Plume radius in both cases as a function of the vertical distance above fire source

Table III.1: plume radius b(z) with the ideal and Heskestad models

Z	Plume radius b(z) (m)									
	Heskestad					Ideal				
	Radloss = 0.20	Radloss = 0.25	Radloss = 0.30	Radloss = 0.35	Radloss = 0.40	$\alpha = 0.10$	$\alpha = 0.20$	$\alpha = 0.25$	$\alpha = 0.30$	$\alpha = 0.35$
0	0.0505	0.0501	0.0498	0.0494	0.0491	0	0	0	0	0
0.0500	0.0535	0.0532	0.0529	0.0525	0.0522	0.0060	0.0120	0.0150	0.0180	0.0210
0.1000	0.0566	0.0563	0.0560	0.0557	0.0553	0.0120	0.0240	0.0300	0.0360	0.0420
0.1500	0.0598	0.0595	0.0592	0.0588	0.0585	0.0180	0.0360	0.0450	0.0540	0.0630
0.2000	0.0629	0.0626	0.0623	0.0620	0.0617	0.0240	0.0480	0.0600	0.0720	0.0840
0.2500	0.0661	0.0658	0.0655	0.0652	0.0649	0.0300	0.0600	0.0750	0.0900	0.1050
0.3000	0.0693	0.0690	0.0687	0.0684	0.0681	0.0360	0.0720	0.0900	0.1080	0.1260
0.3500	0.0725	0.0722	0.0720	0.0717	0.0714	0.0420	0.0840	0.1050	0.1260	0.1470
0.4000	0.0757	0.0755	0.0752	0.0749	0.0746	0.0480	0.0960	0.1200	0.1440	0.1680
0.4500	0.0790	0.0787	0.0785	0.0782	0.0779	0.0540	0.1080	0.1350	0.1620	0.1890
0.5000	0.0822	0.0820	0.0817	0.0815	0.0812	0.0600	0.1200	0.1500	0.1800	0.2100
0.5500	0.0855	0.0853	0.0850	0.0847	0.0845	0.0660	0.1320	0.1650	0.1980	0.2310
0.6000	0.0888	0.0885	0.0883	0.0880	0.0878	0.0720	0.1440	0.1800	0.2160	0.2520
0.6500	0.0921	0.0918	0.0916	0.0913	0.0911	0.0780	0.1560	0.1950	0.2340	0.2730

Chapter III: Calculation, results and discussions

0.7000	0.0954	0.0951	0.0949	0.0947	0.0944	0.0840	0.1680	0.2100	0.2520	0.2940
0.7500	0.0987	0.0984	0.0982	0.0980	0.0977	0.0900	0.1800	0.2250	0.2700	0.3150
0.8000	0.1020	0.1017	0.1015	0.1013	0.1010	0.0960	0.1920	0.2400	0.2880	0.3360
0.8500	0.1053	0.1051	0.1048	0.1046	0.1044	0.1020	0.2040	0.2550	0.3060	0.3570
0.9000	0.1086	0.1084	0.1082	0.1079	0.1077	0.1080	0.2160	0.2700	0.3240	0.3780
0.9500	0.1119	0.1117	0.1115	0.1113	0.1111	0.1140	0.2280	0.2850	0.3420	0.3990
1.0000	0.1152	0.1150	0.1148	0.1146	0.1144	0.1200	0.2400	0.3000	0.3600	0.4200
1.5000	0.1488	0.1486	0.1484	0.1482	0.1480	0.1800	0.3600	0.4500	0.5400	0.6300
2.0000	0.1825	0.1824	0.1822	0.1820	0.1819	0.2400	0.4800	0.6000	0.7200	0.8400
2.5000	0.2164	0.2163	0.2161	0.2160	0.2158	0.3000	0.6000	0.7500	0.9000	1.0500
2.8000	0.2368	0.2367	0.2365	0.2364	0.2363	0.3360	0.6720	0.8400	1.0080	1.1760
2.9000	0.2436	0.2435	0.2433	0.2432	0.2431	0.3480	0.6960	0.8700	1.0440	1.2180

III.3- Axial distribution of the temperature $\Delta T_{ax}(z)$

After the ignition of the flame, the fume spreads upwards, in this part we are going to calculate the temperature varying through the vertical axis with the ideal and the Heskestad model then we compare between them.

We know that the z varies from 0 to 2.9m. The following tables are shrunk to the most useful values of z because it's useless to deal with hundreds of value by taking all the values of the flame height with a step of 0.01 or 0.05m.

III.3.1- Comparison between the ideal and the Heskestad models

Table III.2: plume radius $b(z)$, excess of temperature and the tolerance of the temperature with the ideal model ($\alpha = 0.15$) and the Heskestad models ($Radloss = 0.20$)

Model	Ideal ($\alpha = 0.15$)			Heskestad ($Radloss = 0.20$)		
	$\Delta T(K)$	$\Delta T/T_{amb}$	$b(m)$	$\Delta T(K)$	$\Delta T/T_{amb}$	$b(m)$
0	2218.7	7.4453	0	137.3894	0.4610	0.0505
0.0500	698.90	2.3453	0.0090	109.8409	0.3686	0.0535
0.1000	355.50	1.1930	0.0180	90.1764	0.3026	0.0566
0.1500	220.10	0.7386	0.0270	75.5958	0.2537	0.0598
0.2000	151.80	0.5094	0.0360	64.4521	0.2163	0.0629
0.2500	112.00	0.3758	0.0450	55.7223	0.1870	0.0661
0.3000	86.600	0.2906	0.0540	48.7417	0.1636	0.0693
0.3500	69.300	0.2326	0.0630	43.0621	0.1445	0.0725
0.4000	57.000	0.1913	0.0720	38.3719	0.1288	0.0757
0.4500	47.800	0.1604	0.0810	34.4488	0.1156	0.0790
0.5000	40.800	0.1369	0.0900	31.1303	0.1045	0.0822
1.0000	13.900	0.0466	0.1800	14.3772	0.0482	0.1152
1.5000	7.3000	0.0245	0.2700	8.4979	0.0285	0.1488
2.0000	4.6000	0.0154	0.3600	5.7014	0.0191	0.1825
2.5000	3.2000	0.0107	0.4500	4.1327	0.0139	0.2164
2.5500	3.1000	0.0104	0.4599	4.0146	0.0135	0.2198
2.6000	3.0000	0.0101	0.4680	3.9017	0.0131	0.2232
2.6500	2.9000	0.0094	0.4770	3.7939	0.0127	0.2266

Chapter III: Calculation, results and discussions

2.7000	2.8000	0.0094	0.4860	3.6907	0.0124	0.2300
2.7500	2.7000	0.0091	0.4950	3.5920	0.0121	0.2334
2.8000	2.6000	0.0087	0.5040	3.4974	0.0117	0.2368
2.9000	2.6000	0.0087	0.5220	3.3198	0.0111	0.2436

We notice that the more the plume height increases, the more its radius increases and the more the difference of temperature decreases as well

- Plume radius as a function of the fire height (diagram): the two curves of both models (ideal and Heskestad) increase slightly with same manner.
The ideal model curve is a straight line passing through the origin however, the Heskestad model doesn't.
- The difference of the temperature as a function of the fire height (diagram): between 0 and 0.5m the both curves decrease but not with the same manner (the ideal model curve decreasing is more accentuated) and its first two values of the ideal model are a little bit more exaggerated, nevertheless, the other values are all acceptable.

III.3.2- Calculating ΔT and $\Delta T/T_{amb}$ with different radlosses in the Heskestad model

Table III.3: excess of temperature and the tolerance of the temperature with different radlosses

Z	Heskestad model							
	$\Delta T(K)$ (Radloss = 0.25)	$\Delta T/T_{amb}$	$\Delta T(K)$ (Radloss = 0.30)	$\Delta T/T_{amb}$	$\Delta T(K)$ (Radloss = 0.35)	$\Delta T/T_{amb}$	$\Delta T(K)$ (Radloss = 0.40)	$\Delta T/T_{amb}$
0	131.6035	0.4416	125.6875	0.4218	119.6287	0.4014	113.4125	0.3806
0.0500	105.2151	0.3530	100.4853	0.3372	95.6415	0.3209	90.6716	0.3043
0.1000	86.3788	0.2899	82.4958	0.2768	78.5191	0.2635	74.4390	0.2498
0.1500	72.4122	0.2430	69.1570	0.2321	65.8233	0.2209	62.4029	0.2094
0.2000	61.7378	0.2072	58.9625	0.1979	56.1202	0.1883	53.2041	0.1785
0.2500	53.3757	0.1791	50.9763	0.1711	48.5190	0.1628	45.9978	0.1544
0.3000	46.2486	0.1552	44.5902	0.1496	42.4407	0.1424	40.2354	0.1350
0.3500	41.2486	0.1384	39.3943	0.1322	37.4953	0.1258	35.5469	0.1193
0.4000	36.7560	0.1233	35.1036	0.1178	33.4115	0.1121	31.6753	0.1063
0.4500	32.9981	0.1107	31.5147	0.1058	29.9955	0.1007	28.4369	0.0954
0.5000	29.8193	0.1001	28.4788	0.0956	27.1060	0.0910	25.6975	0.0862
1.0000	13.7717	0.0462	13.1526	0.0441	12.5186	0.0420	11.8681	0.0398
1.5000	8.1400	0.0273	7.7741	0.0261	7.3993	0.0248	7.0148	0.0235
2.0000	5.4613	0.0183	5.2158	0.0175	4.9643	0.0167	4.7064	0.0158
2.5000	3.9587	0.0133	3.7807	0.0127	3.5985	0.0121	3.4115	0.0114
2.5500	3.8455	0.0129	3.6727	0.0123	3.4956	0.0117	3.3140	0.0111
2.6000	3.7374	0.0125	3.5694	0.0120	3.3974	0.0114	3.2208	0.0108

Chapter III: Calculation, results and discussions

2.6500	3.6341	0.0122	3.4708	0.0116	3.3034	0.0111	3.1318	0.0105
2.7000	3.5353	0.0119	3.3764	0.0113	3.2136	0.0108	3.0466	0.0102
2.7500	3.4407	0.0115	3.2860	0.0110	3.1276	0.0105	2.9651	0.0100
2.8000	3.3501	0.0112	3.1995	0.0107	3.0453	0.0102	2.8870	0.0097
2.9000	3.1800	0.0107	3.0370	0.0102	2.8906	0.0097	2.7404	0.0092

- 1- The height of the cool zone Z_{cz} from which $\Delta T / T_{\infty} < 1\%$ (ideal model, $\alpha = 0.15$) is: $Z_{cz} = 2.65\text{m}$ where $\Delta T / T_{\infty} = 0.0094$ (0.94%) and $\Delta T = 2.9000\text{K}$
- 2- The height of the cool zone Z_{cz} from which $\Delta T / T_{\infty} < 1.2\%$ (Heskestad model, $\text{Radloss} = 0.20$) is: $Z_{cz} = 2.8\text{m}$ where $\Delta T / T_{\infty} = 0.0117$ (1.17%) and $\Delta T = 3.4974\text{K}$
- 3-

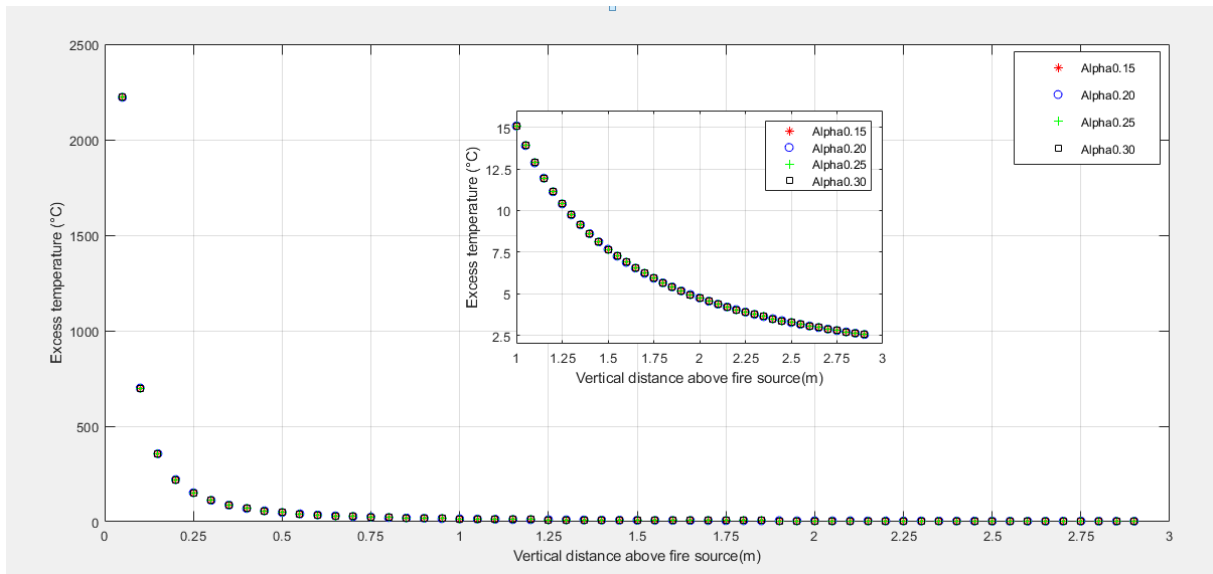


Figure III.4: Diagram of the excess of temperature as a function of the vertical distance above fire in the ideal model

Chapter III: Calculation, results and discussions

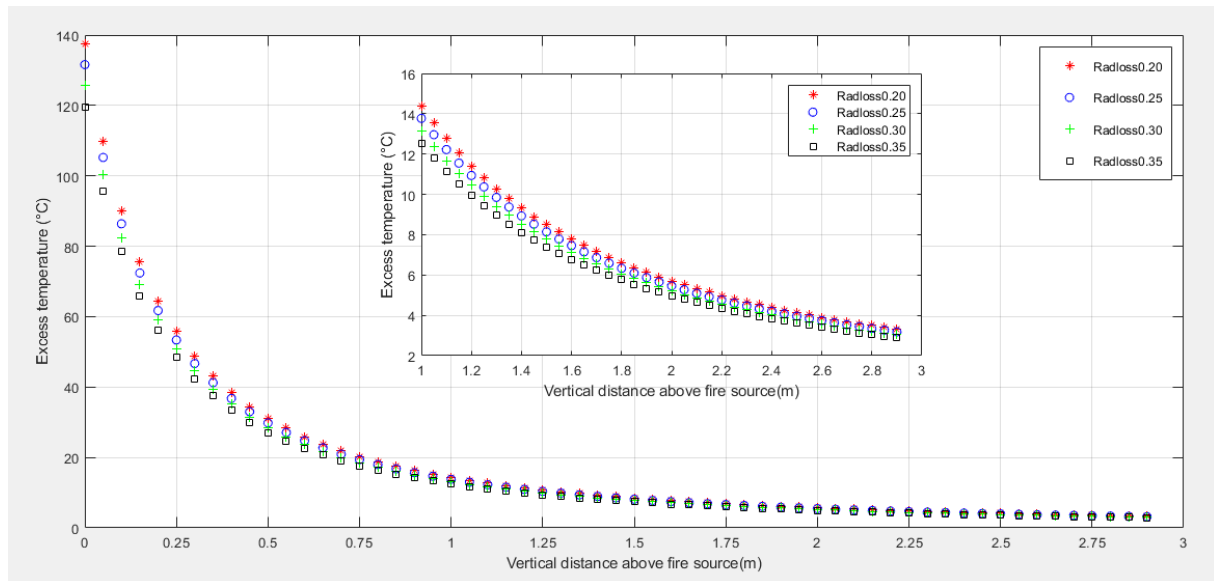


Figure III.5: Diagram of the excess of temperature as a function of the vertical distance above fire in the Heskestad model

From these graphs (of the excess of the temperature) we can deduct roughly that the intersections between the ideal and the Heskestad curves start from a vertical distance close to 1m until 2.9m

In terms of accuracy, calculations of relative error between ΔT of the ideal model and one of the Heskestad model were done and only the closest values with which the tolerance (relative error) is less than 1% were held.

Note:

The ideal model doesn't vary as a function of α , so with any value of α there is always one curve. Therefore, we can say that the ideal model intersects hardly with the Heskestad model in these cases:

- 1- $\alpha = 0.15$ (or other than 0.15) with Radloss = 0.20 when $z = 0.90\text{m}$
- 2- $\alpha = 0.15$ (or other than 0.15) with Radloss = 0.25 when $z = 1\text{m}$
- 3- $\alpha = 0.15$ (or other than 0.15) with Radloss = 0.30 when $z = 1.15\text{m} \ \& \ 1.20\text{m}$
- 4- $\alpha = 0.15$ (or other than 0.15) with Radloss = 0.35 when $z = 1.35\text{m} \text{---} 1.45\text{m}$
- 5- $\alpha = 0.15$ (or other than 0.15) with Radloss = 0.20 when $z = 1.65\text{m} \text{---} 1.85\text{m}$

III.4- Horizontal distribution of the temperature $\Delta T(r, z)$

After reaching the ceiling, the fume starts spreading radially which is our study in this part hence, this formula $\Delta T(r, z) = \Delta T_{ax}(z) e^{[-(1.2r)^2/b^2]}$ fits with this part of calculations

Chapter III: Calculation, results and discussions

III.4.1- Distribution of ΔT in the ideal model

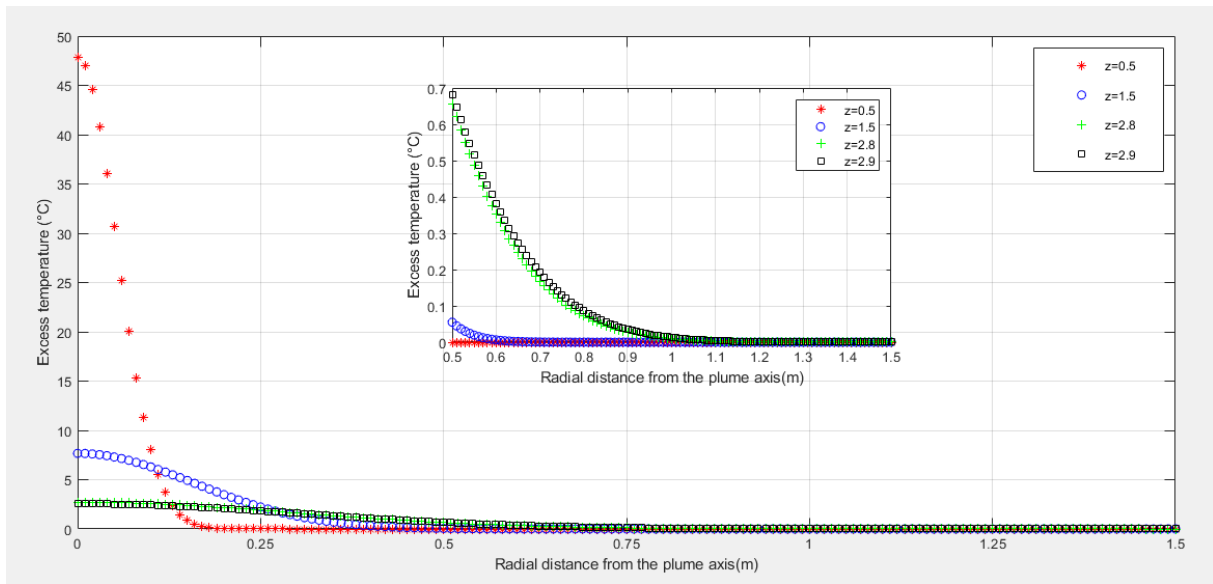


Figure III.6: Diagram of the excess of temperature as a function of the radial distance above fire in the ideal model

Chapter III: Calculation, results and discussions

III.4.1.1- calculating ΔT & $\Delta T/T_{amb}$ of the ideal model

Table III.4: excess of temperature and the tolerance of the temperature at different plume heights with the ideal model

r (m)	Z = 0.5m		Z = 1.5m		Z = 2.8m		Z = 2.9m	
	$\Delta T(K)$	$\Delta T/T_{amb}$	$\Delta T(K)$	$\Delta T/T_{amb}$	$\Delta T(K)$	$\Delta T/T_{amb}$	$\Delta T(K)$	$\Delta T/T_{amb}$
0	47.8676	0.1606	7.6708	0.0257	2.7106	0.0091	2.5566	0.0086
0.0100	47.0241	0.1578	7.6556	0.0257	2.7090	0.0091	2.5552	0.0086
0.0200	44.5819	0.1496	7.6104	0.0255	2.7044	0.0091	2.5512	0.0086
0.0300	40.7900	0.1369	7.5356	0.0253	2.6968	0.0090	2.5445	0.0085
0.0400	36.0171	0.1209	7.4321	0.0249	2.6861	0.0090	2.5351	0.0085
0.0500	30.6917	0.1030	7.3012	0.0245	2.6724	0.0090	2.5230	0.0085
0.0600	25.2402	0.0847	7.1442	0.0240	2.6558	0.0089	2.5084	0.0084
0.0700	20.0319	0.0672	6.9631	0.0234	2.6363	0.0088	2.4912	0.0084
0.0800	15.3430	0.0515	6.7598	0.0227	2.6140	0.0088	2.4716	0.0083
0.0900	11.3412	0.0381	6.5366	0.0219	2.5889	0.0087	2.4495	0.0082
0.1000	8.0903	0.0271	6.2958	0.0211	2.5612	0.0086	2.4250	0.0081
0.1100	5.5696	0.0187	6.0400	0.0203	2.5309	0.0085	2.3982	0.0080
0.1200	3.7004	0.0124	5.7717	0.0194	2.4981	0.0084	2.3693	0.0080
0.1300	2.3726	0.0080	5.4936	0.0184	2.4629	0.0083	2.3382	0.0078
0.1400	1.4681	0.0049	5.2083	0.0175	2.4255	0.0081	2.3050	0.0077
0.1500	0.8767	0.0029	4.9183	0.0165	2.3860	0.0080	2.2700	0.0076
0.1600	0.5053	0.0017	4.6262	0.0155	2.3444	0.0079	2.2331	0.0075
0.1700	0.2810	0.0009	4.3343	0.0145	2.3010	0.0077	2.1945	0.0074
0.1800	0.1508	0.0005	4.0447	0.0136	2.2558	0.0076	2.1543	0.0072
0.1900	0.0781	0.0003	3.7597	0.0126	2.2089	0.0074	2.1126	0.0071
0.2000	0.0391	0.0001	3.4809	0.0117	2.1606	0.0073	2.0695	0.0069
0.2100	0.0188	0.0001	3.2101	0.0108	2.1110	0.0071	2.0251	0.0068
0.2200	0.0088	0.0000	2.9487	0.0099	2.0602	0.0069	1.9796	0.0066
0.2300	0.0039	0.0000	2.6979	0.0091	2.0083	0.0067	1.9331	0.0065
0.2400	0.0017	0.0000	2.4587	0.0083	1.9555	0.0066	1.8857	0.0063
0.2500	0.0007	0.0000	2.2319	0.0075	1.9019	0.0064	1.8375	0.0062
0.2600	0.0003	0.0000	2.0180	0.0068	1.8477	0.0062	1.7886	0.0060
0.2700	0.0001	0.0000	1.8174	0.0061	1.7930	0.0060	1.7392	0.0058
0.2800	0.0000	0.0000	1.6303	0.0055	1.7380	0.0058	1.6894	0.0057
0.2900	0.0000	0.0000	1.4567	0.0049	1.6827	0.0056	1.6392	0.0055
0.3000	0.0000	0.0000	1.2965	0.0044	1.6274	0.0055	1.5889	0.0053

Note:

We were supposed to keep calculating until $r = 2.9m$ but in view of the uselessness of the other results we stopped on $r = 0.3m$, because all the values of $\Delta T/T_{amb}$ start being less than 1% just after the radius $r = 0.22m$.

Chapter III: Calculation, results and discussions

III.4.2- Distribution of ΔT in the Heskestad model

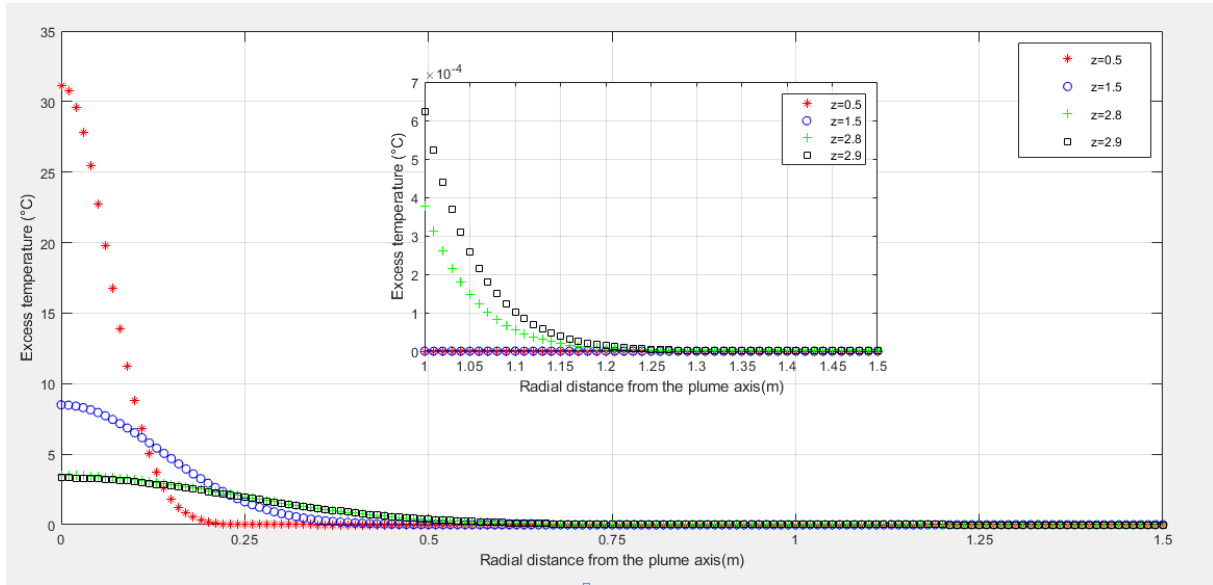


Figure III.7: Diagram of the excess of temperature as a function of the radial distance above fire in the Heskestad model

III.4.2.1- ΔT & $\Delta T/T_{amb}$ values of the Heskestad model

Table III.5: Excess of temperature and the tolerance (relative error) of the temperature at different plume heights with the Heskestad model

R	Z = 0.5m		Z = 1.5m		Z = 2.8m		Z = 2.9m	
	$\Delta T(K)$	$\Delta T/T_{amb}$	$\Delta T(K)$	$\Delta T/T_{amb}$	$\Delta T(K)$	$\Delta T/T_{amb}$	$\Delta T(K)$	$\Delta T/T_{amb}$
0	31.1303	0.1045	8.4979	0.0285	3.4974	0.0117	3.3198	0.0111
0.0100	30.7407	0.1032	8.4754	0.0284	3.4942	0.0117	3.3169	0.0111
0.0200	29.6010	0.0993	8.4082	0.0282	3.4846	0.0117	3.3084	0.0111
0.0300	27.7947	0.0933	8.2975	0.0278	3.4688	0.0116	3.2942	0.0111
0.0400	25.4495	0.0854	8.1449	0.0273	3.4466	0.0116	3.2745	0.0110
0.0500	22.7226	0.0763	7.9529	0.0267	3.4184	0.0115	3.2493	0.0109
0.0600	19.7834	0.0664	7.7243	0.0259	3.3842	0.0114	3.2188	0.0108
0.0700	16.7959	0.0564	7.4626	0.0250	3.3443	0.0112	3.1831	0.0107
0.0800	13.9049	0.0467	7.1716	0.0241	3.2988	0.0111	3.1423	0.0105
0.0900	11.2253	0.0377	6.8555	0.0230	3.2479	0.0109	3.0968	0.0104
0.1000	8.8366	0.0297	6.5187	0.0219	3.1920	0.0107	3.0467	0.0102

Chapter III: Calculation, results and discussions

0.1100	6.7833	0.0228	6.1657	0.0207	3.1314	0.0105	2.9923	0.0100
0.1200	5.0775	0.0170	5.8009	0.0195	3.0662	0.0103	2.9338	0.0098
0.1300	3.7062	0.0124	5.4289	0.0182	2.9970	0.0101	2.8715	0.0096
0.1400	2.6379	0.0089	5.0538	0.0170	2.9240	0.0098	2.8058	0.0094
0.1500	1.8309	0.0061	4.6798	0.0157	2.8475	0.0096	2.7368	0.0092
0.1600	1.2392	0.0042	4.3105	0.0145	2.7680	0.0093	2.6649	0.0089
0.1700	0.8178	0.0027	3.9494	0.0133	2.6858	0.0090	2.5905	0.0087
0.1800	0.5263	0.0018	3.5994	0.0121	2.6012	0.0087	2.5138	0.0084
0.1900	0.3303	0.0011	3.2631	0.0109	2.5148	0.0084	2.4353	0.0082
0.2000	0.2021	0.0007	2.9425	0.0099	2.4267	0.0081	2.3551	0.0079
0.2100	0.1206	0.0004	2.6394	0.0089	2.3375	0.0078	2.2737	0.0076
0.2200	0.0702	0.0002	2.3550	0.0079	2.2475	0.0075	2.1913	0.0074
0.2300	0.0398	0.0001	2.0901	0.0070	2.1569	0.0072	2.1083	0.0071
0.2400	0.0220	0.0001	1.8453	0.0062	2.0663	0.0069	2.0249	0.0068
0.2500	0.0119	0.0000	1.6204	0.0054	1.9758	0.0066	1.9415	0.0065
0.2600	0.0063	0.0000	1.4155	0.0047	1.8858	0.0063	1.8584	0.0062
0.2700	0.0032	0.0000	1.2299	0.0041	1.7967	0.0060	1.7757	0.0060
0.2800	0.0016	0.0000	1.0630	0.0036	1.7086	0.0057	1.6938	0.0057
0.2900	0.0008	0.0000	0.9139	0.0031	1.6219	0.0054	1.6130	0.0054
0.3000	0.0004	0.0000	0.7816	0.0026	1.5368	0.0052	1.5333	0.0051

Note:

We were supposed to keep calculating until $r = 2.9\text{m}$ but in view of the uselessness of the other results we stopped on $r = 0.3\text{m}$, because the values of $\Delta T/T_{\text{amb}}$ start being less than 1% just after the radius $r = 0.20\text{m}$

III.4.3- Plume radius in both models

1-

The radius of the cool zone r_{cz} from which $\Delta T/T_{\infty} < 1\%$ (ideal model $\alpha = 0.15$):

$$Z_{cz} = 2.65\text{m}, \Delta T_{ax}(2.65) = 2.9\text{K} \text{ and } b(z) = (6/5) * \alpha * z$$

Table III.6: the tolerance (relative error) of the temperature and the plume radius with the ideal model

Z (m)	$\Delta T/T_{\infty}$ (%)	r_{cz} (m)	$\Delta T(r,Z)$ (K)	b(z) (m)	$r_{cz}/b(z)$
0.5	0.80	0.1300	2.3726	0.0900	1.4444
1.5	0.99	0.2200	2.9487	0.2700	0.8148

Chapter III: Calculation, results and discussions

2.8	0.91	0.0000	2.7106	0.5040	0.0000
2.9	0.86	0.0000	2.5566	0.5220	0.0000

2-

The radius of the cool zone r_{cz} from which $\Delta T/T_{\infty} < 1\%$ (Heskestad model, Radloss = 0.20): $Z_{cz} = 2.8\text{m}$, and $\Delta T_{ax}(2.8) = 3.4974\text{K}$

TableIII.7: the tolerance (relative error) of the temperature and the plume radius with the Heskestad model

From the table of the plume radius variation vertically we have:

Z (m)	$\Delta T/T_{\infty}$ (%)	r_{cz} (m)	$\Delta T(r,Z)$ (K)	b(z) (m)	$r_{cz}/b(z)$
0.5	0.89	0.1400	2.6379	0.0822	1.703
1.5	0.99	0.2000	2.9425	0.1488	1.344
2.8	0.98	0.1400	2.9240	0.2368	0.591
2.9	0.98	0.1200	2.9338	0.2436	0.493

3-

According to the table of the plume radiuses, at a height of $z = 1.5\text{m}$, the ideal model when $\alpha = 0.20$ reproduces the same value of the radius with the Heskestad model when **Radloss = 0.20** which is equal to 0.360m ($r_{cz} = 0.360\text{m}$). Otherwise, there is no other value of α with which the ideal model reproduces the same radius value, at the same height, with the Heskestad model.

In the following tables, we are going to deal with the most important values of r where we may find the most wanted values of ΔT and $\Delta T/T_{amb}$ so we shrank them as much as we could.

TableIII.8: the tolerance (relative error) of the temperature with different values of α and radloss at $z = 0.5\text{m}$

R	$\Delta T/T_{amb}$										
	Heskestad					Ideal					
	Radloss = 0.20	Radloss = 0.25	Radloss = 0.30	Radloss = 0.35	Radloss = 0.40	$\alpha = 0.10$	$\alpha = 0.15$	$\alpha = 0.20$	$\alpha = 0.25$	$\alpha = 0.30$	$\alpha = 0.35$
0.2500	0.0000	0.0000	0.0000	0.0000	0.0000	0.0000	0.0000	0.0003	0.0029	0.0100	0.0209
0.2600	0.0000	0.0000	0.0000	0.0000	0.0000	0.0000	0.0000	0.0002	0.0021	0.0080	0.0177
0.2700	0.0000	0.0000	0.0000	0.0000	0.0000	0.0000	0.0000	0.0001	0.0015	0.0063	0.0149
0.2800	0.0000	0.0000	0.0000	0.0000	0.0000	0.0000	0.0000	0.0001	0.0011	0.0049	0.0124
0.2900	0.0000	0.0000	0.0000	0.0000	0.0000	0.0000	0.0000	0.0000	0.0007	0.0038	0.0103
0.3000	0.0000	0.0000	0.0000	0.0000	0.0000	0.0000	0.0000	0.0000	0.0005	0.0029	0.0085

From this table we notice that the ideal model reproduces the same zero values of $\Delta T/T_{amb}$ with the Heskestad model (with any of the four radlosses) starting from $r = 0.25\text{m}$ onwards (when $\alpha = 0.10$ and $\alpha = 0.15$) and from $r = 0.29\text{m}$ onwards (when $\alpha = 0.20$), nevertheless,

Chapter III: Calculation, results and discussions

there is no value of ΔT of the ideal model being equal to those of the Heskestad model (in the same cases). So we deduct that with a height of 0.5m both models don't reproduce any similar values

TableIII.9: the tolerance (relative error) of the temperature with different values of α and radloss at $z = 1.5m$

		$\Delta T/T_{amb}$									
R	Heskestad					Ideal					
	Radloss = 0.20	Radloss = 0.25	Radloss = 0.30	Radloss = 0.35	Radloss = 0.40	$\alpha = 0.10$	$\alpha = 0.15$	$\alpha = 0.20$	$\alpha = 0.25$	$\alpha = 0.30$	$\alpha = 0.35$
0.0400	0.0273	0.0261	0.0249	0.0237	0.0225	0.0240	0.0249	0.0253	0.0254	0.0255	0.0256
0.0500	0.0267	0.0254	0.0243	0.0231	0.0219	0.0230	0.0245	0.0250	0.0253	0.0254	0.0255
0.0600	0.0259	0.0247	0.0235	0.0224	0.0212	0.0219	0.0240	0.0247	0.0251	0.0253	0.0254
		ΔT									
R	Heskestad					Ideal					
	Radloss = 0.20	Radloss = 0.25	Radloss = 0.30	Radloss = 0.35	Radloss = 0.40	$\alpha = 0.10$	$\alpha = 0.15$	$\alpha = 0.20$	$\alpha = 0.25$	$\alpha = 0.30$	$\alpha = 0.35$
0.0400	8.1449	7.7771	7.4275	7.0694	6.7021	7.1442	7.4321	7.5356	7.5840	7.6104	7.6264
0.0500	7.9529	7.5801	7.2394	6.8904	6.5323	6.8641	7.3012	7.4606	7.5356	7.5767	7.6015
0.0600	7.7243	7.3461	7.0159	6.6777	6.3307	6.5366	7.1442	7.3700	7.4769	7.5356	7.5712

In this case:

- $\alpha = 0.30$ and Radloss = 0.15 reproduce the same value of $\Delta T/T_{amb}$ at $r = 0.05m$
- $\alpha = 0.30$ and Radloss = 0.25 reproduce the same value of $\Delta T/T_{amb}$ at $r = 0.05m$
- $\alpha = 0.20$ and Radloss = 0.25 reproduce the same value of $\Delta T/T_{amb}$ at $r = 0.06m$

TableIII.10: the tolerance (relative error) of the temperature with different values of α and radloss at $z = 2.8m$

		$\Delta T/T_{amb}$									
R	Heskestad					Ideal					
	Radloss = 0.20	Radloss = 0.25	Radloss = 0.30	Radloss = 0.35	Radloss = 0.40	$\alpha = 0.10$	$\alpha = 0.15$	$\alpha = 0.20$	$\alpha = 0.25$	$\alpha = 0.30$	$\alpha = 0.35$
0.0900	0.0109	0.0104	0.0099	0.0094	0.0089	0.0082	0.0087	0.0089	0.0089	0.0090	0.0090
0.1000	0.0107	0.0102	0.0097	0.0092	0.0088	0.0080	0.0086	0.0088	0.0089	0.0090	0.0090
0.1200	0.0103	0.0097	0.0093	0.0089	0.0084	0.0076	0.0084	0.0087	0.0088	0.0089	0.0090
0.1300	0.0101	0.0095	0.0091	0.0086	0.0082	0.0073	0.0083	0.0086	0.0088	0.0089	0.0089
0.1400	0.0098	0.0092	0.0088	0.0084	0.0080	0.0071	0.0081	0.0085	0.0087	0.0088	0.0089
0.1600	0.0093	0.0087	0.0083	0.0079	0.0075	0.0066	0.0079	0.0084	0.0086	0.0088	0.0089
0.1700	0.0090	0.0084	0.0080	0.0077	0.0073	0.0063	0.0077	0.0083	0.0086	0.0087	0.0088
0.1800	0.0087	0.0081	0.0078	0.0074	0.0070	0.0060	0.0076	0.0082	0.0085	0.0087	0.0088
0.1900	0.0084	0.0078	0.0075	0.0071	0.0068	0.0057	0.0074	0.0081	0.0084	0.0086	0.0088
0.2200	0.0075	0.0069	0.0066	0.0063	0.0060	0.0049	0.0069	0.0078	0.0082	0.0085	0.0086
0.2700	0.0060	0.0054	0.0052	0.0049	0.0047	0.0036	0.0060	0.0072	0.0078	0.0082	0.0084
		$\Delta T(K)$									
R	Heskestad					Ideal					

Chapter III: Calculation, results and discussions

	Radloss = 0.20	Radloss = 0.25	Radloss = 0.30	Radloss = 0.35	Radloss = 0.40	$\alpha =$ 0.10	$\alpha =$ 0.15	$\alpha =$ 0.20	$\alpha =$ 0.25	$\alpha =$ 0.30	$\alpha =$ 0.35
0.0900	3.2479	10.7088	6.1713	5.8738	5.5686	5.3517	2.5889	7.0106	7.2414	7.3700	7.4486
0.1000	3.1920	8.4220	5.8459	5.5641	5.2750	4.9183	2.5612	6.8641	7.1442	7.3012	7.3975
0.1200	3.0662	4.8286	5.1568	4.9083	4.6532	4.0447	2.4981	6.5366	6.9242	7.1442	7.2803
0.1300	2.9970	3.5200	4.8021	4.5706	4.3331	3.6194	2.4629	6.3575	6.8022	7.0566	7.2146
0.1400	2.9240	2.5020	4.4464	4.2321	4.0122	3.2101	2.4255	6.1696	6.6728	6.9631	7.1442
0.1600	2.7680	1.1718	3.7474	3.5668	3.3814	2.4587	2.3444	5.7717	6.3941	6.7598	6.9904
0.1700	2.6858	0.7721	3.4110	3.2466	3.0779	2.1233	2.3010	5.5639	6.2458	6.6506	6.9072
0.1800	2.6012	2.4246	2.3156	2.2040	2.0895	1.7930	2.2558	2.4445	2.5371	2.5889	2.6207
0.1900	2.5148	2.3367	2.2317	2.1241	2.0137	1.7104	2.2089	2.4158	2.5181	2.5754	2.6106
0.2200	2.2475	2.0668	1.9739	1.8787	1.7811	1.4620	2.0602	2.3229	2.4556	2.5309	2.5774
0.2700	1.7967	1.6185	1.5458	1.4713	1.3948	1.0696	1.7930	2.1483	2.3359	2.4445	2.5124

In this case:

- $\alpha = 0.20$ and Radloss = 0.40 reproduce the same value of $\Delta T/T_{amb}$ at $r = 0.09m$
- $\alpha = 0.25$ and Radloss = 0.40 reproduce the same value of $\Delta T/T_{amb}$ at $r = 0.09m$
- $\alpha = 0.20$ and Radloss = 0.40 reproduce the same value of $\Delta T/T_{amb}$ at $r = 0.10m$
- $\alpha = 0.15$ and Radloss = 0.40 reproduce the same value of $\Delta T/T_{amb}$ at $r = 0.12m$
- $\alpha = 0.30$ and Radloss = 0.35 reproduce the same value of $\Delta T/T_{amb}$ at $r = 0.12m$
- $\alpha = 0.20$ and Radloss = 0.35 reproduce the same value of $\Delta T/T_{amb}$ at $r = 0.13m$
- $\alpha = 0.30$ and Radloss = 0.30 reproduce the same value of $\Delta T/T_{amb}$ at $r = 0.14m$
- $\alpha = 0.35$ and Radloss = 0.30 reproduce the same value of $\Delta T/T_{amb}$ at $r = 0.14m$
- $\alpha = 0.15$ and Radloss = 0.35 reproduce the same value of $\Delta T/T_{amb}$ at $r = 0.16m$
- $\alpha = 0.15$ and Radloss = 0.35 reproduce the same value of $\Delta T/T_{amb}$ at $r = 0.17m$
- $\alpha = 0.30$ and Radloss = 0.20 reproduce the same value of $\Delta T/T_{amb}$ at $r = 0.18m$
- $\alpha = 0.15$ and Radloss = 0.25 reproduce the same value of $\Delta T/T_{amb}$ at $r = 0.22m$
- $\alpha = 0.15$ and Radloss = 0.20 reproduce the same value of $\Delta T/T_{amb}$ at $r = 0.27m$

Table III.11: the tolerance (relative error) of the temperature with different values of α and radloss at $z = 2.9m$

R	$\Delta T/T_{amb}$										
	Heskestad					Ideal					
	Radloss = 0.20	Radloss = 0.25	Radloss = 0.30	Radloss = 0.35	Radloss = 0.40	$\alpha =$ 0.10	$\alpha =$ 0.15	$\alpha =$ 0.20	$\alpha =$ 0.25	$\alpha =$ 0.30	$\alpha =$ 0.35
0.1200	0.0098	0.0097	0.0093	0.0089	0.0084	0.0072	0.0080	0.0082	0.0083	0.0084	0.0085
0.1300	0.0096	0.0095	0.0091	0.0086	0.0082	0.0070	0.0078	0.0082	0.0083	0.0084	0.0084
0.1400	0.0094	0.0092	0.0088	0.0084	0.0080	0.0068	0.0077	0.0081	0.0083	0.0084	0.0084
0.1500	0.0092	0.0090	0.0086	0.0082	0.0077	0.0066	0.0076	0.0080	0.0082	0.0083	0.0084
0.1600	0.0089	0.0087	0.0083	0.0079	0.0075	0.0063	0.0075	0.0080	0.0082	0.0083	0.0084
0.1800	0.0084	0.0081	0.0078	0.0074	0.0070	0.0058	0.0072	0.0078	0.0081	0.0082	0.0083
0.1900	0.0082	0.0078	0.0075	0.0071	0.0068	0.0056	0.0071	0.0077	0.0080	0.0082	0.0083

Chapter III: Calculation, results and discussions

0.2000	0.0079	0.0075	0.0072	0.0069	0.0065	0.0053	0.0069	0.0076	0.0080	0.0081	0.0083
0.2200	0.0074	0.0069	0.0066	0.0063	0.0060	0.0048	0.0066	0.0074	0.0078	0.0080	0.0082
0.2400	0.0068	0.0063	0.0060	0.0058	0.0055	0.0043	0.0063	0.0072	0.0077	0.0080	0.0081
0.2800	0.0057	0.0051	0.0049	0.0047	0.0044	0.0034	0.0057	0.0068	0.0074	0.0077	0.0080
	$\Delta T(K)$										
R	Heskestad					Ideal					
	Radloss = 0.20	Radloss = 0.25	Radloss = 0.30	Radloss = 0.35	Radloss = 0.40	$\alpha =$ 0.10	$\alpha =$ 0.15	$\alpha =$ 0.20	$\alpha =$ 0.25	$\alpha =$ 0.30	$\alpha =$ 0.35
0.1200	2.9338	2.9017	2.7713	2.6377	2.5006	2.1543	2.3693	2.4495	2.4875	2.5084	2.5211
0.1300	2.8715	2.8302	2.7030	2.5727	2.4390	2.0912	2.3382	2.4313	2.4757	2.5001	2.5150
0.1400	2.8058	2.7550	2.6311	2.5043	2.3742	2.0251	2.3050	2.4119	2.4630	2.4912	2.5084
0.1500	2.7368	2.6764	2.5561	2.4329	2.3064	1.9565	2.2700	2.3912	2.4495	2.4817	2.5014
0.1600	2.6649	2.5949	2.4782	2.3587	2.2362	1.8857	2.2331	2.3693	2.4351	2.4716	2.4938
0.1800	2.5138	2.4246	2.3156	2.2040	2.0895	1.7392	2.1543	2.3218	2.4038	2.4495	2.4774
0.1900	2.4353	2.3367	2.2317	2.1241	2.0137	1.6643	2.1126	2.2964	2.3869	2.4375	2.4686
0.2000	2.3551	2.2475	2.1465	2.0430	1.9369	1.5889	2.0695	2.2700	2.3693	2.4250	2.4592
0.2200	2.1913	2.0668	1.9739	1.8787	1.7811	1.4379	1.9796	2.2140	2.3317	2.3982	2.4393
0.2400	2.0249	1.8855	1.8007	1.7139	1.6249	1.2889	1.8857	2.1543	2.2912	2.3693	2.4176
0.2800	1.6938	1.5321	1.4632	1.3927	1.3203	1.0065	1.6894	2.0251	2.2023	2.3050	2.3693

In this case:

- $\alpha = 0.30$ and Radloss = 0.40 reproduce the same value of $\Delta T/T_{amb}$ at $r = 0.12m$
- $\alpha = 0.20$ and Radloss = 0.40 reproduce the same value of $\Delta T/T_{amb}$ at $r = 0.13m$
- $\alpha = 0.30$ and Radloss = 0.35 reproduce the same value of $\Delta T/T_{amb}$ at $r = 0.14m$
- $\alpha = 0.35$ and Radloss = 0.35 reproduce the same value of $\Delta T/T_{amb}$ at $r = 0.14m$
- $\alpha = 0.25$ and Radloss = 0.35 reproduce the same value of $\Delta T/T_{amb}$ at $r = 0.15m$
- $\alpha = 0.30$ and Radloss = 0.30 reproduce the same value of $\Delta T/T_{amb}$ at $r = 0.16m$
- $\alpha = 0.15$ and Radloss = 0.40 reproduce the same value of $\Delta T/T_{amb}$ at $r = 0.16m$
- $\alpha = 0.30$ and Radloss = 0.20 reproduce the same value of $\Delta T/T_{amb}$ at $r = 0.18m$
- $\alpha = 0.25$ and Radloss = 0.25 reproduce the same value of $\Delta T/T_{amb}$ at $r = 0.18m$
- $\alpha = 0.20$ and Radloss = 0.30 reproduce the same value of $\Delta T/T_{amb}$ at $r = 0.18m$
- $\alpha = 0.25$ and Radloss = 0.25 reproduce the same value of $\Delta T/T_{amb}$ at $r = 0.18m$
- $\alpha = 0.30$ and Radloss = 0.20 reproduce the same value of $\Delta T/T_{amb}$ at $r = 0.19m$
- $\alpha = 0.15$ and Radloss = 0.35 reproduce the same value of $\Delta T/T_{amb}$ at $r = 0.19m$
- $\alpha = 0.15$ and Radloss = 0.35 reproduce the same value of $\Delta T/T_{amb}$ at $r = 0.20m$
- $\alpha = 0.20$ and Radloss = 0.20 reproduce the same value of $\Delta T/T_{amb}$ at $r = 0.22m$
- $\alpha = 0.15$ and Radloss = 0.30 reproduce the same value of $\Delta T/T_{amb}$ at $r = 0.22m$
- $\alpha = 0.15$ and Radloss = 0.25 reproduce the same value of $\Delta T/T_{amb}$ at $r = 0.24m$
- $\alpha = 0.15$ and Radloss = 0.20 reproduce the same value of $\Delta T/T_{amb}$ at $r = 0.28m$

Chapter III: Calculation, results and discussions

III.5- Calculations on the flow of the stratified fumes (Alpert 1979)[23]

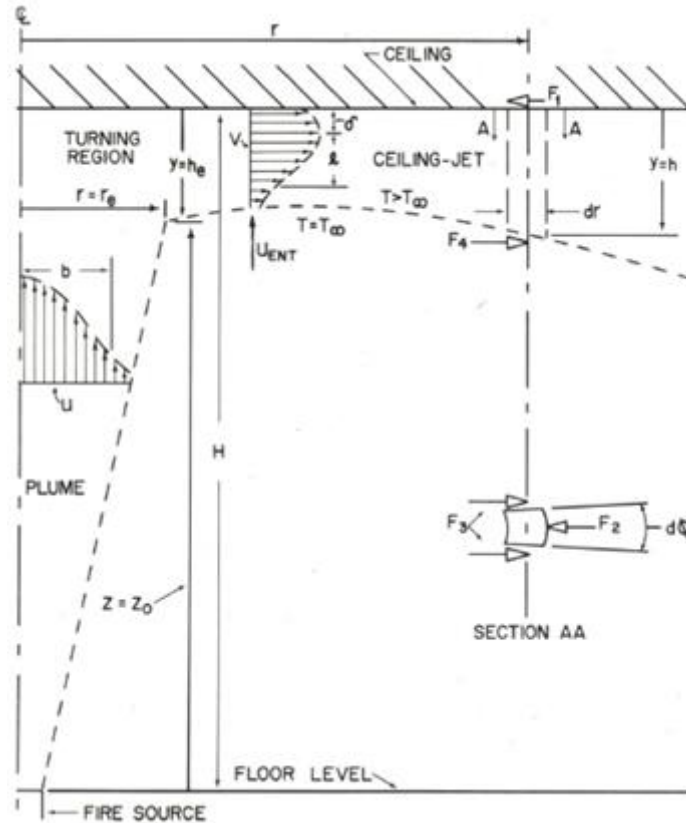


Figure III.8: Schematic figure of Ceiling Jet Flow

$$\Delta T_m = T_{\max} - T_{\infty} = 16.9 \dot{Q}^{2/3} (H - z_0)^{-5/3} \quad \text{for } r \leq 0.18 H \quad (\text{III-11})$$

$R \leq 0.18 H$: turning region zone

$$\Delta T_m = T_{\max} - T_{\infty} = 5.38 (\dot{Q}/r)^{2/3} (H - z_0)^{-1} \quad \text{for } r < 0.18 H < 2 H \quad (\text{III-12})$$

Radial distribution of the temperature $\Delta T_{\max}(r)$

- 0) $T_{\text{centerline}}$ is the temperature just beneath the ceiling where $r = 0$, so to find it we calculate $\Delta T_m(r = 0)$ i.e. ΔT_m of the first interval where it's constant.

In the study of the ceiling jets flame we consider two heights of the fire pool: $H_{\text{pool}} = 0$ and $H_{\text{pool}} = 0.5\text{m}$

1st case $H_{\text{pool}} = 0$:

$$H = H_{\text{ceiling}} - H_{\text{pool}} = 2.9 - 0 = 2.9\text{m}$$

We know that $0.18 \cdot H < r < 2 \cdot H$ i.e. $r_{\min} = 0.18 \cdot H = 0.522\text{m}$ and $r_{\max} = 2 \cdot H = 5.8\text{m}$

According to Alpert model 1972, the heat release rate is thus: $668 \text{ kW} \leq \dot{Q} \leq 98 \text{ MW}$

$$Z_0 = -0.34793783\text{m} \rightarrow \Delta T_{\text{centerline}} = 256.6309\text{K} \rightarrow T_{\text{centerline}} = 554.7809\text{K}$$

$$Z_0 = 0 \rightarrow \Delta T_{\text{centerline}} = 309.9738\text{K} \rightarrow T_{\text{centerline}} = 608.2138\text{K}$$

Chapter III: Calculation, results and discussions

TableIII.12: the tolerance (relative error) and the excess of the temperature in the Alpert 1972 case when $H_{pool} = 0$

$Q = 1125\text{kW}$				
$z_0 = -0.3479378 \text{ m}$			$z_0 = 0$	
R	$\Delta T \text{ (K)}$	$\Delta T/T_{amb}$	$\Delta T \text{ (K)}$	$\Delta T/T_{amb}$
0.5220	276.3732	0.9274	309.5321	1.0387
0.5720	260.0233	0.8726	291.2205	0.9772
0.6220	245.8948	0.8252	275.3969	0.9242
0.6720	233.5411	0.7837	261.5611	0.8777
5.5220	57.3516	0.1925	64.2325	0.2155
5.5720	57.0080	0.1913	63.8477	0.2143
5.6220	56.6695	0.1902	63.4686	0.2130
5.6720	56.3359	0.1890	63.0950	0.2117
5.7220	56.0073	0.1879	62.7269	0.2105
5.7720	55.6834	0.1869	62.3642	0.2093

The temperature decreases with the increasing of the plume radius. In our case we stopped at $r = 2*H = 5.8\text{m}$ where the tolerance can't be less than 5%, so the closest value to T_{∞} is 353.8334K if $z_0 = -0.3479378 \text{ m}$ and 360.5142.4805K if $z_0 = 0$

Chapter III: Calculation, results and discussions

- When $z_0 = -0.3479378\text{m}$:

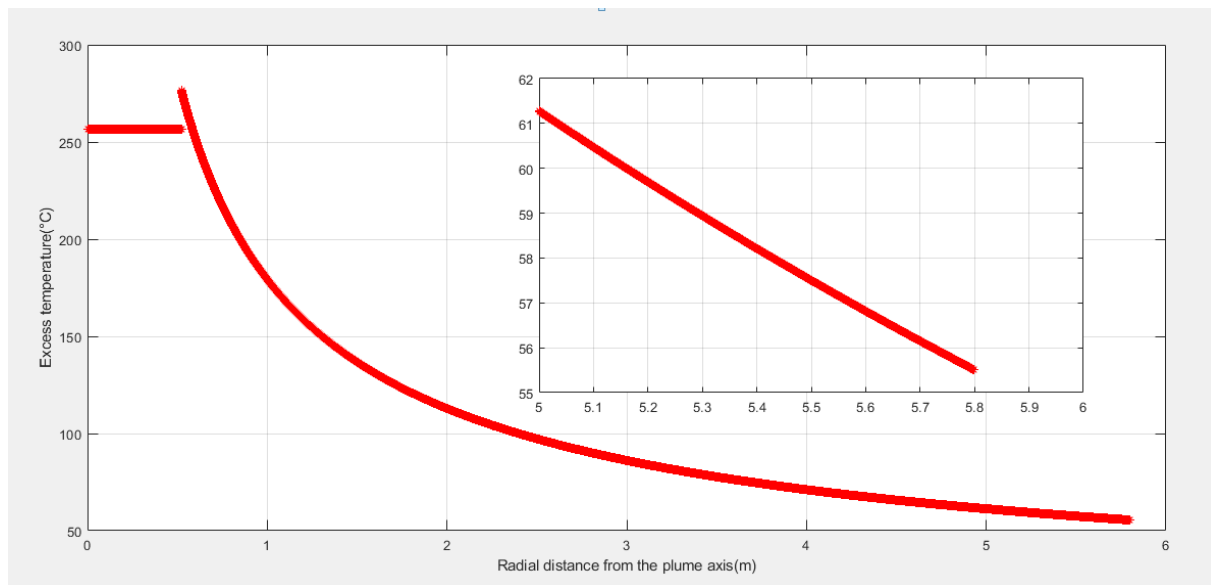


Figure III.9: Diagram of the excess temperature as a function of the radial distance ($z_0 = -0.3479378\text{m}$ and $H_{\text{pool}} = 0$)

We notice from this graph that the excess of temperature stays constant in the first interval, while it decreases in the second, but the most remarkable detail is that this decreasing doesn't start from the same value that the excess of temperature is equal to in the first interval, but it starts with a value greater than $\Delta T_{\text{centerline}}$ until it reaches to it after some centimeters of r and all that is due to $Z_0 = -0.3479378\text{m}$ instead of a null value

- 1) $r = r_{\text{max}} = 5.8\text{m} \rightarrow \Delta T = \Delta T_{\text{max,limite}} = \Delta T(5.8) = 55.5040 \rightarrow T_{\text{max_limit}} = 353.6540\text{K}$
and $(\Delta T_{\text{max}}/T_{\text{amb}})_{\text{limite}} = 0.1862$
- 2) $\Delta T_{\text{max}} = 276.3732\text{K}$ which is definitely the highest

Chapter III: Calculation, results and discussions

- When $z_0 = 0$:

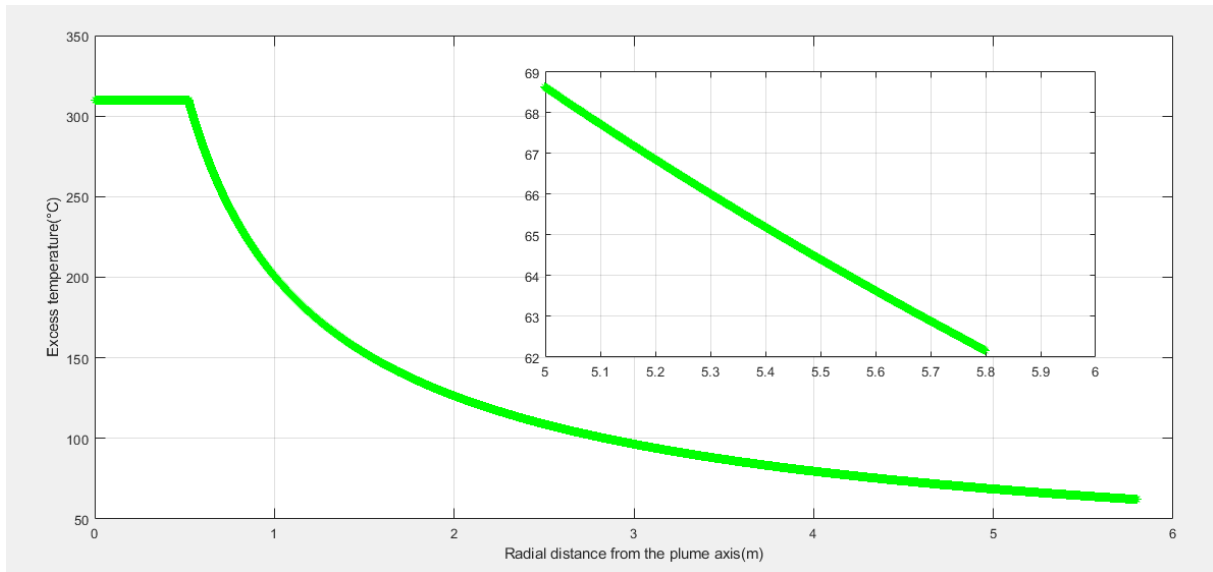


Figure III.10: Diagram of the excess temperature as a function of the radial distance ($z_0 = 0$ and $H = 0$)

We notice from this graph that the excess of temperature stays constant in the first interval and starts decreasing in the second from the same value (from $\Delta T_{\text{centerline}}$)

- 1) $r = r_{\text{max}} = 5.8\text{m} \rightarrow \Delta T = \Delta T_{\text{max, limite}} = \Delta T(5.8) = 62.1633\text{K} \rightarrow T_{\text{max, limite}} = 360.3133\text{K}$ and $(\Delta T_{\text{max}}/T_{\text{amb}})_{\text{limite}} = 0.2085\text{K}$
- 2) $\Delta T_{\text{max}} = 309.5321\text{K}$ which is definitely the highest

2nd case $H_{\text{pool}} = 0.5\text{m}$:

$$H = H_{\text{ceiling}} - H_{\text{pool}} = 2.9 - 0.5 = 2.4\text{m}$$

We know that $0.18 \cdot H < r < 2 \cdot H$ i.e. $r_{\text{min}} = 0.18 \cdot H = 0.432\text{m}$ and $r_{\text{max}} = 2 \cdot H = 4.8\text{m}$

$$Z_0 = -0.34793783\text{m} \rightarrow \Delta T_{\text{centerline}} = 339.0863\text{K} \rightarrow T_{\text{centerline}} = 637.2363\text{K}$$

$$Z_0 = 0 \rightarrow \Delta T_{\text{centerline}} = 424.9159\text{K} \rightarrow T_{\text{centerline}} = 723.0659\text{K}$$

Table III.13: the tolerance (relative error) and the excess of the temperature in the Alpert 1972 case when $H_{\text{pool}} = 0.5\text{m}$

	$\dot{Q} = 1125\text{kW}$			
	$z_0 = -0.3479378\text{ m}$		$z_0 = 0$	
$r(\text{m})$	$\Delta T (\text{K})$	$\Delta T/T_{\text{amb}}$	$\Delta T (\text{K})$	$\Delta T/T_{\text{amb}}$

Chapter III: Calculation, results and discussions

0.4320	370.5850	1.2436	424.3103	1.5534
0.4820	344.4919	1.1560	394.4343	1.4440
0.5320	322.5542	1.0824	369.3161	1.3521
0.5820	303.8051	1.0195	347.8490	1.2735
4.5320	77.3304	0.2595	88.5413	0.3241
4.5820	76.7668	0.2576	87.8960	0.3218
4.6320	76.2134	0.2557	87.2624	0.3195
4.6820	75.6698	0.2539	86.6400	0.3172
4.7320	75.1359	0.2521	86.0286	0.3150
4.7820	74.6112	0.2504	85.4279	0.3128

The temperature decreases with the increasing of the plume radius. In our case we stopped at $r = 2*H = 4.8\text{m}$ where the tolerance can't be less than 5%, so the closest value to T_{∞} is 372.7612K if $Z_0 = -0.3479378\text{ m}$ and 383.5779K if $Z_0 = 0$

Chapter III: Calculation, results and discussions

- When $z_0 = -0.3479378\text{m}$:

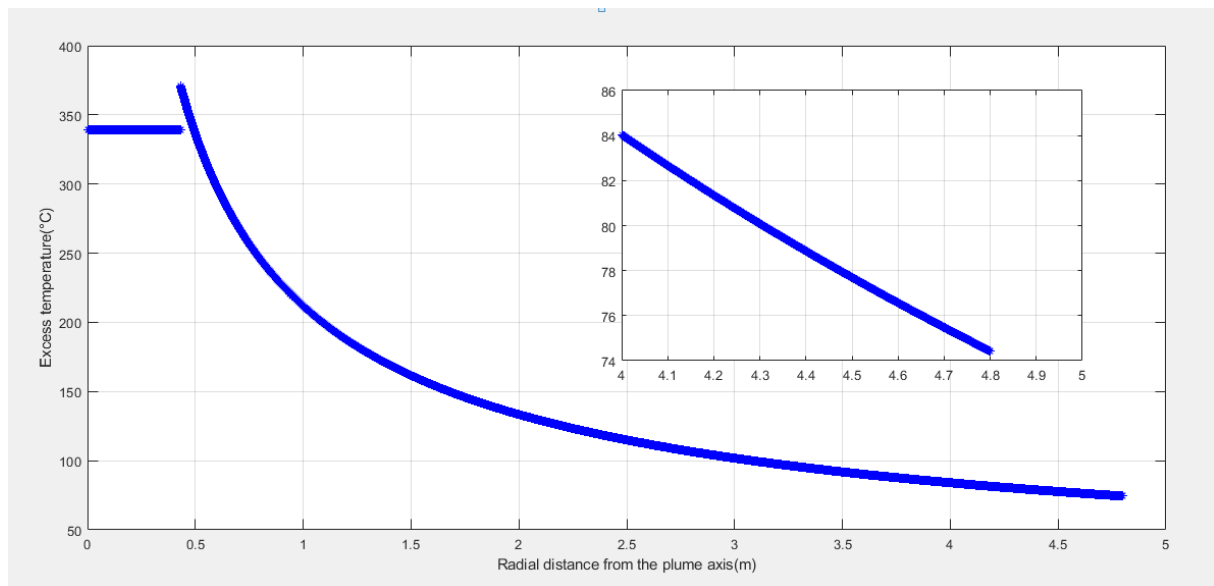


Figure III.11: Diagram of the excess temperature as a function of the radial distance ($z_0 = -0.3479378\text{m}$ and $H_{\text{pool}} = 0,5\text{m}$)

We notice from this graph that the excess of temperature stays constant in the first interval, while it decreases in the second, but the most remarkable detail is that this decreasing doesn't start from the same value the excess of temperature is equal to in the first interval, but it starts with a value greater than $\Delta T_{\text{centerline}}$ until it reaches to it after some centimeters of r and all that is due to $Z_0 = -0.3479378\text{m}$ instead of a null value

$$1) \quad r = r_{\text{max}} = 4.8\text{m} \rightarrow \Delta T = \Delta T_{\text{max,limite}} = \Delta T(4.8) = 74.4246\text{K} \rightarrow T_{\text{max_limit}} = 372.5746\text{K} \text{ and } (\Delta T_{\text{max}}/T_{\text{amb}})_{\text{limite}} = 0.2496\text{K}$$

$$2) \quad \Delta T_{\text{max}} = 370.5850 \text{ K which is definitely the highest}$$

- When $z_0 = 0$:

Chapter III: Calculation, results and discussions

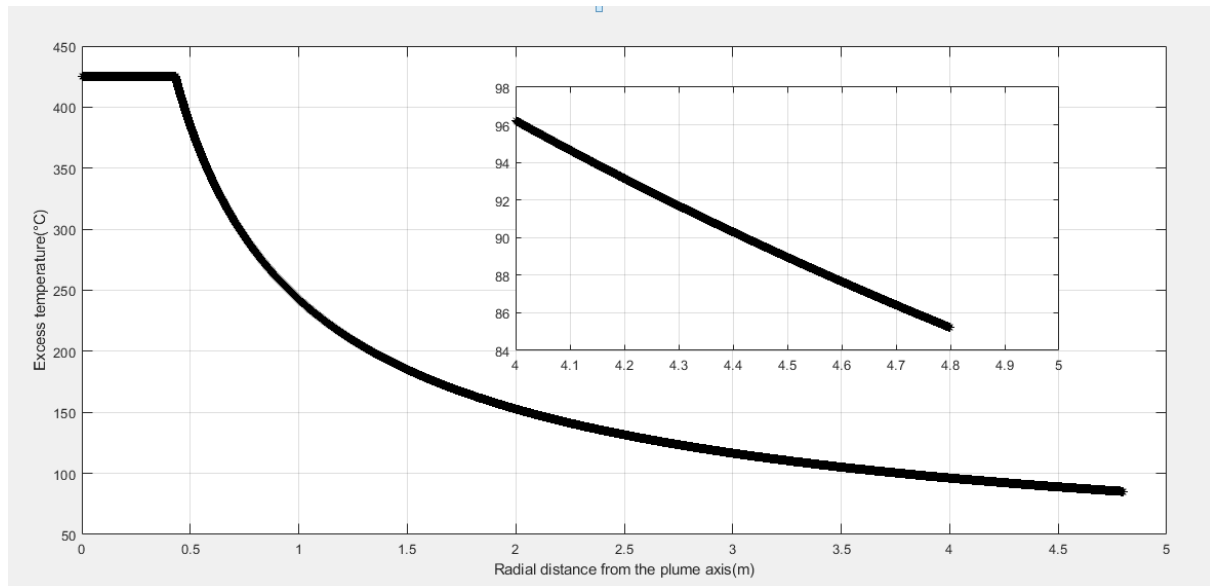


Figure III.12: Diagram of the excess temperature as a function of the radial distance ($z_0 = 0$ and $H_{pool} = 0,5m$)

We notice from this graph that the excess of temperature stays constant in the first interval and starts decreasing in the second from the same value (from $\Delta T_{centerline}$)

- 1) $r = r_{max} = 4.8m \rightarrow \Delta T = \Delta T_{max,limite} = \Delta T(4.8) = 85.2142K \rightarrow T_{max_limit} = 383.3642K$
and $(\Delta T_{max}/T_{amb})_{limite} = 0.2858K$
- 2) $\Delta T_{max} = 424.3103K$ which is definitely the highest

Note:

According to the four graphs and the two tables we got, we notice that there is an issue whenever $z_0 \neq 0$ because:

- Firstly, the two graphs of $H_{pool} = 0$ and $H_{pool} = 0.5m$ when $z_0 = -0.3479378m$ are not continuous at the turning region point.
- Secondly the maximum value of the ΔT we have in the table is greater than ΔT_{max} we got from the first interval ($\Delta T_{centerline}$), meaning, $\Delta T_{max} \neq \Delta T_{centerline}$ although they are supposed to be equal to each other.

In that case we need to study the continuity of the two formulas to find at which point they must intersect.

For the function to be continuous, both equations must be equal to each other, hence:

$$16.9 (HRR)^{2/3} (H - z_0)^{-5/3} = 5.38 HRR^{2/3} / r^{2/3} (H - z_0)^{-1} \rightarrow 16.9 r^{2/3} = 5.38 (H - z_0)^{2/3} \rightarrow r = 0.1796 (H - z_0)$$

Chapter III: Calculation, results and discussions

- 1- if $z_0 = 0$ then, the function is continuous at $\frac{r}{H} = 0.1796 \approx 0.18$ and consequently:
- $$\Delta T_m = T_{\max} - T_{\infty} = 16.9 \dot{Q}^{2/3} (H - z_0)^{-5/3} \quad r \leq 0.18 H$$
- $$\Delta T_m = T_{\max} - T_{\infty} = 5.38 (\dot{Q}/r)^{2/3} (H - z_0)^{-1} \quad 0.18 H < r < 2 H$$
- 2- if $z_0 \neq 0$ then, the function is continuous at $\frac{r}{H - z_0} = 0.1796 \approx 0.18$ and consequently:
- $$\Delta T_m = T_{\max} - T_{\infty} = 16.9 \dot{Q}^{2/3} (H - z_0)^{-5/3} \quad r \leq 0.18 (H - z_0)$$
- $$\Delta T_m = T_{\max} - T_{\infty} = 5.38 (\dot{Q}/r)^{2/3} (H - z_0)^{-1} \quad 0.18 (H - z_0) < r < 2 (H - z_0)$$

In this case we must keep up calculating with the new intervals:

$$\Delta T_m = T_{\max} - T_{\infty} = 16.9 \dot{Q}^{2/3} (H - z_0)^{-5/3} \quad \mathbf{r \leq 0.18 (H - z_0)} \quad \text{(III.13)}$$

$$\Delta T_m = T_{\max} - T_{\infty} = 5.38 (\dot{Q}/r)^{2/3} (H - z_0)^{-1} \quad \mathbf{0.18 (H - z_0) < r < 2 (H - z_0)} \quad \text{(III.14)}$$

1st case $H_{\text{pool}} = 0$:

$$H = H_{\text{ceiling}} - H_{\text{pool}} = 2.9 - 0 = 2.9\text{m}$$

We know that $0.18*(H - z_0) < r < 2*(H - z_0)$ and:

- If $z_0 = 0$ $r_{\min} = 0.18*(H - z_0) = 0.522\text{m}$ and $r_{\max} = 2*(H - z_0) = 5.800\text{m}$
- If $z_0 = -0.3479378\text{m}$ $r_{\min} = 0.18*(H - z_0) = 0.585\text{m}$ and $r_{\max} = 2*(H - z_0) = 6.500\text{m}$

According to Alpert model 1972, the heat release rate is thus: $668 \text{ kW} \leq \dot{Q} \leq 98 \text{ MW}$

If we take $\dot{Q} = 1125 \text{ kW}$ as formerly then:

$$z_0 = -0.3479378\text{m} \rightarrow \Delta T_{\text{centerline}} = 256.6309\text{K} \rightarrow T_{\text{centerline}} = 554.7809\text{K}$$

$$z_0 = 0 \rightarrow \Delta T_{\text{centerline}} = 309.9738\text{K} \rightarrow T_{\text{centerline}} = 607.1238\text{K}$$

Chapter III: Calculation, results and discussions

1- $z_0 = 0$:

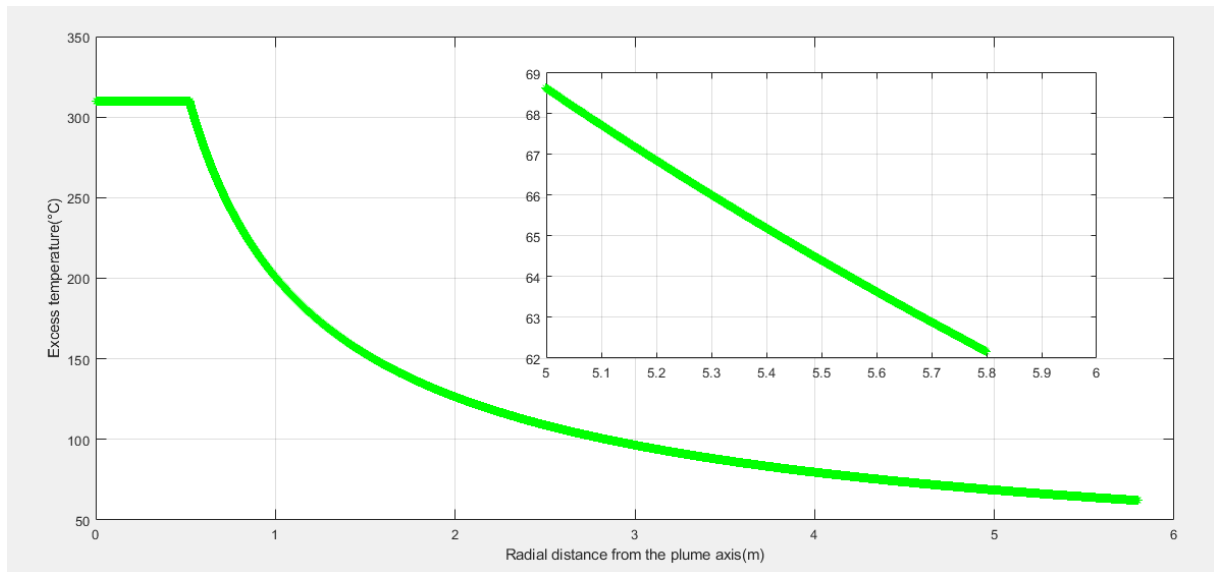


Figure III.13: Diagram of the excess temperature as a function of the radial distance ($z_0 = 0$ and $H = 0$)

We notice from this graph that the excess of temperature is constant in the first interval and starts decreasing in the second from the same value (from $\Delta T_{\text{centerline}}$)

Table III.14: the tolerance (relative error) and the excess of the temperature in the Alpert 1972 case when $H_{\text{pool}} = 0$ and $z = 0$ with the new intervals

r(m)	ΔT (K)	$\Delta T/T_{\text{amb}}$
0.5220	309.5321	1.0387
0.5720	291.2205	0.9772
0.6220	275.3969	0.9242
0.6720	261.5611	0.8777
5.5220	64.2325	0.2155
5.5720	63.8477	0.2143
5.6220	63.4686	0.2130

Chapter III: Calculation, results and discussions

5.6720	63.0950	0.2117
5.7220	62.7269	0.2105
5.7720	62.3642	0.2093

The temperature decreases with the increasing of the plume radius. In our case we stopped at $r = 2*H = 5.8\text{m}$ where the tolerance can't be less than 5%, so the closest value to T_{∞} is 360.5142K

3) $r = r_{\max} = 5.8\text{m} \rightarrow \Delta T = \Delta T_{\max, \text{limite}} = \Delta T(5.8) = 62.1633\text{K} \rightarrow T_{\max, \text{limit}} = 360.3133\text{K}$ and $(\Delta T_{\max}/T_{\text{amb}})_{\text{limite}} = 0.2085\text{K}$.

4) $\Delta T_{\max} = 309.9738\text{K}$ which is definitely the highest.

As we have seen in the first case about tolerance:

$r > 49.4360\text{m}$ and $H_{\text{pool}} = 0$ and $Z_0 = 0 \rightarrow \Delta T/T_{\text{amb}} = 0.2093$ (20.93%) where $r_{\infty} = 5.7720\text{m} \rightarrow r/H = 1.9903\text{m} \in [0.18, 2.0]$

5) At the turning region, $r = 0.18*H = \mathbf{0.522\text{m}}$

a- The ideal model:

$b(z = 2.9) = 0.348\text{m}$ when $\alpha = 0.10$

$b(z = 2.9) = \mathbf{0.522\text{m}}$ when $\alpha = 0.15$

$b(z = 2.9) = 0.696\text{m}$ when $\alpha = 0.20$

$b(z = 2.9) = 0.870\text{m}$ when $\alpha = 0.25$

$b(z = 2.9) = 1.044\text{m}$ when $\alpha = 0.30$

$b(z = 2.9) = 1.218\text{m}$ when $\alpha = 0.35$

b- The Heskestad model:

Radloss = 0 $\rightarrow b(z = 2.9) = 0.4311\text{m}$

Radloss = 0.20 $\rightarrow b(z = 2.9) = 0.4206\text{m}$

Radloss = 0.30 $\rightarrow b(z = 2.9) = 0.4149\text{m}$

Radloss = 0.40 $\rightarrow b(z = 2.9) = 0.4089\text{m}$

In this case we take b_{\max} where $\alpha = \mathbf{0.15}$, for the reason of the equality between r and b_{\max} in the same case, however, the other value either of the ideal model or the Heskestad model are far being equal to r

Chapter III: Calculation, results and discussions

2- $z_0 = -0.3479378$ m:

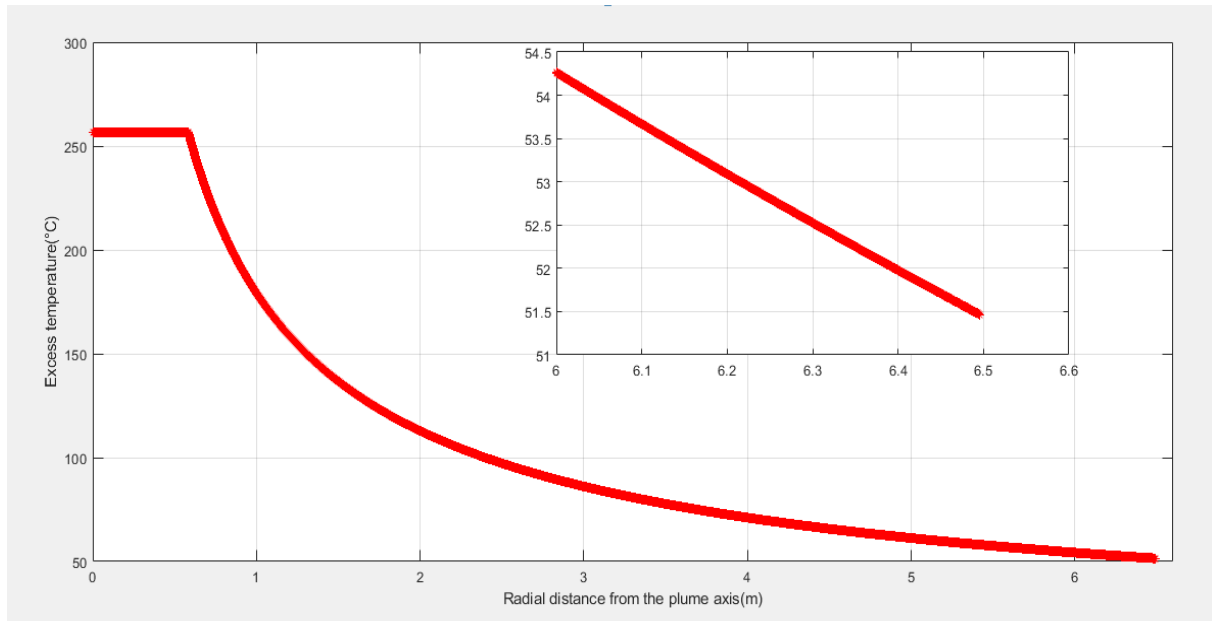


Figure III.14: Diagram of the excess temperature as a function of the radial distance ($z_0 = -0.3479378$ m and $H_{\text{pool}} = 0$)

With the new intervals we could reach to a continuous graph, so now with any value of z_0 , the graph keeps being continuous at the turning region point such as, the excess of temperature remains constant in the first interval then it decreases in the second from the same value (from $\Delta T_{\text{centerline}}$).

Table III.15: the tolerance (relative error) and the excess of the temperature in the Alpert 1972 case when $H_{\text{pool}} = 0$ and $z = -0.3479378$ m with the new intervals

r(m)	ΔT (K)	$\Delta T/T_{\text{amb}}$
0.585	256.2651	0.8599
0.635	242.6218	0.8142
0.685	230.6603	0.7740
0.735	220.0717	0.7385
6.235	52.8935	0.1775

Chapter III: Calculation, results and discussions

6.285	52.6126	0.1766
6.335	52.3354	0.1756
6.385	52.0618	0.1747
6.435	51.7918	0.1738
6.485	51.5252	0.1729

The temperature decreases with the increasing of the plume radius. In our case we stopped at $r = 2*(H - z_0) = 6.5\text{m}$ where the tolerance can't be less than 5%, so the closest value to T_∞ is 349.6752K

- 3) $r = r_{\max} = 5.8\text{m} \rightarrow \Delta T = \Delta T_{\max, \text{limite}} = \Delta T(6.5) = 51.4439 \rightarrow T_{\max, \text{limit}} = 349.5939\text{K}$
 and $(\Delta T_{\max}/T_{\text{amb}})_{\text{limite}} = 0.1725$
- 4) $\Delta T_{\max} = 256.2651\text{K}$ which is definitely the highest

$$\Delta T_m = T_{\max} - T_\infty = 5.38 * (\text{HRR}/r)^{2/3} * (H - Z_0)^{-1}$$

$$\Delta T/T_{\text{amb}} < 0.05 \rightarrow \Delta T < 14.91 \rightarrow 5.38 * (\text{HRR}/r)^{2/3} * (H - Z_0)^{-1} < 14.9 \rightarrow 1/[(H-Z_0)*r^{2/3}] < 0.0256 \rightarrow 39.0625/(H-Z_0) < r^{2/3} \rightarrow 244.1406/(H-Z_0)^{3/2} < r$$

- $H_{\text{pool}} = 0$ and $z_0 = -0.3479378\text{m} \rightarrow r > \mathbf{41.7089\text{m}}$

$\Delta T/T_{\text{amb}}$ is impossible to be less than 5% whatever was the value of Z_0 in any of both cases of H_{pool} ($H_{\text{pool}} = 0$ and $H_{\text{pool}} = 0.5$), unless if r was as big as a radial distance being equal to 41.7089m and thus, it's irrational for a compartment of 15m of width to have a radius of at least three times its breadth. In that case, we take the least value of $\Delta T/T_{\text{amb}}$ where our calculations stopped:

- $H_{\text{pool}} = 0$ and $z_0 = -0.3479378\text{m} \rightarrow \Delta T/T_{\text{amb}} = 0.1729$ (17.29%) where $r_\infty = 6.485\text{m} \rightarrow r/(H - z_0) = 1.9967\text{m} \in [0.18, 2.0]$

5) At the turning region, $r = 0.18*(H - z_0) = \mathbf{0.5846\text{m}}$

a- The ideal model:

$$b(z = 2.9) = 0.348\text{m} \text{ when } \alpha = 0.10$$

$$b(z = 2.9) = \mathbf{0.522\text{m}} \text{ when } \alpha = 0.15$$

Chapter III: Calculation, results and discussions

$$b(z = 2.9) = 0.696\text{m when } \alpha = 0.20$$

$$b(z = 2.9) = 0.870\text{m when } \alpha = 0.25$$

$$b(z = 2.9) = 1.044\text{m when } \alpha = 0.30$$

$$b(z = 2.9) = 1.218\text{m when } \alpha = 0.35$$

b- The Heskestad model:

$$\text{Radloss} = 0 \rightarrow b(z = 2.9) = 0.4828\text{m}$$

$$\text{Radloss} = 0.20 \rightarrow b(z = 2.9) = 0.4711\text{m}$$

$$\text{Radloss} = 0.30 \rightarrow b(z = 2.9) = 0.4647\text{m}$$

$$\text{Radloss} = 0.40 \rightarrow b(z = 2.9) = 0.4579\text{m}$$

In this case we take b_{\max} where $\alpha = 0.15$, for the reason of the equality between r and b_{\max} in the same case, however, the other values either of the ideal model or the Heskestad model are far being equal to r .

2nd case $H_{\text{pool}} = 0.5\text{m}$:

$$H = H_{\text{ceiling}} - H_{\text{pool}} = 2.9 - 0.5 = 2.4\text{m}$$

We know that $0.18*(H - z_0) < r < 2*(H - z_0)$ and:

- If $z_0 = 0$ then, $r_{\min} = 0.18*H = 0.4320\text{m}$ and $r_{\max} = 2*H = 4.8\text{m}$
- If $z_0 = -0.3479378\text{m}$ then, $r_{\min} = 0.18*(H - z_0) = 0.4946\text{m}$ and $r_{\max} = 2*(H - z_0) = 5.4959\text{m} \approx 5.5\text{m}$

$$z_0 = -0.3479378\text{m} \rightarrow \Delta T_{\text{centerline}} = 339.0863\text{K} \rightarrow T_{\text{centerline}} = 637.2363\text{K}$$

$$z_0 = 0 \rightarrow \Delta T_{\text{centerline}} = 424.9159\text{K} \rightarrow T_{\text{centerline}} = 723.0659\text{K}$$

Chapter III: Calculation, results and discussions

1- $z_0 = 0$:

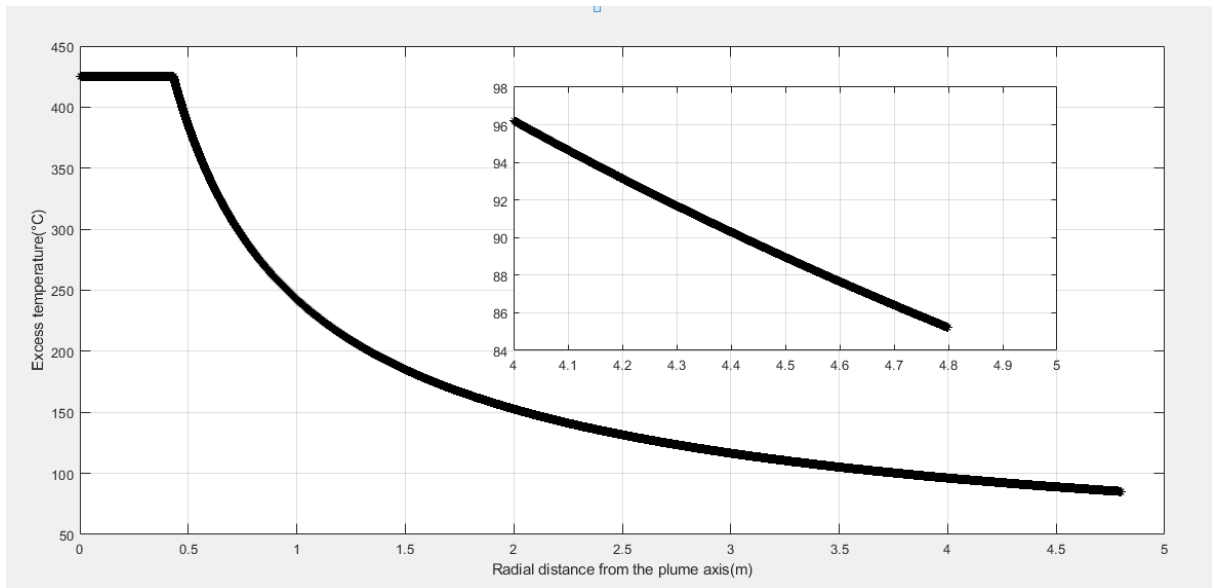


Figure III.15: Diagram of the excess temperature as a function of the radial distance ($z_0 = 0$ and $H_{\text{pool}} = 0,5\text{m}$)

We notice from this graph that the excess of temperature is constant in the first interval and starts decreasing in the second from the same value (from $\Delta T_{\text{centerline}}$).

Table III.16: the tolerance (relative error) and the excess of the temperature in the Alpert 1972 case when $H_{\text{pool}} = 0.5$ and $z = 0\text{m}$ with the new intervals

r(m)	ΔT (K)	$\Delta T/T_{\text{amb}}$
0.4320	424.3103	1.5534
0.4820	394.4343	1.4440
0.5320	369.3161	1.3521
0.5820	347.8490	1.2735
4.5320	88.5413	0.3241
4.5820	87.8960	0.3218

Chapter III: Calculation, results and discussions

4.6320	87.2624	0.3195
4.6820	86.6400	0.3172
4.7320	86.0286	0.3150
4.7820	85.4279	0.3128

The temperature decreases with the increasing of the plume radius. In our case we stopped at $r = 2 * H = 4.8m$ where the tolerance can't be less than 5%, so the closest value to T_{∞} is 383.5779K.

3) $r = r_{max} = 4.8m \rightarrow \Delta T = \Delta T_{max,limite} = \Delta T(4.8) = 85.2142K \rightarrow T_{max_limit} = 383.3642K$
and $(\Delta T_{max}/T_{amb})_{limite} = 0.2858K$

4) $\Delta T_{max} = 424.3103K$ which is definitely the highest

As we have seen in the first case ever about tolerance:

- $r > 65.6634m$

- $\Delta T/T_{amb} = 0.3128$ (31.28%) where $r_{\infty} = 4.7820m \rightarrow r/H = 1.9925m \in [0.18, 2.0]$

5) At the turning region, $r = 0.18 * H = 0.4320m$:

a- The ideal model:

$b(z = 2.9) = 0.348m$ when $\alpha = 0.10$

$b(z = 2.9) = 0.522m$ when $\alpha = 0.15$

$b(z = 2.9) = 0.696m$ when $\alpha = 0.20$

$b(z = 2.9) = 0.870m$ when $\alpha = 0.25$

$b(z = 2.9) = 1.044m$ when $\alpha = 0.30$

$b(z = 2.9) = 1.218m$ when $\alpha = 0.35$

b- The Heskestad model:

Radloss = 0 $\rightarrow b(z = 2.9) = 0.4311m$

Radloss = 0.20 $\rightarrow b(z = 2.9) = 0.4206m$

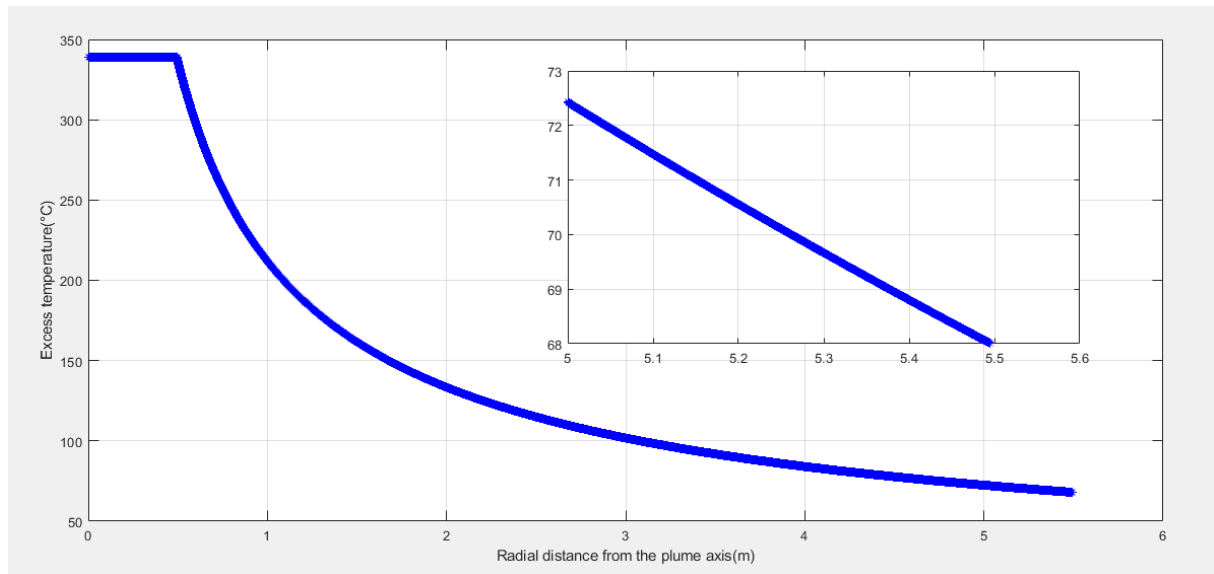
Radloss = 0.30 $\rightarrow b(z = 2.9) = 0.4149m$

Radloss = 0.40 $\rightarrow b(z = 2.9) = 0.4089m$

$b_{max} = 0.4320m$ is the closest value to r so it's the most accepted as we proofed before by calculating.

2- $z_0 = -0.3479378m$:

Chapter III: Calculation, results and discussions



FigureIII.16: Diagram of the excess temperature as a function of the radial distance ($z_0 = -0.3479378\text{m}$ and $H_{\text{pool}} = 0,5\text{m}$)

With the new intervals we could reach to a continuous graph, so now with any value of z_0 , the graph keeps being continuous at the turning region point such as, the excess of temperature remains constant in the first interval then it decreases in the second from the same value (from $\Delta T_{\text{centerline}}$)

TableIII.17: the tolerance (relative error) and the excess of the temperature in the Alpert 1972 case when $H_{\text{pool}} = 0.5\text{m}$ and $z = -0.3479378\text{m}$ with the new intervals

r(m)	ΔT (K)	$\Delta T/T_{\text{amb}}$
0.4956	338.6030	1.1363
0.5456	317.5484	1.0656
0.5956	299.4882	1.0050
0.6456	283.7945	0.9523
5.2456	70.1564	0.2354
5.2956	69.7140	0.2339
5.3456	69.2785	0.2325

Chapter III: Calculation, results and discussions

5.3956	68.8498	0.2310
5.4456	68.4276	0.2296
5.4956	68.0119	0.2282

The temperature decreases with the increasing of the plume radius. In our case we stopped at $r = 2*(H - z_0) = 5.495\text{m}$ where the tolerance can't be less than 5%, so the closest value to T_∞ is 366.1619K.

3) $r = r_{\max} = 5.5\text{m} \rightarrow \Delta T = \Delta T_{\max, \text{limite}} = \Delta T(5.5) = 67.9676\text{K} \rightarrow T_{\max, \text{limit}} = 366.1176\text{K}$ and $(\Delta T_{\max}/T_{\text{amb}})_{\text{limite}} = 0.2280\text{K}$.

4) $\Delta T_{\max} = 338.6030\text{K}$ which is definitely the highest.

As we have seen in the first case ever about tolerance:

- $r > 53.5957\text{m}$

- $\Delta T/T_{\text{amb}} = 0.2282$ (22.82%) where $r_\infty = 5.4950\text{m} \rightarrow r/(H - z_0) = 1.9997\text{m} \in [0.18, 2.0]$

5) At the turning region, $r = 0.18*(H - z_0) = 0.4946\text{m}$

a- The ideal model:

$b(z = 2.9) = 0.348\text{m}$ when $\alpha = 0.10$

$b(z = 2.9) = 0.522\text{m}$ when $\alpha = 0.15$

$b(z = 2.9) = 0.696\text{m}$ when $\alpha = 0.20$

$b(z = 2.9) = 0.870\text{m}$ when $\alpha = 0.25$

$b(z = 2.9) = 1.044\text{m}$ when $\alpha = 0.30$

$b(z = 2.9) = 1.218\text{m}$ when $\alpha = 0.35$

b- The Heskestad model:

Radloss = 0 $\rightarrow b(z = 2.9) = 0.4828\text{m}$

Radloss = 0.20 $\rightarrow b(z = 2.9) = 0.4711\text{m}$

Radloss = 0.30 $\rightarrow b(z = 2.9) = 0.4647\text{m}$

Radloss = 0.40 $\rightarrow b(z = 2.9) = 0.4579\text{m}$

$b_{\max} = 0.4828\text{m}$ is the closest value for so it's the most accepted as we proofed before by calculating.

Chapter III: Calculation, results and discussions

III.6- Calculations on the flow of the stratified fumes (Alpert 2011)

$$T_{max} - T_{\infty} = 16.9\dot{Q}_c^{2/3} (H - Z_0)^{-5/3} \quad \text{For } \frac{r}{H-Z_0} \leq 0.134 \quad (\text{III.15})$$

$$T_{max} - T_{\infty} = 6.721\dot{Q}_c^{2/3} (H - Z_0)^{-5/3} \left(\frac{r}{H-Z_0}\right)^{-0.6545} \quad \text{For } \frac{r}{H-Z_0} > 0.134 \quad (\text{III.16})$$

$Q_{conv} = (1-\text{radloss}) * \dot{Q}$, we take $\text{radloss} = 0.25$ we get hence, $Q_{conv} = 843.75\text{kW}$

0) Checking the continuity at $r = 0.134 * (H - z_0)$

- For $r/(H-z_0) \leq 0.134$: $r/(H-z_0)$ can be equal to 0.134 which involves the continuity in the first interval

a- $H_{pool} = 0$ and $z_0 = -0.3479378\text{m} \rightarrow T_{max} - T_{\infty} = 211.8441\text{K}$

b- $H_{pool} = 0.5\text{m}$ and $z_0 = -0.3479378\text{m} \rightarrow T_{max} - T_{\infty} = 279.9096\text{K}$

- For $r/(H-z_0) > 0.134$:

a- $H_{pool} = 0$ and $z_0 = -0.3479378\text{m} \rightarrow H = 2.9\text{m} \rightarrow \Delta T (0.134) = 313.9594\text{K}$

b- $H_{pool} = 0.5\text{m}$ and $z_0 = -0.3479378\text{m} \rightarrow H = 2.4\text{m} \rightarrow \Delta T (0.134) = 414.8345\text{K}$

According to the calculations we got in both intervals, the function is not continuous at 0.134 because no value of ΔT , in the first interval, of any of the two cases ($H_{pool} = 0$ and $H_{pool} = 0.5\text{m}$) is equal to the other value of ΔT of the second interval at 0.134.

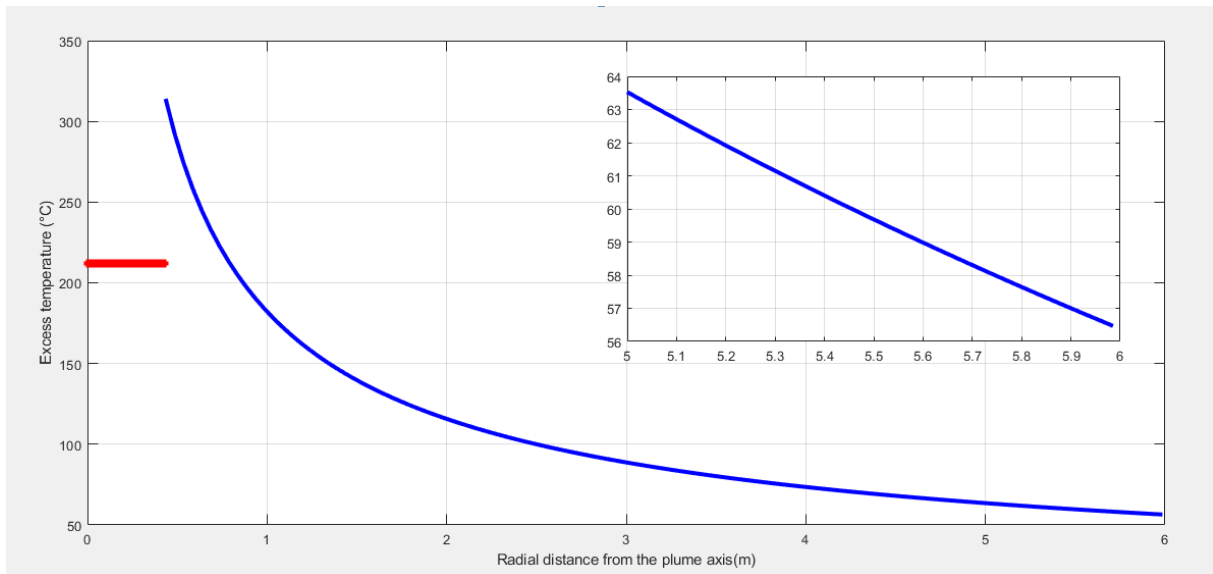
1) **Determination of $T_{centerline}$:**

1st case $H_{pool} = 0$ and $z_0 = -0.3479378\text{m}$:

In the 1st interval: $\Delta T_{centerline} = 211.8441\text{K} \rightarrow T_{centerline} = 509.9941\text{K}$ and $\Delta T/T_{amb} = 0.7105$

$\Delta T_{max} = 313.9594\text{K} \rightarrow T_{max} = 612.1094\text{K}$ and $(\Delta T/T_{amb})_{max} = 1.0530$

Chapter III: Calculation, results and discussions



FigureIII.17: Diagram of the excess temperature as a function the radial distance ($H_{\text{pool}} = 0$ and $z_0 = -0.3479378\text{m}$)

$$H = H_{\text{ceiling}} - H_{\text{pool}} = 2.9 - 0 = 2.9\text{m}$$

We know that $0.134*(H-z_0) < r$ i.e. r_{min} tends to $0.134*(H-z_0) = 0.4352\text{m}$

TableIII.18: the tolerance (relative error) and the excess of the temperature in the Alpert 2011 case when $H_{\text{pool}} = 0$ and $z_0 = -0.3479378\text{m}$

r(m)	ΔT (K)	$\Delta T/T_{\text{amb}}$
0.4352	313.9594	1.0536
0.4852	292.3895	0.9812
0.5352	274.2107	0.9202
0.5852	258.6418	0.8679
5.7352	58.0684	0.1949
5.7852	57.7394	0.1938
5.8352	57.4151	0.1927
5.8852	57.0954	0.1916

Chapter III: Calculation, results and discussions

5.9352	56.7801	0.1905
5.9852	56.4692	0.1895

2nd case, $H_{pool} = 0.5\text{m}$ and $z_0 = -0.3479378\text{m}$:

In the 1st interval: $\Delta T_{\text{centerline}} = 279.9096\text{K} \rightarrow T_{\text{centerline}} = 578.0596\text{K}$ and $\Delta T/T_{\text{amb}} = 0.9388$

$\Delta T_{\text{max}} = 414.8345\text{K} \rightarrow T_{\text{max}} = 712.9845\text{K}$ and $(\Delta T/T_{\text{amb}})_{\text{max}} = 1.3914$

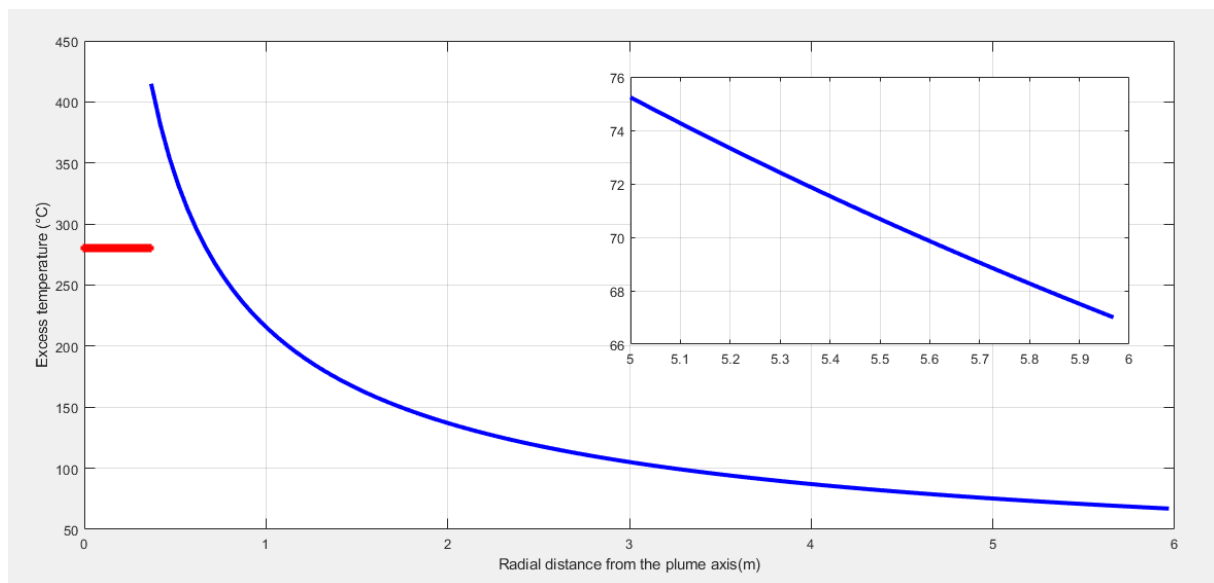


Figure III.18: Diagram of the excess temperature as a function the radial distance ($H_{pool} = 0.5\text{m}$ and $z_0 = -0.3479378\text{m}$)

$$H = H_{\text{ceiling}} - H_{\text{pool}} = 2.9 - 0.5 = 2.4\text{m}$$

We know that $0.134 \cdot (H - z_0) < r$ i.e. r_{min} tends to $0.134 \cdot (H - z_0) = 0.3682\text{m}$

Table III.19: the tolerance (relative error) and the excess of the temperature in the Alpert 2011 case when $H_{pool} = 0.5$ and $z_0 = -0.3479378\text{m}$

r(m)	ΔT (K)	$\Delta T/T_{\text{amb}}$
0.3682	414.8345	1.3921
0.4182	381.6656	1.2808
0.4682	354.4730	1.1895

Chapter III: Calculation, results and discussions

0.5182	331.6984	1.1131
5.7182	68.9077	0.2312
5.7682	68.5161	0.2299
5.8182	68.1302	0.2286
5.8682	67.7497	0.2273
5.9182	67.3745	0.2261
5.9682	67.0046	0.2248

The graphs are not continuous at 0.134 and $\Delta T_{\text{centerline}} \neq \Delta T_{\text{max}}$.

What we must do is finding at which point they may be continuous. So for the function to be continuous at 0.134, both equations give the same value at the same point (0.134) hence:

$$16.9 \dot{Q}_c^{2/3} (H - z_0)^{-5/3} = 6.721 \dot{Q}_c^{2/3} (H - z_0)^{-5/3} \left(\frac{r}{H - z_0} \right)^{-0.6545}$$

We can divide both sides by $\dot{Q}_c^{2/3} (H - z_0)^{-5/3}$ since it's a constant value so we get:

$$16.9 = 6.721 * \left(\frac{r}{H - z_0} \right)^{-0.6545} \rightarrow \left(\frac{r}{H - z_0} \right)^{-0.6545} = 2.5145 \rightarrow \frac{r}{H - z_0} = 0.2444.$$

Consequently the function is continuous at 0.2444 and the new interval we must work with is therefore:

$$T_{\text{max}} - T_{\infty} = 16.9 \dot{Q}_c^{2/3} (H - z_0)^{-5/3} \quad \text{For } \frac{r}{H - z_0} \leq \mathbf{0.2444} \quad (\text{III.17})$$

$$T_{\text{max}} - T_{\infty} = 6.721 \dot{Q}_c^{2/3} (H - z_0)^{-5/3} \left(\frac{r}{H - z_0} \right)^{-0.6545} \quad \text{For } \frac{r}{H - z_0} > \mathbf{0.2444} \quad (\text{III.18})$$

2) Checking the continuity: $r = 0.2444 * (H - z_0)$

- For $r/(H - z_0) \leq \mathbf{0.2444}$:

$r/(H - z_0)$ can be equal to 0.2444 which involves the continuity in the first interval

c- $H_{\text{pool}} = 0$ and $z_0 = -0.3479378\text{m} \rightarrow T_{\text{max}} - T_{\infty} = 211.8441\text{K}$ and $r \leq \mathbf{0.7938m}$

d- $H_{\text{pool}} = 0.5\text{m}$ and $z_0 = -0.3479378\text{m} \rightarrow T_{\text{max}} - T_{\infty} = 279.9096\text{K}$ and $r \leq \mathbf{0.6716m}$

- For $r/(H - z_0) > \mathbf{0.2444}$:

Chapter III: Calculation, results and discussions

- c- $H_{\text{pool}} = 0$ and $z_0 = -0.3479378\text{m} \rightarrow H = 2.9\text{m} \rightarrow \Delta T (0.2444) = 211.8612\text{K}$ and $r > 0.7938\text{m}$
- d- $H_{\text{pool}} = 0.5\text{m}$ and $z_0 = -0.3479378\text{m} \rightarrow H = 2.4\text{m} \rightarrow \Delta T (0.2444) = 279.9321\text{K}$ and $r > 0.6716\text{m}$

According to the calculations we got in both intervals, the function is continuous at 0.2444

3) Determination of $T_{\text{centerline}}$:

1st case $H_{\text{pool}} = 0$ and $z_0 = -0.3479378\text{m}$:

In the 1st interval: $\Delta T_{\text{centerline}} = 211.8441\text{K} \rightarrow T_{\text{centerline}} = 509.9941\text{K}$ and $\Delta T/T_{\text{amb}} = 0.7105$

$\Delta T_{\text{max}} = 211.8612\text{K} \rightarrow T_{\text{max}} = 510.0112\text{K}$ and $(\Delta T/T_{\text{amb}})_{\text{max}} = 0.7106$

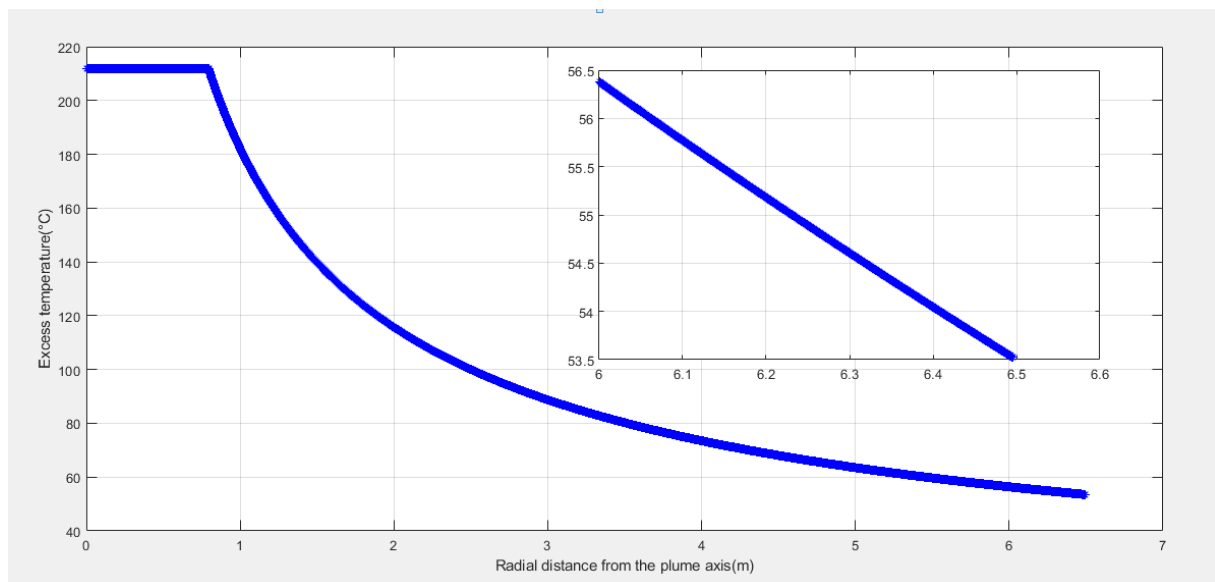


Figure III.19: Diagram of the excess temperature as a function the radial distance ($H_{\text{pool}} = 0$ and $z_0 = -0.3479378\text{m}$)

$$H = H_{\text{ceiling}} - H_{\text{pool}} = 2.9 - 0 = 2.9\text{m}$$

We know that $0.2444*(H-z_0) < r$ i.e. r_{min} tends to $0.2444*(H-z_0) = 0.7938\text{m}$

Table III.20: the tolerance (relative error) and the excess of the temperature in the Alpert 2011 case when $H_{\text{pool}} = 0$ and $z_0 = -0.3479378\text{m}$ with the new intervals

$r(\text{m})$	$\Delta T (\text{K})$	$\Delta T/T_{\text{amb}}$
0.7938	211.8612	0.7109
0.8438	203.5581	0.6831

Chapter III: Calculation, results and discussions

0.8938	196.0312	0.6578
0.9438	189.1704	0.6348
5.7438	58.0116	0.1947
5.7938	57.6835	0.1936
5.8438	57.3600	0.1925
5.8938	57.0410	0.1914
5.9438	56.7265	0.1904
5.9938	56.4163	0.1893

2nd case, $H_{\text{pool}} = 0.5\text{m}$ and $z_0 = -0.3479378\text{m}$:

In the 1st interval: $\Delta T_{\text{centerline}} = 279.9096\text{K} \rightarrow T_{\text{centerline}} = 578.0596\text{K}$ and $\Delta T/T_{\text{amb}} = 0.9388$

$\Delta T_{\text{max}} = 279.9321\text{K} \rightarrow T_{\text{max}} = 578.0821\text{K}$ and $(\Delta T/T_{\text{amb}})_{\text{max}} = 0.9389$

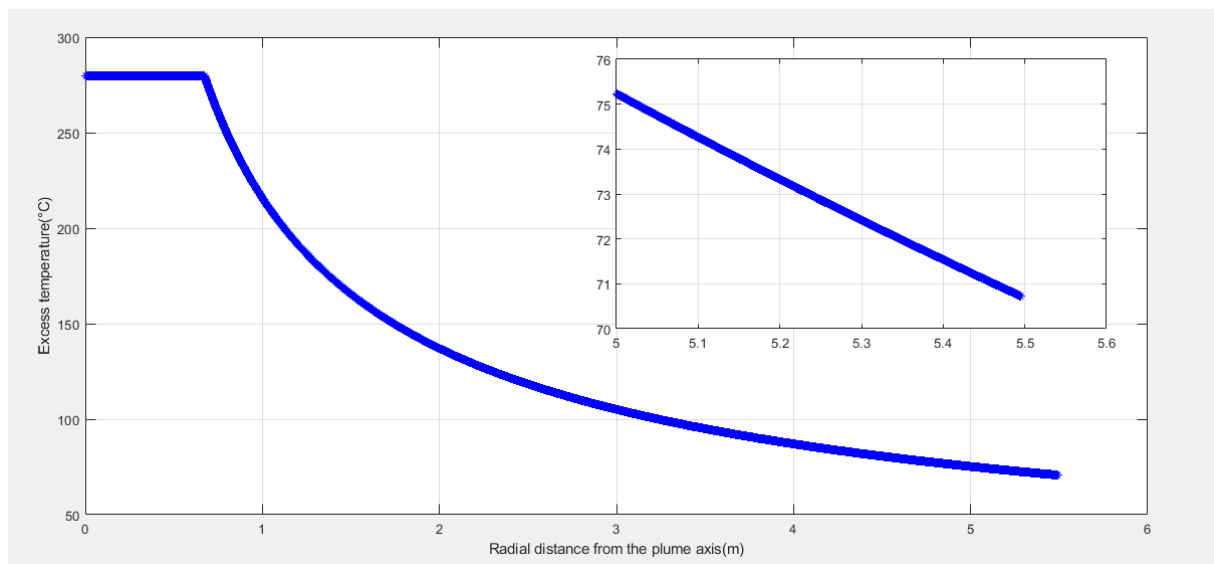


Figure III.20: Diagram of the excess temperature as a function of the radial distance ($H_{\text{pool}} = 0.5\text{m}$ and $z_0 = -0.3479378\text{m}$)

$$H = H_{\text{ceiling}} - H_{\text{pool}} = 2.9 - 0.5 = 2.4\text{m}$$

We know that $0.2444 \cdot (H - z_0) < r$ i.e. r_{min} tends to $0.2444 \cdot (H - z_0) = 0.6716\text{m}$

Chapter III: Calculation, results and discussions

TableIII.21: the tolerance (relative error) and the excess of the temperature in the Alpert 2011 case when $H_{pool} = 0.5m$ and $z_0 = -0.3479378m$ with the new intervals

r(m)	ΔT (K)	$\Delta T/T_{amb}$
0.6716	279.9321	0.9394
0.7216	267.0800	0.8962
0.7716	255.6220	0.8578
0.8216	245.3302	0.8233
5.7216	68.8810	0.2311
5.7716	68.4899	0.2298
5.8216	68.1043	0.2285
5.8716	67.7242	0.2273
5.9216	67.3494	0.2260
5.9716	66.9798	0.2248

$$4) \Delta T/T_{amb} < 0.05 \rightarrow \Delta T = T_{max} - T_{\infty} < 14.9 \rightarrow 6.721 \dot{Q}_c^{2/3} (H - z_0)^{-5/3} \left(\frac{r}{H - z_0} \right)^{-0.6545} < 14.9$$

$$\rightarrow (H - z_0)^{-1.0122} * r^{-0.6545} < 0.0248 \rightarrow (H - z_0)^{1.0122} * r^{0.6545} > 40.2770 \rightarrow r^{0.6545} > 40.3226 / (H - z_0)^{1.0122}$$

$$\rightarrow r > 11.2417 / (H - z_0)^{(1/0.6622)} \rightarrow r > 283.8518 / (H - z_0)^{1.5465}$$

- $H_{pool} = 0m$ and $z_0 = -0.3479378m \rightarrow r > 45.91m$
- $H_{pool} = 0.5m$ and $Z_0 = -0.3479378m \rightarrow r > 59.45m$

It's impossible for $\Delta T/T_{amb}$ to be less than 5% whatever was the value of z_0 in any of both cases of H_{pool} ($H_{pool} = 0$ and $H_{pool} = 0.5$), unless if r was as big as a radius being equal respectively to (45.91m and $r = 59.45m$) thus, it's irrational for a compartment of 15m of width to have a radius of at least three times its breadth. In that case, we take the least value of $\Delta T/T_{amb}$ where our calculations stopped:

Chapter III: Calculation, results and discussions

- $H_{\text{pool}} = 0\text{m}$ and $z_0 = -0.3479378\text{m} \rightarrow \Delta T/T_{\text{amb}} = 0.1893$ (18.93%) where $r_{\infty} = 5.9938\text{m}$
 $\rightarrow r/(H-z_0) = 1.845\text{m} \in [0.134, \infty]$
- $H_{\text{pool}} = 0.5\text{m}$ and $z_0 = -0.3479378\text{m} \rightarrow \Delta T/T_{\text{amb}} = 0.2248$ (22.48%) where $r_{\infty} = 5.9716\text{m} \rightarrow r/(H-z_0) = 2.173\text{m} \in [0.134, \infty]$

Note:

Calculating the values of ΔT and $\Delta T/T_{\text{amb}}$, we stopped at $r = 6\text{m}$, because if we kept calculating until a tolerance less than 0.05, we would have some hundreds of values, which is useless and illogical for a radius of more than 45m

- 5) $\Delta T_{\text{max_limit}} = \Delta T(r_{\text{max}})$, so we take $r_{\text{max}} = 6\text{m}$ as a radius maximal value of our calculations and even as a radius that can be fitted with the dimension of the compartment, as a result:

$$H_{\text{pool}} = 0 \text{ and } z_0 = -0.3479378\text{m}: r_{\text{max}} = 6\text{m} \rightarrow \Delta T_{\text{max_limit}} = 56.3782\text{K} \rightarrow \mathbf{T_{\text{max_limit}} = 354.5281\text{K}}$$

$$H_{\text{pool}} = 0.5\text{m} \text{ and } z_0 = -0.3479378\text{m}: r_{\text{max}} = 6\text{m} \rightarrow \Delta T_{\text{max_limit}} = 66.7721\text{K} \rightarrow \mathbf{T_{\text{max_limit}} = 364.9221\text{K}}$$

- 6) Comparison of plume maximum radius (b_{max}) with the turn.R radius **with** radloss = 20%, 30%, 40% in the Heskestad model:

The turning region radius is $r = 0.2444*(H-z_0)$:

$$H_{\text{pool}} = 0; z_0 = -0.3479378\text{m} \rightarrow r = 0.7938\text{m}$$

$$H_{\text{pool}} = 0.5; z_0 = -0.3479378\text{m} \rightarrow r = 0.6716\text{m}$$

Heskestad model $\rightarrow b(z) = 0.12 * (T_0/T_{\text{amb}})^{1/2} * (z-z_0)$: $z_0 = -0.3479378\text{m}$

- Radloss = 0% : $b(z = 2.9) = \mathbf{0.4828\text{m}}$
- Radloss = 20% : $b(z = 2.9) = \mathbf{0.4711\text{m}}$
- Radloss = 30% : $b(z = 2.9) = \mathbf{0.4647\text{m}}$
- Radloss = 40% : $b(z = 2.9) = \mathbf{0.4579\text{m}}$

The four values of b_{max} are less than the two values of the turning region radius. In this case, we take the greatest value of b_{max} which is the closest to r_{turn_r} so, we consider that $b_{\text{max}} =$

Chapter III: Calculation, results and discussions

0.4828m is the most fittable and, therefore, the radiation losses we take in the model of Alpert 2011 is: $\text{radloss} = 0\%$.

Chapter III: Calculation, results and discussions

Note

If we don't consider the three ratios of radloss without taking radloss = 0% in consideration, then the closest b_{max} to $r_{turn,r}$ is 0.4711m and hence, the radiation losses we take in the model of Alpert 2011 is: radloss = 20%.

$$\Delta T_m = T_{max} - T_{\infty} = 5.38(HRR / r)^{2/3} (H - z_0)^{-1} \quad 0.18 (H - z_0) < r < 2 (H - z_0)$$

- Radloss = 0% → $Q_c = 1125kW$
- Radloss = 20% → $Q_c = 900kW$
- Radloss = 30% → $Q_c = 787.5kW$
- Radloss = 40% → $Q_c = 675kW$

TableIII.22: Recapitulating table of the previous flame parameters

The following table recapitulates all the results we got with the new interval:

	$T_{centerline}$ (°C)	Turning region situated at $r = ?$ of the plume axis (m)	Plume radius at the ceiling b_{max} (m)	$b_{max}/Turn.R$	T_{max} at the turning region (°C)	T_{max} at b_{max} (°C)	$T_{max-limit}$ (°C)
Alpert 1972 $\alpha_{rad} =$ 0%; 20%; 30%; 40% $H_{pool} = 0$; $z_0 = 0$	333.9738	0.5220	- 0.4828 (Radloss= 0%) - 0.4711 (radloss= 20%) - 0.4647 (radloss= 30%) - 0.4579 (radloss= 40%)	- 0.9249 (radloss= 0%) - 0.9025 (radloss= 20%) - 0.8902 (radloss= 30%) - 0.8772 (radloss= 40%)	334.5321	- 351.0677 (radloss= 0%) - 356.4443 (radloss= 20%) - 359.4805 (radloss= 30%) - 362.7838 (radloss= 40%)	87.1633
Alpert 1972 α_{rad} = 0%; 20%; 30%; 40% $H_{pool} = 0$; $z_0 \neq 0$	281.6309	0.5846	- 0.4828 (Radloss= 0%) - 0.4711 (radloss= 20%) - 0.4647 (radloss= 30%) - 0.4579 (radloss= 40%)	- 0.8259 (Radloss= 0%) - 0.8059 (Radloss= 20%) - 0.7949 (Radloss= 30%) - 0.7833 (Radloss=	281.2651	- 316.1375 (radloss= 0%) - 320.9381 (radloss= 20%) - 323.6491 (radloss= 30%) - 326.5985	76.4439

Chapter III: Calculation, results and discussions

				40%)		(radloss=40%)	
Alpert 1972 $\alpha_{rad} = 0\%, 20\% ; 30\% ; 40\%$ $H_{pool} = 0.5 ; z_0 = 0$	449.9159	0.4320	- 0.4828 (Radloss= 0%) - 0.4711 (radloss= 20%) - 0.4647 (radloss= 30%) - 0.4579 (radloss= 40%)	- 1.1176 (radloss= 0%) - 1.0905 (radloss= 20%) - 1.0757 (radloss= 30%) - 1.0600 (radloss= 40%)	449.3103	- 418.9985 (radloss= 0%) - 425.4952 (radloss= 20%) - 429.1640 (radloss= 30%) - 433.1555 (radloss= 40%)	110.2142
Alpert 1972 $\alpha_{rad} = 0\% ; 20\% ; 30\% ; 40\%$ $H_{pool} = 0.5 ; z_0 \neq 0$	364.0863	0.4946	- 0.4828 (Radloss= 0%) - 0.4711 (radloss= 20%) - 0.4647 (radloss= 30%) - 0.4579 (radloss= 40%)	- 0.9761 (Radloss= 0%) - 0.9525 (Radloss= 20%) - 0.9395 (Radloss= 30%) - 0.9258 (Radloss= 40%)	363.6030	- 369.1113 (radloss= 0%) - 374.7854 (radloss= 20%) - 377.9896 (radloss= 30%) - 381.4757 (radloss= 40%)	92.9676
Alpert 2011 $\alpha_{rad} = 0\% ; 20\% ; 30\% ; 40\%$ $H_{pool} = 0 ; z_0 \neq 0$	- 281.6309 (Radloss = 0%) - 246.1578 (radloss= 20%) - 227.3210 (radloss= 30%) - 207.5617 (radloss= 40%)	0.7938	- 0.4828 (Radloss= 0%) - 0.4711 (radloss= 20%) - 0.4647 (radloss= 30%) - 0.4579 (radloss= 40%)	- 0.6082 (radloss= 0%) - 0.5935 (radloss= 20%) - 0.5854 (radloss= 30%) - 0.5768 (radloss= 40%)	- 281.6507 (Radloss = 0%) - 246.1748 (radloss= 20%) - 227.3366 (radloss= 30%) - 207.5758 (radloss= 40%)	- 318.3494 (radloss= 0%) - 323.0975 (radloss= 20%) - 325.7782 (radloss= 30%) - 328.6942 (radloss= 40%)	81.4163
Alpert 2011 $\alpha_{rad} = 0\% ; 20\% ; 30\% ; 40\%$ $H_{pool} =$	- 364.0863 (Radloss = 0%) - 317.2157 (radloss= 20%)	0.6716	- 0.4828 (Radloss= 0%) - 0.4711 (radloss= 20%) - 0.4647 (radloss= 30%) - 0.4579 (radloss= 40%)	- 0.7189 (radloss= 0%) - 0.7015 (radloss= 20%) - 0.6919 (radloss= 30%) - 0.6818 (radloss	- 364.1123 (Radloss = 0%) - 317.2381 (radloss= 20%)	- 372.4316 (radloss= 0%) - 378.0550 (radloss= 20%) - 381.2299 (radloss=	91.7721

Chapter III: Calculation, results and discussions

0.5; z ₀ ≠0	- 292.3266 (radloss= 30%) - 266.2187 (radloss= 40%)		= 40%)	- 292.3471 (radloss= 30%) - 266.2372 (radloss= 40%)	30%) - 384.6835 (radloss= 40%)
------------------------	--	--	--------	--	--

In this on coming part of calculations, we work with the new intervals that lead us to the continuous functions.

III.7- Alpert's Correlations - Ceiling Jets 1972 for "maximum" temperature

For $r/(H-z_0) \leq 0,18$:

$$T_{\max} - T_{\infty} = 16.9 \dot{Q}^{2/3} (H - z_0)^{-5/3}$$

For $r/(H-z_0) > 0,18$:

$$T_{\max} - T_{\infty} = 5.38(\dot{Q}/r)^{2/3} (H - z_0)^{-1}$$

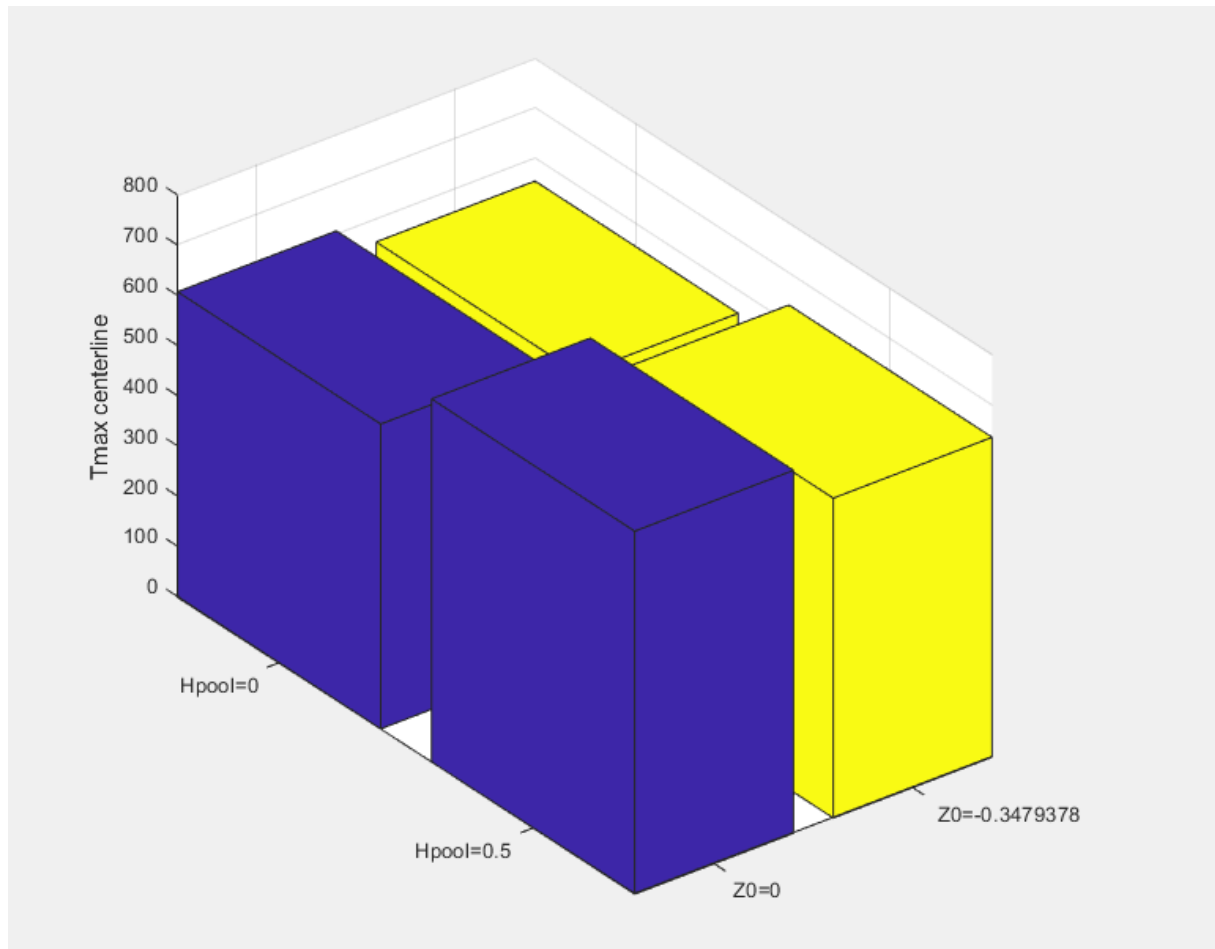
At $r = 0.18(H-z_0)$: turning region (Turn.R)

The distance between the fire pool vertical axis and the inner face of the door is $r_{\max 1} = 7\text{m}$

The distance between the fire pool vertical axis and the inner face of the window is $r_{\max 2} = 1.5\text{m}$

Chapter III: Calculation, results and discussions

1)



FigureIII.21: Histogram showing the centerline maximum temperature for the Alpert 1972 model when $H_{pool} = 0$ and $H_{pool} = 0.5\text{m}$

$H_{pool} = 0:$

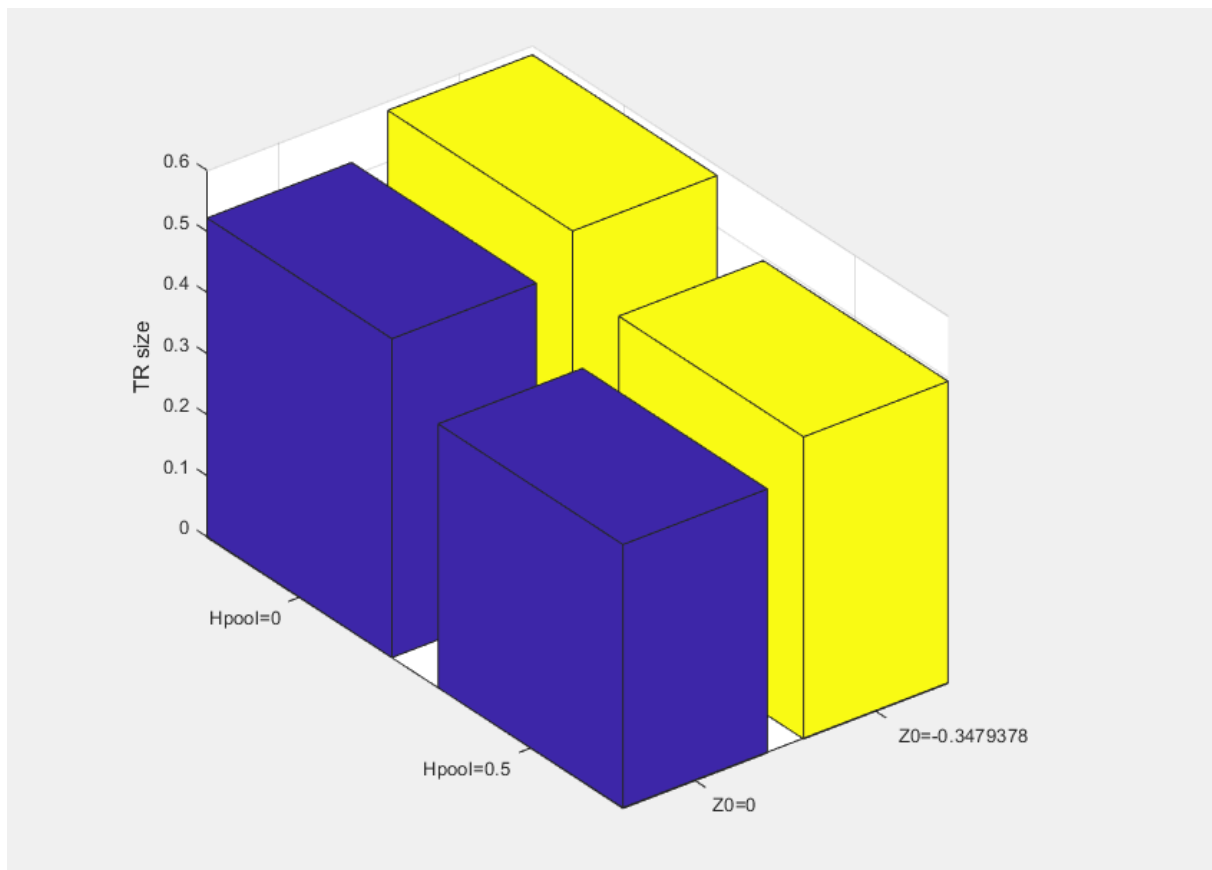
- $z_0 = 0 \rightarrow T_{\max_centerline}(r = 0) = 607.1238\text{K}$
- $z_0 = -0.3479378\text{m} \rightarrow T_{\max_centerline}(r = 0) = 554.7809\text{K}$

$H_{pool} = 0.5:$

- $z_0 = 0 \rightarrow T_{\max_centerline}(r = 0) = 723.0659\text{K}$
- $z_0 = -0.3479378\text{m} \rightarrow T_{\max_centerline}(r = 0) = 637.2363\text{K}$

Chapter III: Calculation, results and discussions

2)



FigureIII.22: Histogram showing the turning region size for the Alpert 1972 model when $H_{pool} = 0$ and $H_{pool} = 0.5m$

$H_{pool}=0$:

- $z_0 = 0 \rightarrow r_{turn_r} = 0.5220m$
- $z_0 = -0.3479378m \rightarrow r_{turn_r} = 0.5846m$

$H_{pool}=0.5$:

- $z_0 = 0 \rightarrow r_{turn_r} = 0.432m$
- $z_0 = -0.3479378m \rightarrow r_{turn_r} = 0.4946m$

Chapter III: Calculation, results and discussions

3)

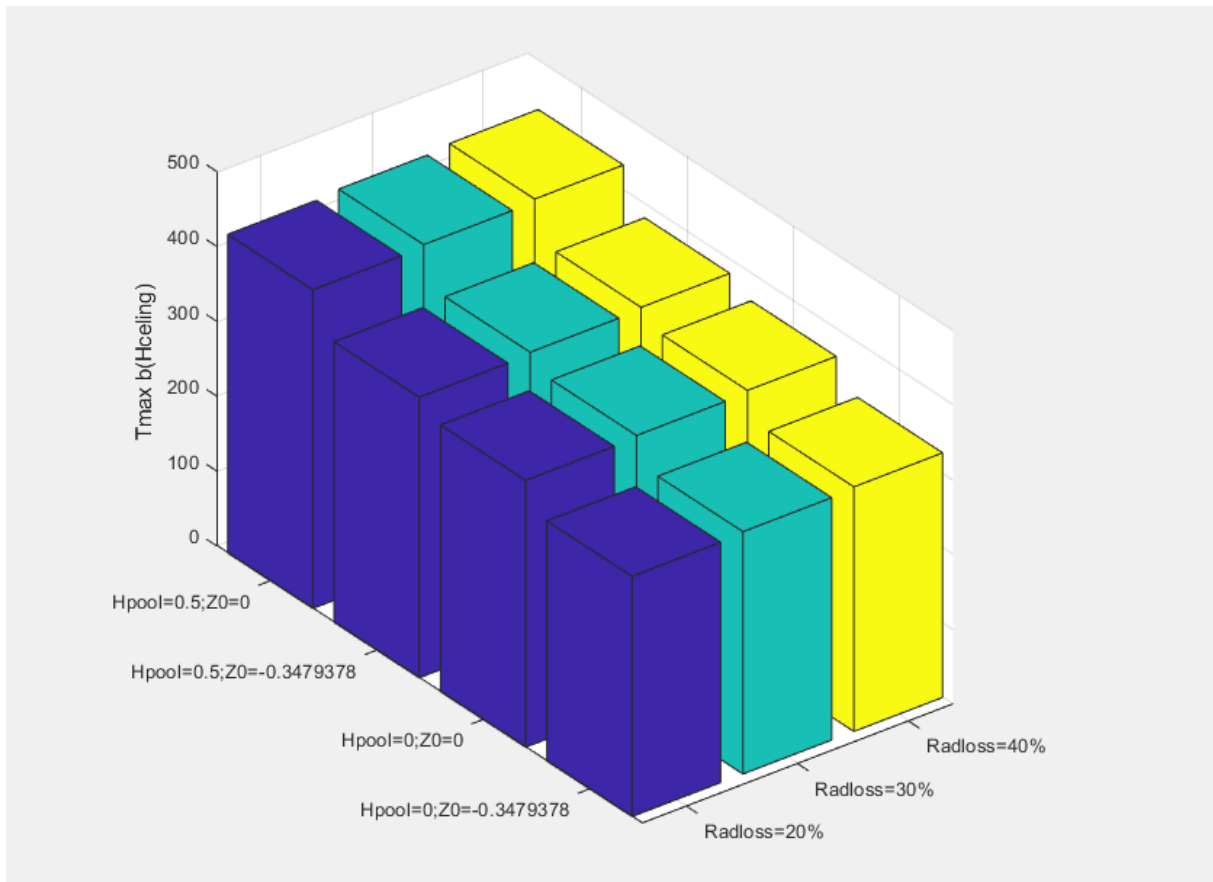


Figure III.23: Histogram showing the maximum temperature depending on the maximum plume radius at the ceiling for the Alpert 1972 model when $H_{pool} = 0$ and $H_{pool} = 0.5m$

$H_{pool}=0$:

- $z_0 = 0$
 - Radloss = 20% $\rightarrow T_{max_bmax} = 356.4443^{\circ}C$
 - Radloss = 30% $\rightarrow T_{max_bmax} = 359.4805^{\circ}C$
 - Radloss = 40% $\rightarrow T_{max_bmax} = 362.7838^{\circ}C$
- $z_0 = -0.3479378m$
 - Radloss = 20% $\rightarrow T_{max_bmax} = 320.9381^{\circ}C$
 - Radloss = 30% $\rightarrow T_{max_bmax} = 323.6491^{\circ}C$
 - Radloss = 40% $\rightarrow T_{max_bmax} = 326.5985^{\circ}C$

$H_{pool}=0.5$:

- $z_0 = 0$

Chapter III: Calculation, results and discussions

Radloss = 20% → $T_{\max_bmax} = 425.4952^{\circ}\text{C}$

Radloss = 30% → $T_{\max_bmax} = 429.1640^{\circ}\text{C}$

Radloss = 40% → $T_{\max_bmax} = 433.1555^{\circ}\text{C}$

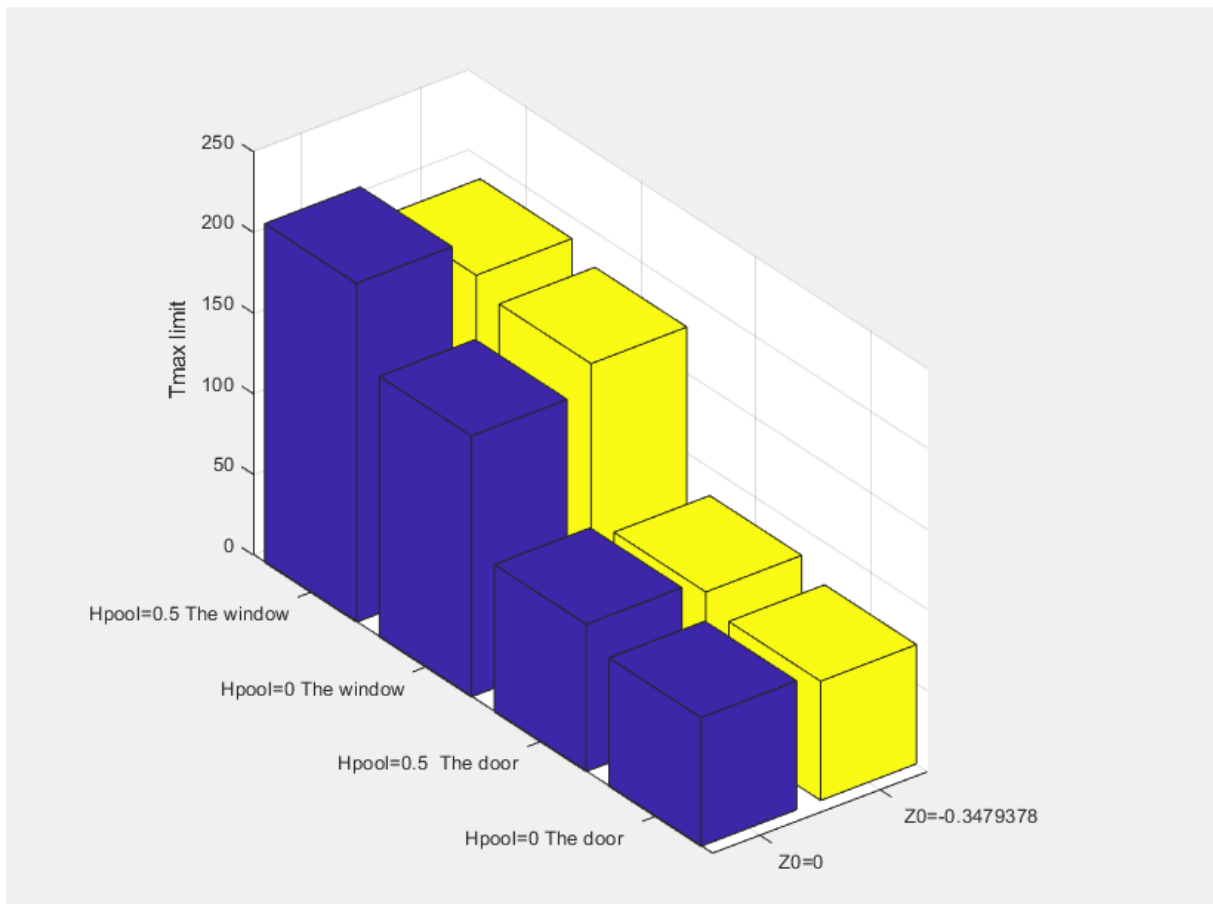
- $z_0 = -0.3479378\text{m}$

Radloss = 20% → $T_{\max_bmax} = 374.7854^{\circ}\text{C}$

Radloss = 30% → $T_{\max_bmax} = 377.9896^{\circ}\text{C}$

Radloss = 40% → $T_{\max_bmax} = 381.4757^{\circ}\text{C}$

4)



FigureIII.24: Histogram showing the maximum temperature at the door and the window for the Alpert 1972 model when $H_{\text{pool}} = 0$ and $H_{\text{pool}} = 0.5\text{m}$

Door:

$H_{\text{pool}} = 0:$

- $z_0 = 0 \rightarrow T_{\max_limit1} = 79.8390^{\circ}\text{C}$

- $z_0 = -0.3479378\text{m} \rightarrow T_{\max_limit1} = 73.9641^{\circ}\text{C}$

$H_{\text{pool}} = 0.5\text{m}:$

Chapter III: Calculation, results and discussions

- $z_0 = 0 \rightarrow T_{\max_limit1} = 91.2634^\circ\text{C}$
- $z_0 = -0.3479378\text{m} \rightarrow T_{\max_limit1} = 82.8733^\circ\text{C}$

Window:

$H_{\text{pool}} = 0$:

- $z_0 = 0 \rightarrow T_{\max_limit2} = 178.1411^\circ\text{C}$
- $z_0 = -0.3479378\text{m} \rightarrow T_{\max_limit2} = 161.7358^\circ\text{C}$

$H_{\text{pool}} = 0.5\text{m}$:

- $z_0 = 0 \rightarrow T_{\max_limit2} = 210.0455^\circ\text{C}$
- $z_0 = -0.3479378\text{m} \rightarrow T_{\max_limit2} = 186.6155^\circ\text{C}$

5)

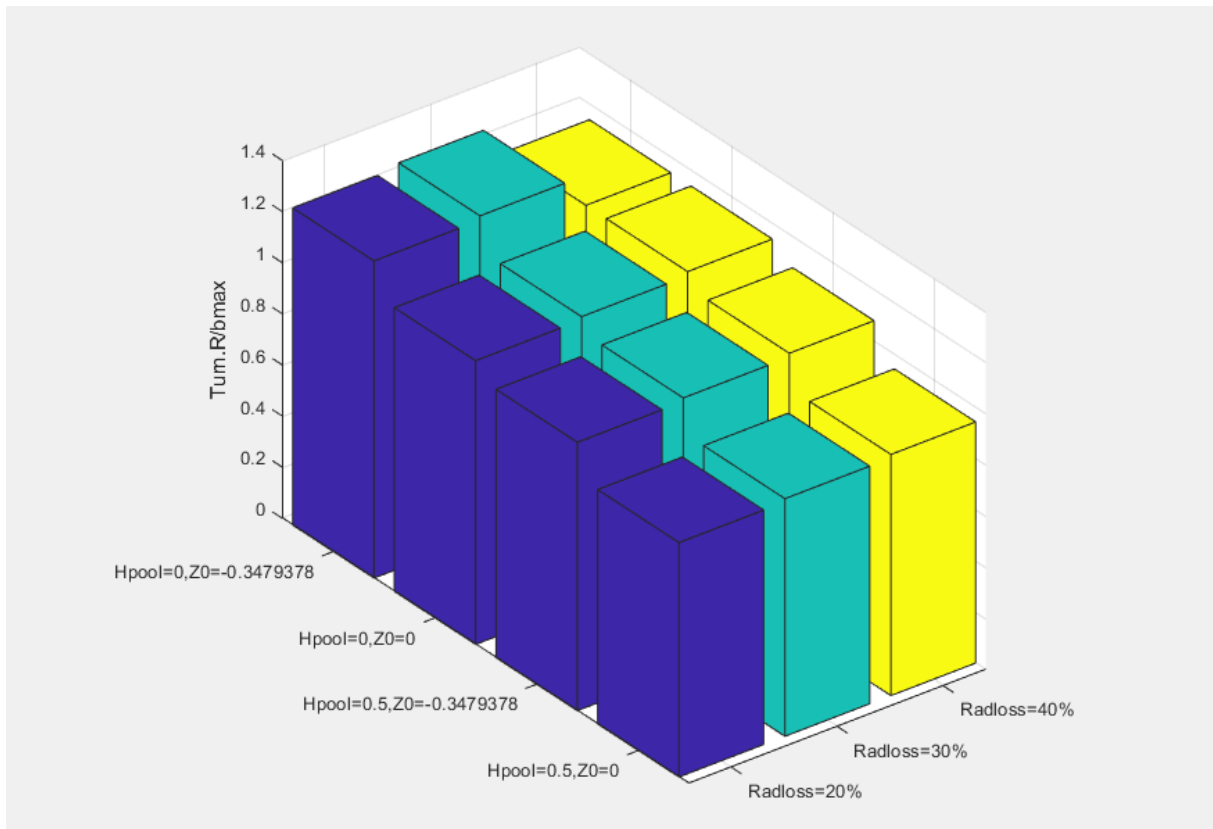


Figure III.25: Histogram showing the ratio between the turning region size and the maximum plume radius at the ceiling for the Alpert 1972 model when $H_{\text{pool}} = 0$ and $H_{\text{pool}} = 0.5\text{m}$

	Alpert 1972 $H_{\text{pool}} = 0$;	Alpert 1972 $H_{\text{pool}} = 0$;	Alpert 1972 $H_{\text{pool}} = 0.5$;	Alpert 1972 $H_{\text{pool}} = 0.5$;
--	--	--	--	--

Chapter III: Calculation, results and discussions

	$z_0 = 0$	$z_0 = -0.3479378$	$z_0 = 0$	$z_0 = -0.3479378$
Turn.R/ b_{max}	- 1.1080 (radloss= 20%)	- 1.2408 (Radloss= 20%)	- 0.9170 (radloss= 20%)	- 1.0499 (Radloss= 20%)
	- 1.1233 (radloss= 30%)	- 1.2580 (Radloss= 30%)	- 0.9296 (radloss= 30%)	- 1.0644 (Radloss= 30%)
	- 1.1400 (radloss= 40%)	- 1.2767 (Radloss= 40%)	- 0.9434 (radloss= 40%)	- 1.0801 (Radloss= 40%)

$H_{pool}=0$:

- $z_0 = 0$
 - Radloss = 20% → Turn.R/ b_{max} = **1.1080**
 - Radloss = 30% → Turn.R/ b_{max} = **1.1233**
 - Radloss = 40% → Turn.R/ b_{max} = **1.1400**
- $z_0 = -0.3479378m$
 - Radloss = 20% → Turn.R/ b_{max} = **1.2408**
 - Radloss = 30% → Turn.R/ b_{max} = **1.2580**
 - Radloss = 40% → Turn.R/ b_{max} = **1.2767**

$H_{pool}= 0.5m$:

- $z_0 = 0$
 - Radloss = 20% → Turn.R/ b_{max} = **0.9170**
 - Radloss = 30% → Turn.R/ b_{max} = **0.9296**
 - Radloss = 40% → Turn.R/ b_{max} = **0.9434**
- $z_0 = -0.3479378m$
 - Radloss = 20% → Turn.R/ b_{max} = **1.0499**
 - Radloss = 30% → Turn.R/ b_{max} = **1.0644**
 - Radloss = 40% → Turn.R/ b_{max} = **1.0801**

III.8- Alpert's Correlations - Ceiling Jets 2011 for maximum temperature

$$T_{max} - T_{\infty} = 16.9 \dot{Q}_c^{2/3} (H - Z_0)^{-5/3} \quad \text{For } \frac{r}{H-Z_0} \leq 0.2444$$

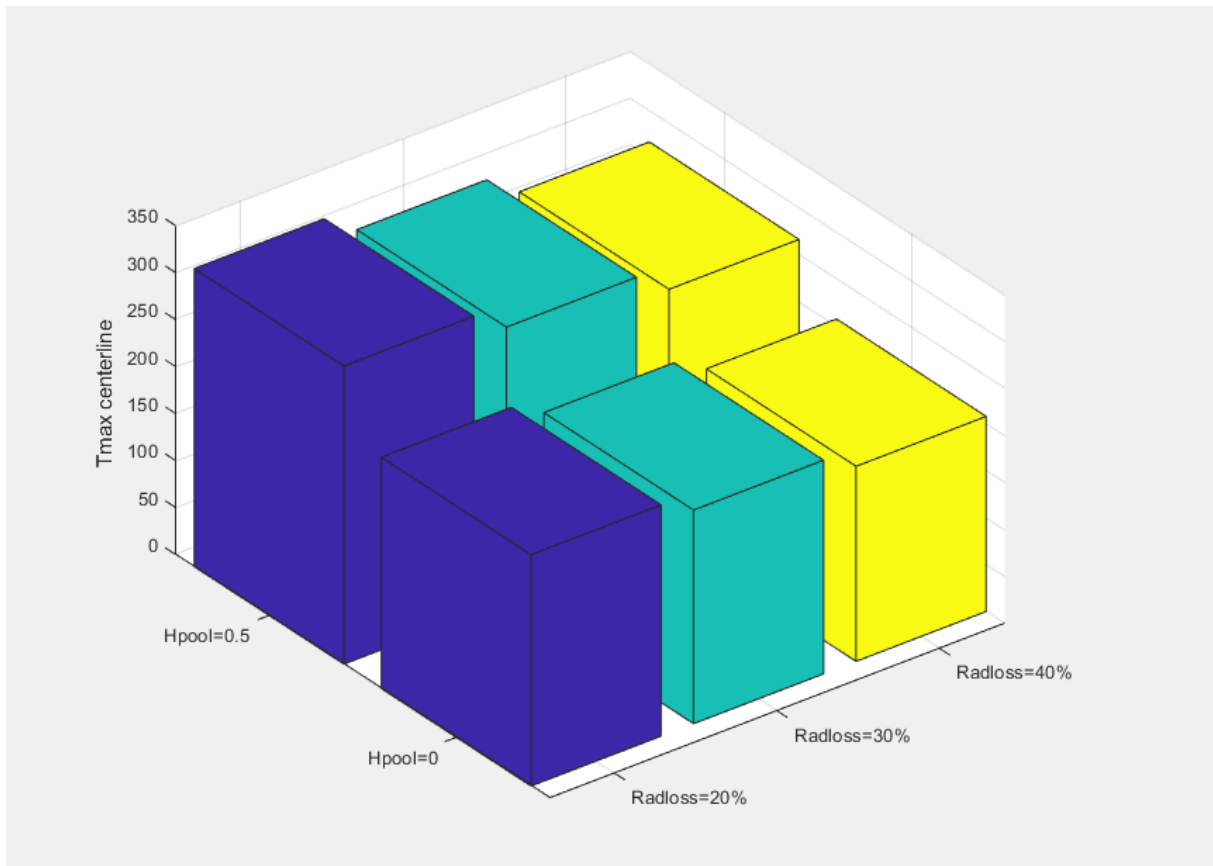
$$T_{max} - T_{\infty} = 6.721 \dot{Q}_c^{2/3} (H - Z_0)^{-5/3} \left(\frac{r}{H-Z_0} \right)^{-0.6545} \quad \text{For } \frac{r}{H-Z_0} > 0.2444$$

Chapter III: Calculation, results and discussions

At $r = 0.2444(H - z_0)$: turning region (Turn.R)

Chapter III: Calculation, results and discussions

6)



FigureIII.26: Histogram showing the centerline maximum temperature for the Alpert 2011 model when $H_{\text{pool}} = 0$ and $H_{\text{pool}} = 0.5\text{m}$

$H_{\text{pool}}=0$:

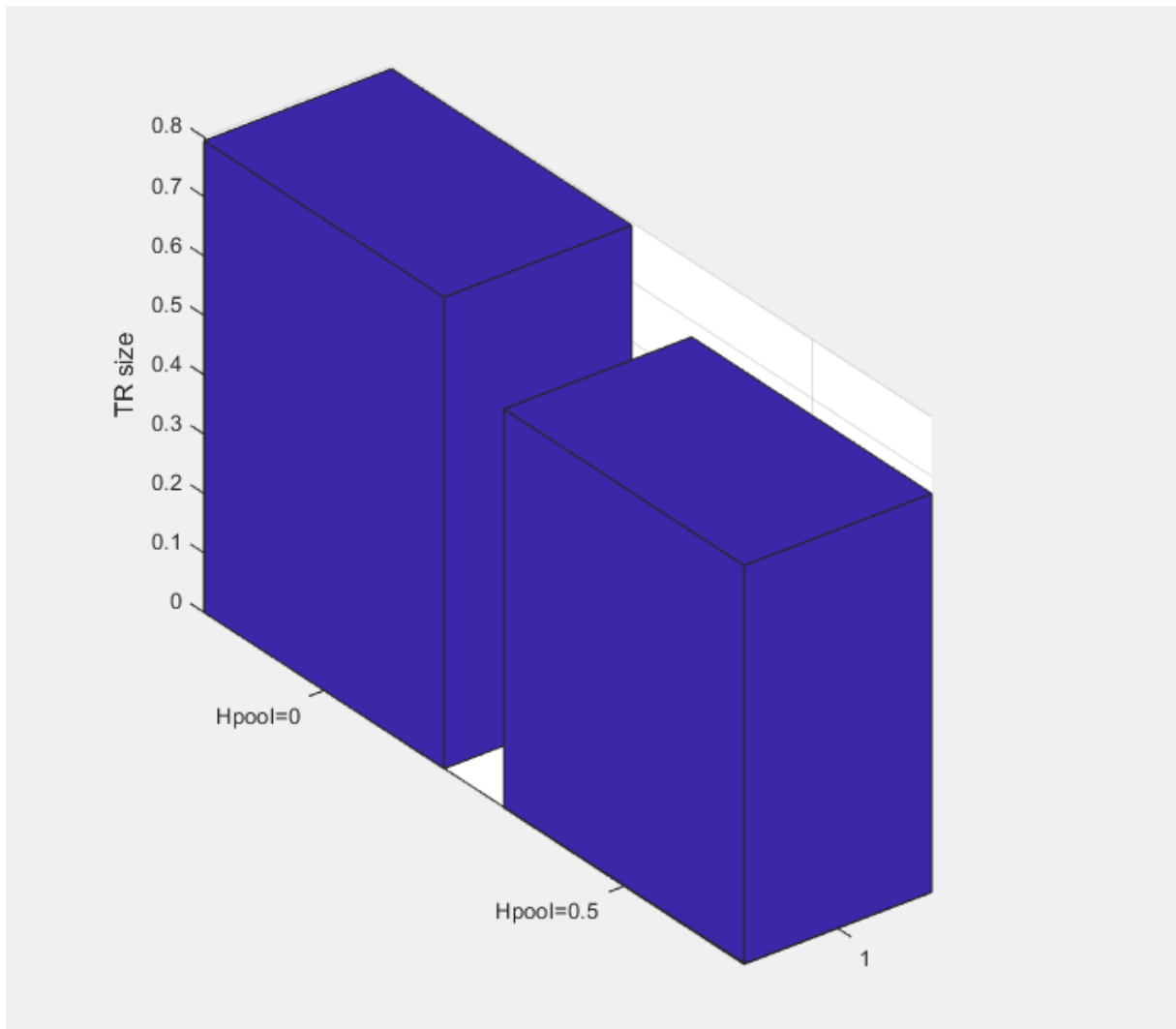
- Radloss = 20% $\rightarrow T_{\text{max_centerline}}(r = 0) = 246.1578^{\circ}\text{C}$
- Radloss = 30% $\rightarrow T_{\text{max_centerline}}(r = 0) = 227.3210^{\circ}\text{C}$
- Radloss = 40% $\rightarrow T_{\text{max_centerline}}(r = 0) = 207.5617^{\circ}\text{C}$

$H_{\text{pool}}=0.5$:

- Radloss = 20% $\rightarrow T_{\text{max_centerline}}(r = 0) = 317.2157^{\circ}\text{C}$
- Radloss = 30% $\rightarrow T_{\text{max_centerline}}(r = 0) = 292.3266^{\circ}\text{C}$
- Radloss = 40% $\rightarrow T_{\text{max_centerline}}(r = 0) = 266.2187^{\circ}\text{C}$

Chapter III: Calculation, results and discussions

7)



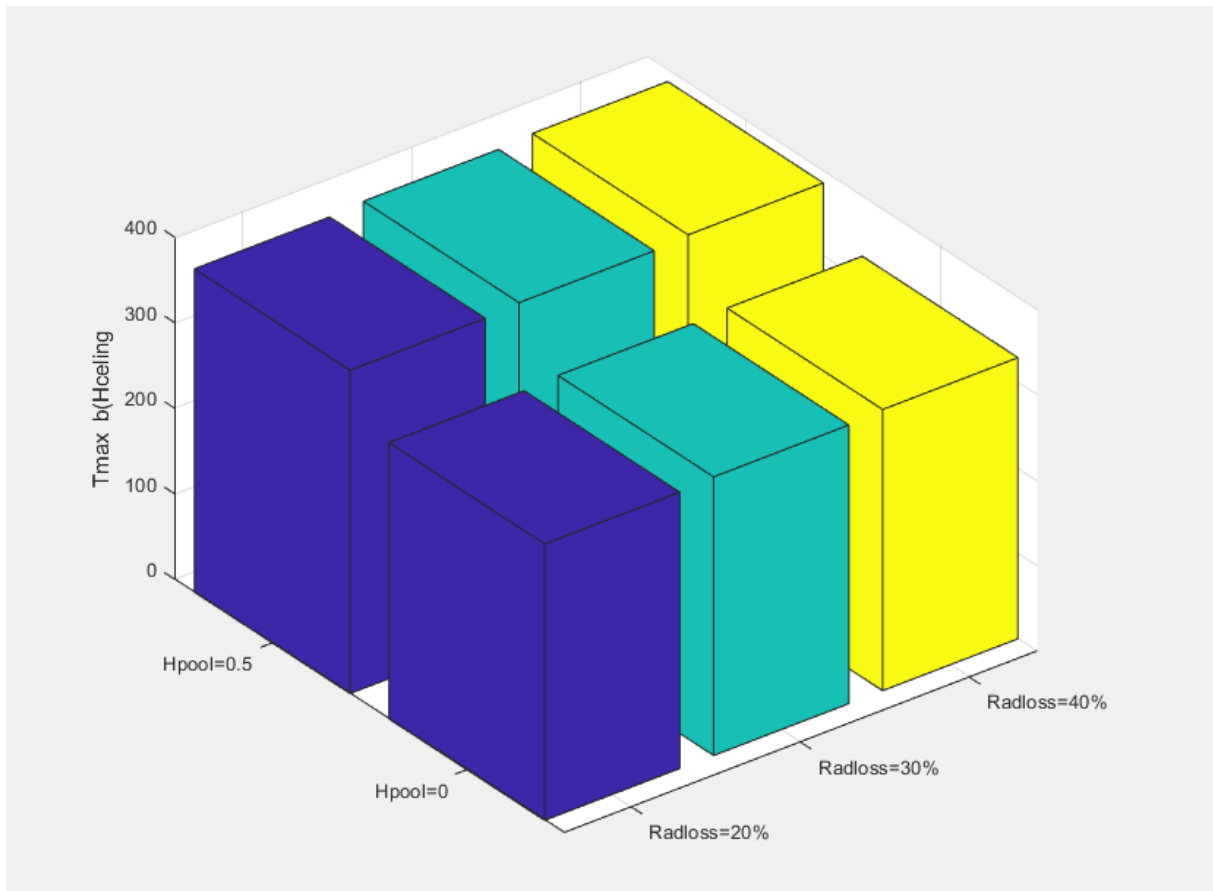
FigureIII.27: Histogram showing the turning region size for the Alpert 2011 model when $H_{pool} = 0$ and $H_{pool} = 0.5m$

$H_{pool} = 0 \rightarrow r_{turn_r} = 0.7938m$

$H_{pool} = 0.5 \rightarrow r_{turn_r} = 0.6716m$

Chapter III: Calculation, results and discussions

8)



FigureIII.28: Histogram showing the maximum temperature depending on the maximum plume radius at the ceiling for the Alpert 2011 model when $H_{pool} = 0$ and $H_{pool} = 0.5m$

$H_{pool} = 0$:

- Radloss = 20% $\rightarrow T_{max_bmax} = 323.0975^{\circ}C$
- Radloss = 30% $\rightarrow T_{max_bmax} = 325.7782^{\circ}C$
- Radloss = 40% $\rightarrow T_{max_bmax} = 328.6942^{\circ}C$

$H_{pool} = 0.5m$:

- Radloss = 20% $\rightarrow T_{max_bmax} = 378.0550^{\circ}C$
- Radloss = 30% $\rightarrow T_{max_bmax} = 381.2299^{\circ}C$
- Radloss = 40% $\rightarrow T_{max_bmax} = 384.6835^{\circ}C$

Chapter III: Calculation, results and discussions

9)

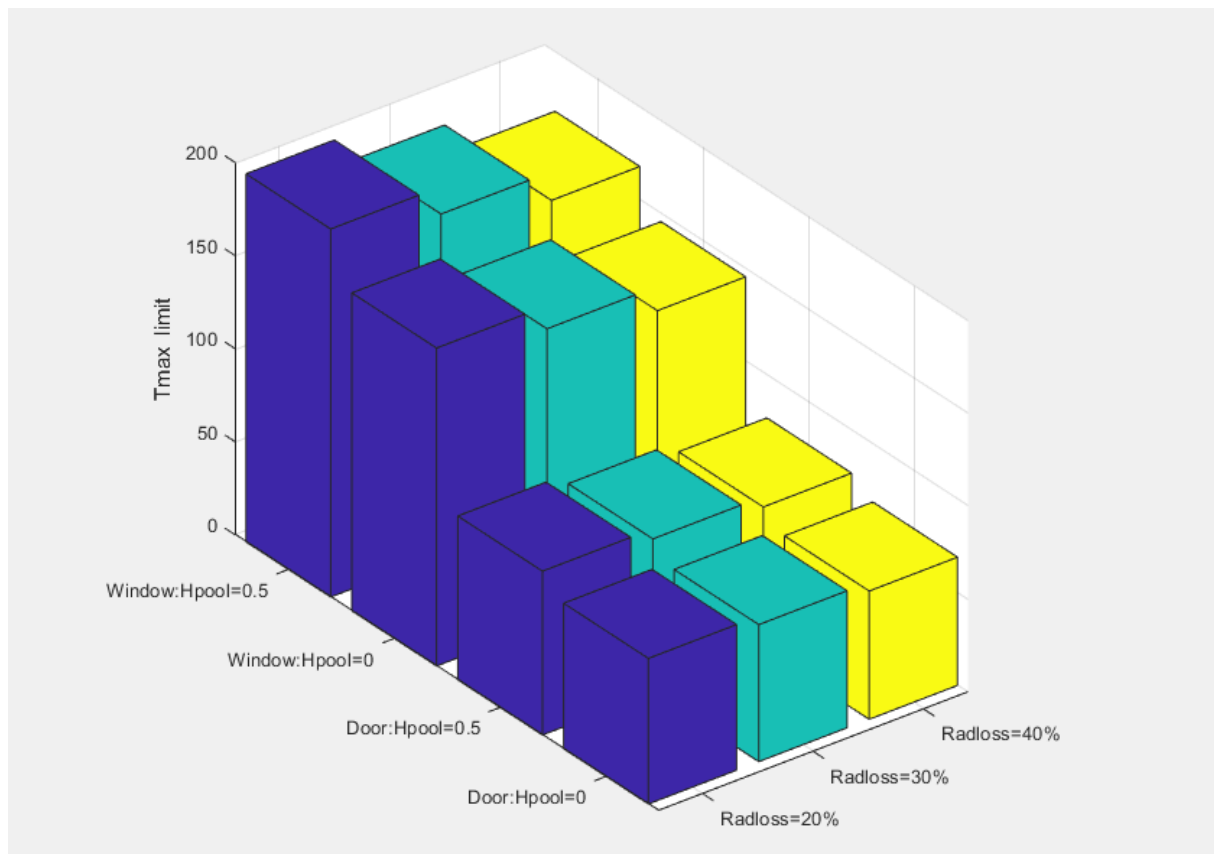


Figure III.29: Histogram showing the maximum temperature at the door and the window for the Alpert 2011 model when $H_{pool} = 0$ and $H_{pool} = 0.5$ m

Door:

$H_{pool} = 0$:

- $z_0 = -0.3479378$ m

Radloss = 20% → $T_{max_limit1} = 78.2084^\circ\text{C}$

Radloss = 30% → $T_{max_limit1} = 73.6764^\circ\text{C}$

Radloss = 40% → $T_{max_limit1} = 68.9225^\circ\text{C}$

$H_{pool} = 0.5$:

- $z_0 = -0.3479378$ m

Radloss = 20% → $T_{max_limit2} = 88.0179^\circ\text{C}$

Radloss = 30% → $T_{max_limit2} = 82.6505^\circ\text{C}$

Radloss = 40% → $T_{max_limit2} = 77.0501^\circ\text{C}$

Window:

Chapter III: Calculation, results and discussions

$H_{\text{pool}} = 0$:

- $z_0 = -0.3479378\text{m}$

Radloss = 20% → $T_{\text{max_limit1}} = 170.8293^\circ\text{C}$

Radloss = 30% → $T_{\text{max_limit1}} = 158.4085^\circ\text{C}$

Radloss = 40% → $T_{\text{max_limit1}} = 145.3795^\circ\text{C}$

$H_{\text{pool}} = 0.5\text{m}$:

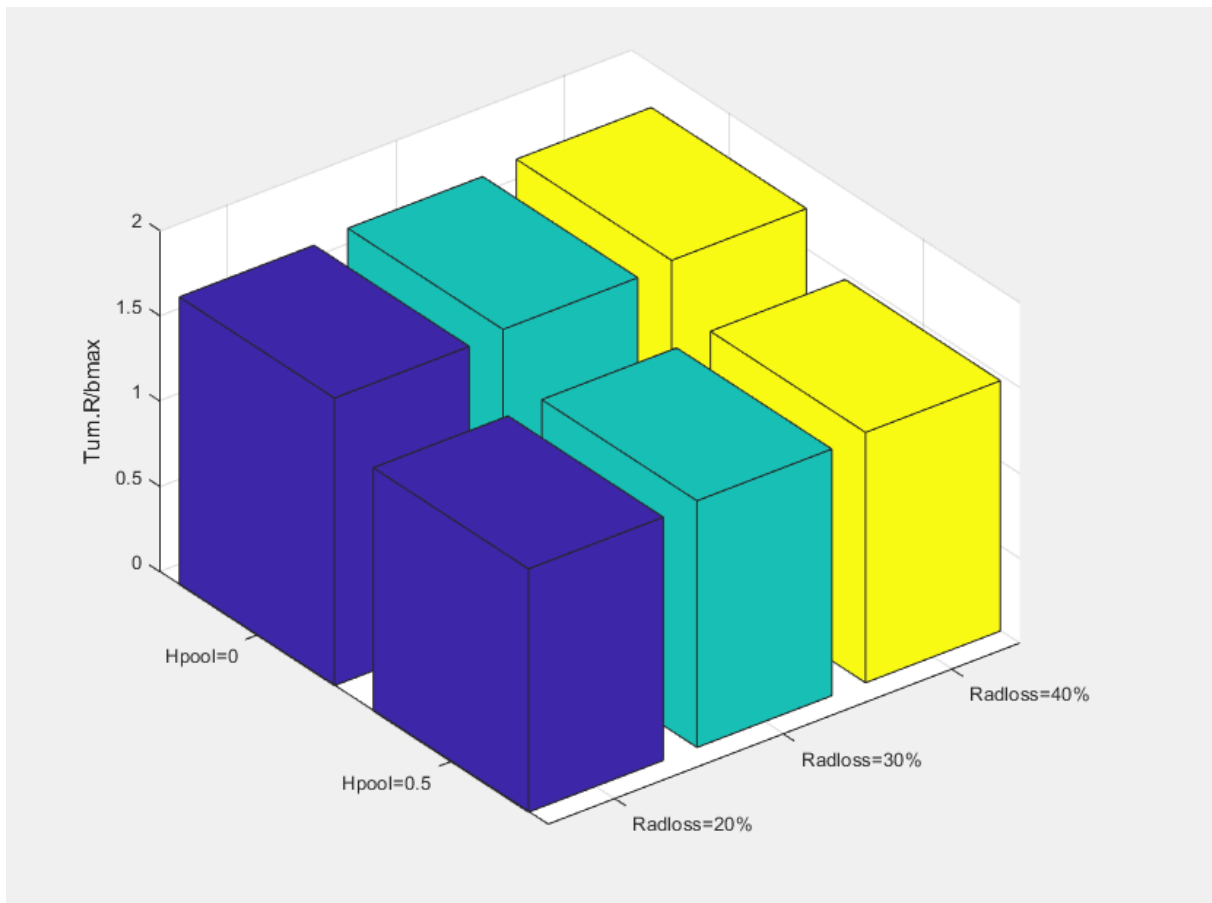
- $z_0 = -0.3479378\text{m}$

Radloss = 20% → $T_{\text{max_limit2}} = 197.7146^\circ\text{C}$

Radloss = 30% → $T_{\text{max_limit2}} = 183.0039^\circ\text{C}$

Radloss = 40% → $T_{\text{max_limit2}} = 167.5728^\circ\text{C}$

10)



FigureIII.30: Histogram showing the ratio between the turning region size and the maximum plume radius at the ceiling for the Alpert 2011 model when $H_{\text{pool}} = 0$ and $H_{\text{pool}} = 0.5\text{m}$

Chapter III: Calculation, results and discussions

	Alpert 2011 $H_{pool} = 0; z_0 = -0.3479378$	Alpert 2011 $H_{pool} = 0.5m; z_0 = -0.3479378m$
Turn.R/ b_{max}	<ul style="list-style-type: none"> - 1.6849 (radloss= 20%) - 1.7082 (radloss= 30%) - 1.7337 (radloss= 40%) 	<ul style="list-style-type: none"> - 1.4255 (radloss= 20%) - 1.4453 (radloss= 30%) - 1.4667(radloss= 40%)

$H_{pool} = 0$:

- Radloss = 20% → Turn.R/ b_{max} = **1.6849**
- Radloss = 30% → Turn.R/ b_{max} = **1.7082**
- Radloss = 40% → Turn.R/ b_{max} = **1.7337**

$H_{pool} = 0.5$:

- Radloss = 20% → Turn.R/ b_{max} = **1.4255**
- Radloss = 30% → Turn.R/ b_{max} = **1.4453**
- Radloss = 40% → Turn.R/ b_{max} = **1.4667**

III.9- Comparison between Alpert 1972 & Alpert 2011($z_0 = -0.3479378m$; $H_{pool} = 0.5m$)

11)

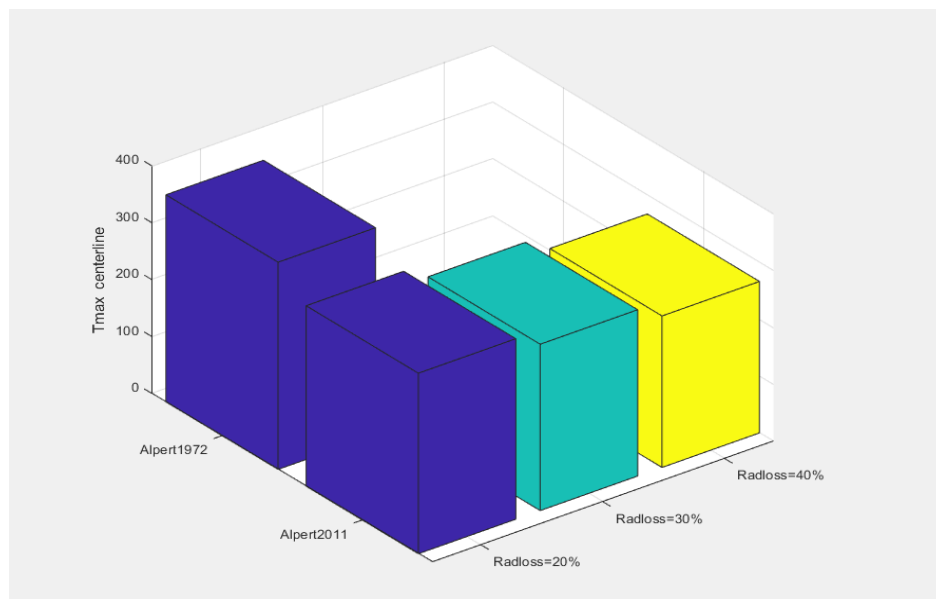


Figure III.31: Histogram showing the centerline maximum temperature for both models of Alpert 1972 and Alpert 2011 when $H_{pool} = 0.5m$

Chapter III: Calculation, results and discussions

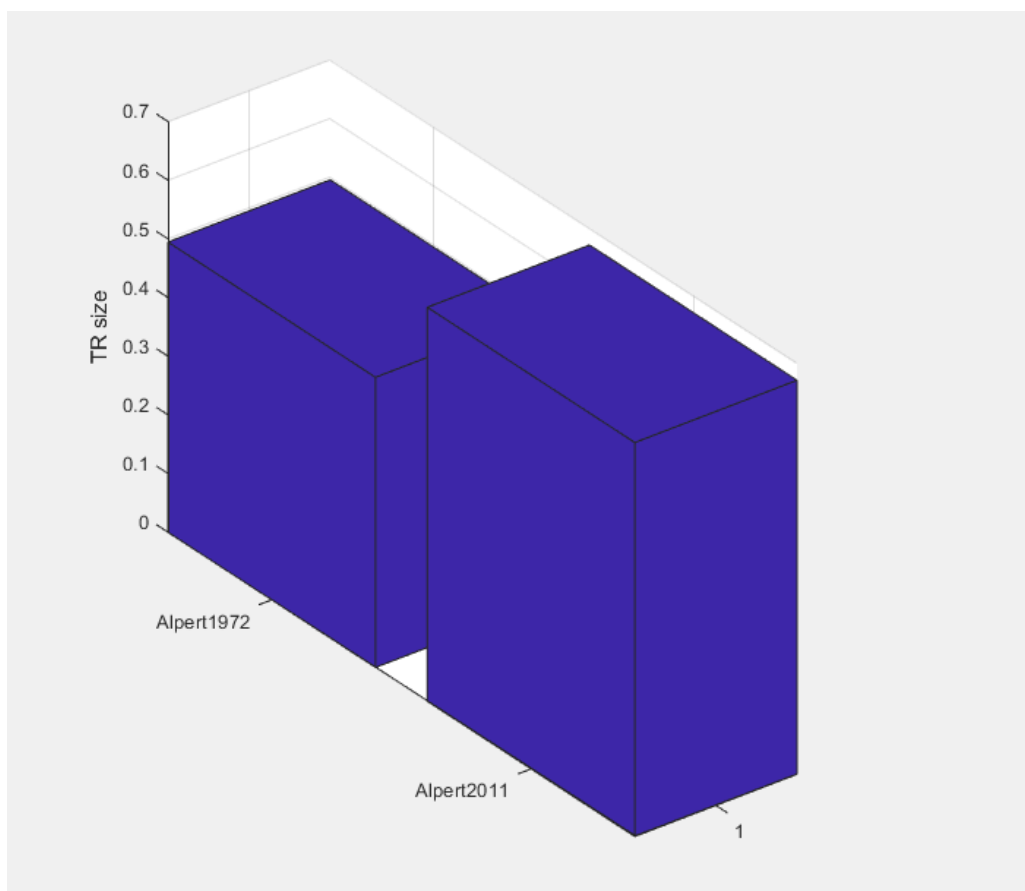
Alpert 1972:

- $T_{\text{centerline}} = 364.0863^{\circ}\text{C}$

Alpert 2011:

- $T_{\text{centerline}} = 317.2157^{\circ}\text{C}$ (radloss= 20%)
- $T_{\text{centerline}} = 292.3266^{\circ}\text{C}$ (radloss= 30%)
- $T_{\text{centerline}} = 266.2187^{\circ}\text{C}$ (radloss = 40%)

12)



FigureIII.32: Histogram showing the turning region size for both models of Alpert 1972 and Alpert 2011 when $H_{\text{pool}} = 0.5\text{m}$

Chapter III: Calculation, results and discussions

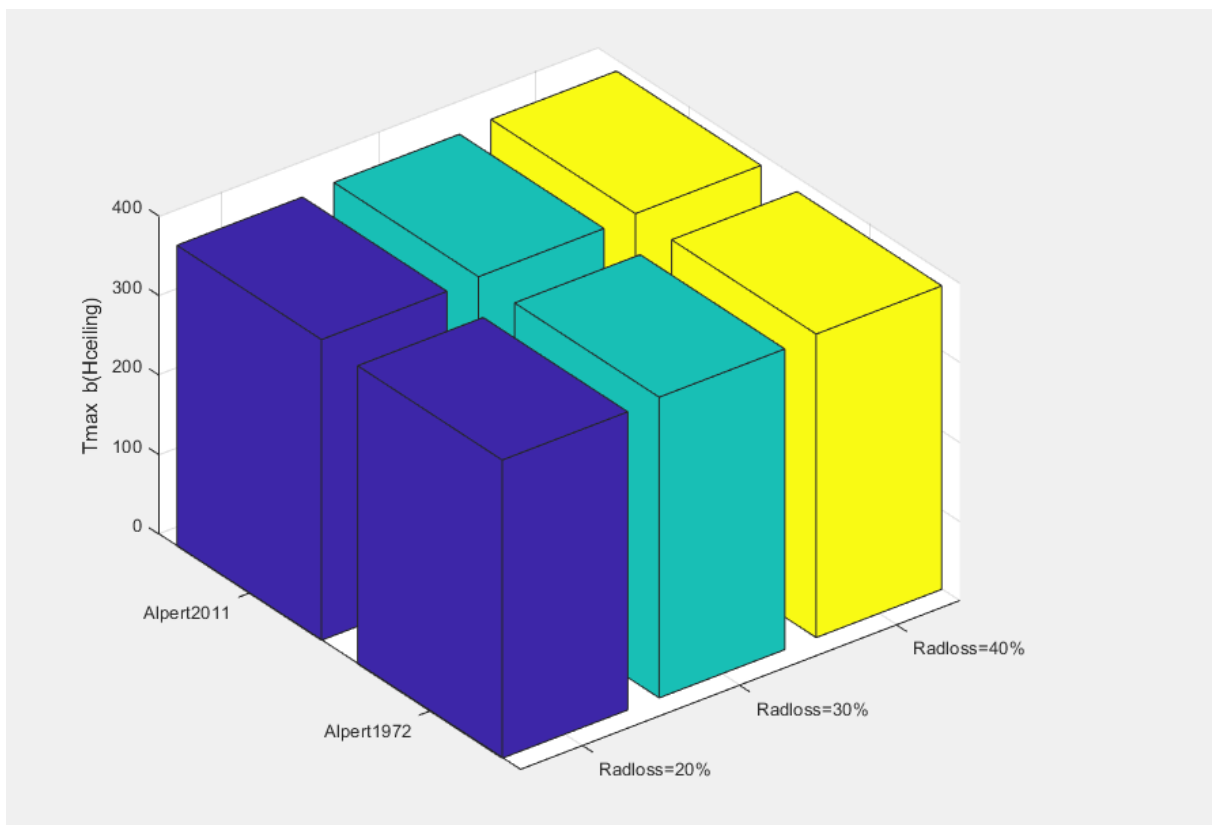
Alpert 1972:

- $r_{\text{Turn}_R} = 0.4946\text{m}$

Alpert 2011:

- $r_{\text{Turn}_R} = 0.6716\text{m}$

13)



FigureIII.33: Histogram showing the maximum temperature depending on the maximum plume radius at the ceiling for both models of Alpert 1972 and Alpert 2011 when $H_{\text{pool}} = 0.5\text{m}$

Alpert 1972:

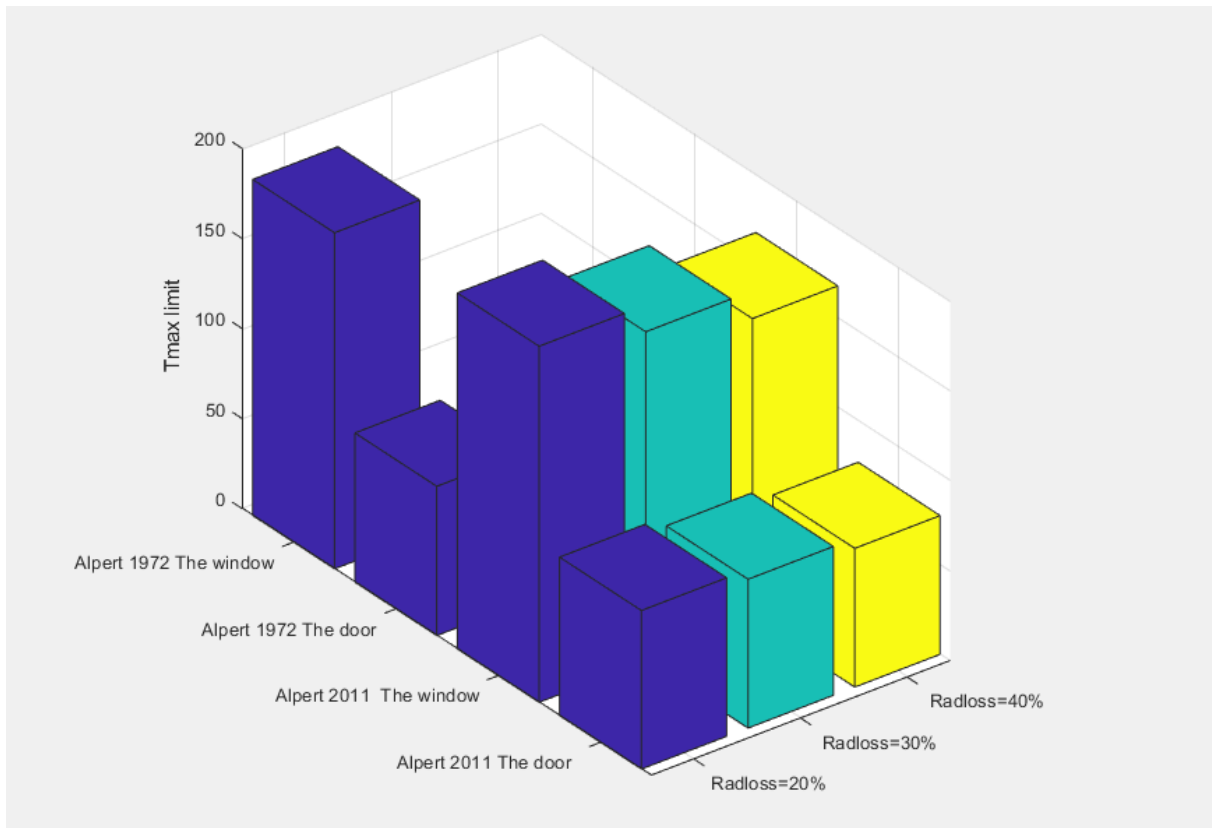
- Radloss = 20% → $T_{\text{max_bmax}} = 374.7854^{\circ}\text{C}$
- Radloss = 30% → $T_{\text{max_bmax}} = 377.9896^{\circ}\text{C}$
- Radloss = 40% → $T_{\text{max_bmax}} = 381.4757^{\circ}\text{C}$

Alpert 2011:

Chapter III: Calculation, results and discussions

- Radloss = 20% → $T_{\max_bmax} = 378.0550^{\circ}\text{C}$
- Radloss = 30% → $T_{\max_bmax} = 381.2299^{\circ}\text{C}$
- Radloss = 40% → $T_{\max_bmax} = 384.6835^{\circ}\text{C}$

14)



FigureIII.34: Histogram showing the maximum temperature at the door and the window for both models of Alpert 1972 and Alpert 2011 when $H_{\text{pool}} = 0.5\text{m}$

Alpert 1972:

- **the door**

$$T_{\max_limit1} = 82.8733^{\circ}\text{C}$$

- **the window**

$$T_{\max_limit2} = 186.6155^{\circ}\text{C}$$

Alpert 2011:

- **the door**

$$\text{Radloss} = 20\% \rightarrow T_{\max_limit2} = 88.0179^{\circ}\text{C}$$

Chapter III: Calculation, results and discussions

Radloss = 30% → $T_{\max_limit2} = 82.6505^{\circ}\text{C}$

Radloss = 40% → $T_{\max_limit2} = 77.0501^{\circ}\text{C}$

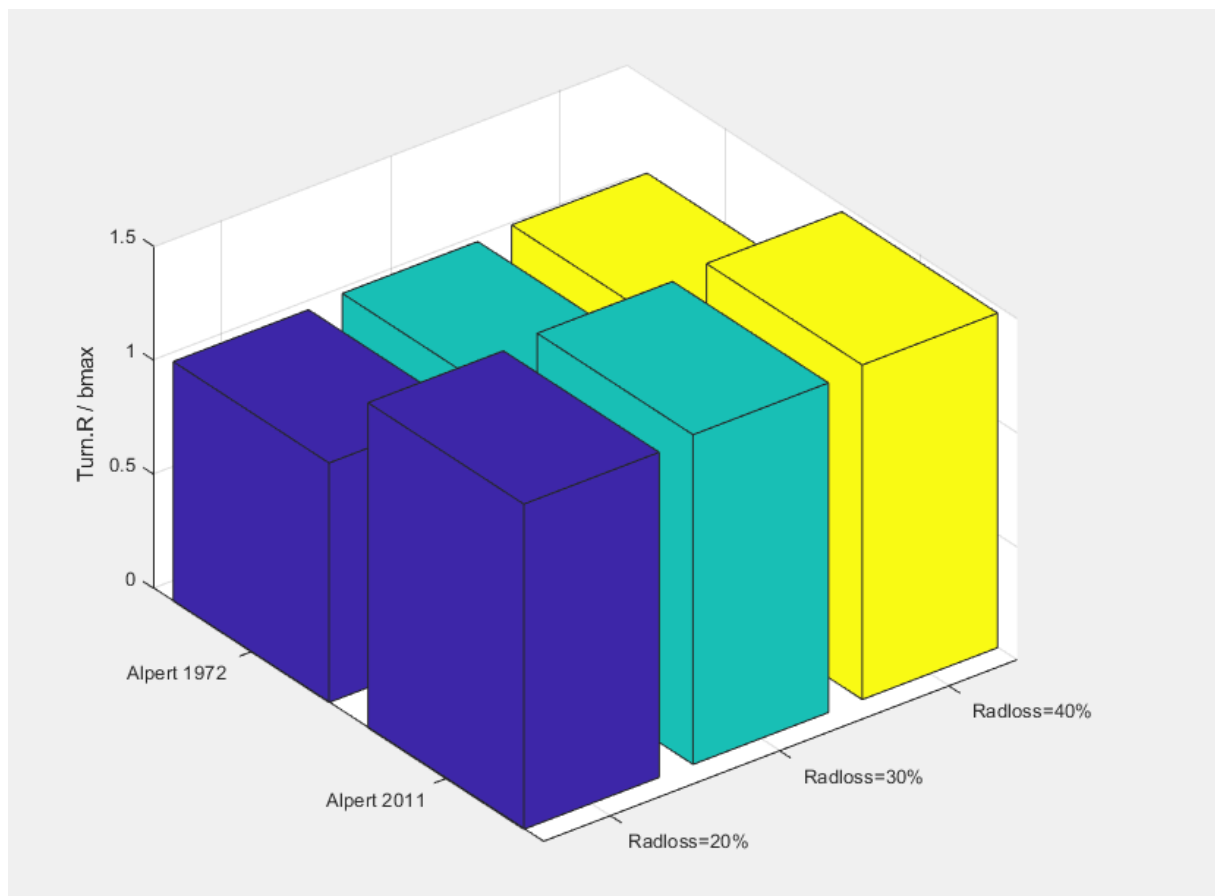
- **the window**

Radloss = 20% → $T_{\max_limit2} = 197.7146^{\circ}\text{C}$

Radloss = 30% → $T_{\max_limit2} = 183.0039^{\circ}\text{C}$

Radloss = 40% → $T_{\max_limit2} = 167.5728^{\circ}\text{C}$

15)



FigureIII.35: Histogram showing the ratio between the turning region size and the maximum plume radius at the ceiling for both models of Alpert 1972 and Alpert 2011 when $H_{\text{pool}} = 0.5\text{m}$

Alpert 1972:

- Radloss = 20% → $\text{Turn.R} / b_{\max} = 1.0499$

- Radloss = 30% → $\text{Turn.R} / b_{\max} = 1.0644$

- Radloss = 40% → $\text{Turn.R} / b_{\max} = 1.0801$

Chapter III: Calculation, results and discussions

Alpert 2011:

- Radloss = 20% → Turn.R/ b_{\max} = **1.4255**
- Radloss = 30% → Turn.R/ b_{\max} = **1.4453**
- Radloss = 40% → Turn.R/ b_{\max} = **1.4667**

III.10- Conclusion

In this chapter, we tried to calculate the variation of the fume temperature generated by the fire pool in an enclosed space (confined room). We were able to reach to some results, more or less rational, after changing the intervals with which we could get to the continuity of Alpert's functions at a new point. In fact, the former intervals weren't wrong but they treat a special case when the virtual height is zero, while the new intervals generalize the formulas making them valid with any virtual height.

General conclusion

The current study represents a numerical investigation on the flame behavior and the fume spreading within a confined or a semi-confined or an open room.

Two types of heat transfer modes that relate to the phenomenon we have studied (radiative and convective) have been shown schematically. The phenomenon of fire is always more difficult to model, especially in the case of complex geometries with different parameters. The numerical study by means of the calculation code of the fire dynamics (FDS) makes it possible to build a rich bibliographic base in the field of safety and prevention against fire.

At the research level, this work has allowed us to get to the bottom of the problem by using commercial software in a field as important for researchers as for engineers. Among the parametric analyzes carried out during this work, some of them have been shown in this thesis. Thermal parameters play a major role in the protection against thermal effects and more specifically burns.

The fire pool, releasing a heat rate, is localized in the compartment with unconfined ceiling jet using a specific dimension of the fire and using thermocouples on the ceiling to get results for the maximum temperature of the hot gases near the ceiling. These results were calculated with simple correlative models (Alpert and Heskestad).

Correlative results are usually derived from experimental results and the numerical models are used to solve differential equations.

The confrontation between correlative, two zones and CFD models can improve the knowledge state on the ceiling-jets and probably helps the fire engineers to enhance the performance of the fire protection devices.

Bibliography

- [1] Carleton University, 82.583 (CVG ****), FIRE DYNAMICS II, Winter 2003, Lecture #2
- [2] INERIS, S.JOLLE ; Formation du savoir et des outils dans le domaine des risques majeurs- Modélisation de feux industriels ; Rapport d'étude, Réf : DRA-14-141478-03176A, 13/03/2014.
- [3] J. G. Quintiere, "Chap 11, Compartment Fires,," in *Fundamentals of Fire Phenomena*, March 2006..
- [4] Lamballais Pierre-Louis ; www.Flashover.fr
- [5] K.Lambert & K.Desmet ; L'attaque à l'intérieur-Principe de bases lors des feux compartimentés ; Livre ; Centre de formation des pompiers de Bruxelles asbl ; 04/02/2008.
- [6] BSEF, Powering science and technologies, www.bsef.com
- [7] [feuerwehr](http://feuerwehr.de), www.feuerwehr.de
- [8] Hartin Ed, Compartment fire development, www.firehouse.com
- [9] S.Deniau, Etude des flux thermiques d'un feu de graisses soleval, Rapport d'étude, Ref : N°15545649, 25/05/2016.
- [10] E.Guillaum, Effets du feu sur les personnes, Synthèse bibliographique, Laboratoire National de métrologie et d'essais (LNE) de Trappes, juillet 2006.
- [11] A.Oliveira, Conception et développement de capteurs et vêtements intelligents pour le suivi et la protection des pompier, thèse de doctorat, L'institut National des Sciences Appliquées de Lyon, 20/01/2011.
- [12] E. 1991-1-2, Eurocode 1—basis of design and actions on structures—part 1—2:actions on structures exposed to fire, 2002.
- [13] Heskestad, G., 'Fire Plumes', SEPE Handbook of Fire Protection Engineering, 2nd ed., National Fire Protection Association, Quincy MA 1995.
- [14] A. S. J. P. R. a. P. B. Gonc, alo Ferraz, «Thermal Analysis of Hollow Steel Columns Exposed to Localised Fires,» *Fire Technology*, 2016.

- [15] Björn Karlsson James G. Quintiere, Enclosure Fire Dynamics, Björn Karlsson, Ph.D., James G. Quintiere, Ph.D.M.E., 1999.
- [16] Morton, B.R., Taylor, G.I. and Turner, J.S., , «Turbulent Gravitational Correction From Maintained and Instantaneous Sources.,» *Proc. R. Soc. Lond.A*, pp. 1-23, 1956.
- [17] Ingason H, Li YZ, «Model scale tunnel fire tests with longitudinal ventilation,» *Fire Safety Journal*, pp. 371-384, 2010.
- [18] Ingason H, Li YZ, "Model scale tunnel fire tests with point extraction ventilation.," *Journal of Fire Protection Engineering*, pp. 5-36, 2011.
- [19] S. L. a. J. W. Wei Yao, «Numerical Prediction of Effects of Gravity on the Centerline Temperature and Velocity of Axi-symmetric Fire Plumes,» *Journal of Fire Sciences* , 2007.
- [20] Gunnar Heskestad, Michael A. Delichatsios, «The Initial Convective Flow in Fire,» *Fire Safety Journal*, 1989.
- [21] Alpert, R.L, «Turbulent Ceiling-Jet Induced by Large-Scale Fires,» *Combustion Science*
- [22] David D. Evans, «CEILING JET FLOWS,» *Fire Protection Engineering*, DiNenno, P.J., et al., 2004, pp. 2/32-2/39 .
- [23] Alpert, R.L, “Calculations of response time of ceiling mounted fire detectors”, *Fire Technology* Vol. 8, 1972.
- [24] Johansson, Nils; Wahlqvist, Jonathan; Van Hees, Patrick, "Simple Ceiling Jet Correlation
- [25] McCaffrey, G., 'Fire Plumes', *SEPE Handbook of Fire Protection Engineering*, 2nd ed., National Fire Protection Association, Quincy MA 1995.
- [26] Desanghere, S. – “*External structure heating determination due to fire*”, Phd Thesis, National Institute of Applied Science of Rouen, France, 2006, 301 p.

Annex:

applications of FDS

1- Starting an FDS Calculation (Single Processor Version)

Sample input files are provided with the program for new users who are encouraged to first run a sample calculation before attempting to write an input file. Assuming that an input file called FIRELESS.fds exists in some directory, run the program either in a DOS or Unix command prompt as follows:

Open up a Command Prompt window (click Start, then Run, then type “cmd”), and change directories (“cd”) to where the input file for the case is located, then run the code by typing at the command prompt `fds5 job_name.fds`

The character string FIRELESS is usually designated within the input file as the CHID. It is recommended that the name of the input file and the CHID be the same so that all of the files associated with a given calculation have a consistent name. The progress of a simulation is indicated by diagnostic output that is written out onto the screen. Detailed diagnostic information is automatically written to a file CHID.out, where CHID is a character string, usually the same as FIRELESS, designated in the input file. Screen output can be redirected to a file via the alternative command `fds5 fireless.fds > fireless.err`

Note that it is also possible to associate the extension “fds” with the FDS executable directly, thereby making FDS run by double-clicking on the input file. If you do this, note that error messages will be written to the .out file. Also, if you associate the input file with the FDS executable, be careful not to accidentally double click on the input file when trying to edit it. This action will cause previously generated output files to be over-written.

Depending on the type of installation, you may need to set various path or environment variables in order to invoke FDS without a full path reference to the executable. The easiest way to do this is via an “alias” in your shell start-up script. For the example below, it is assumed that `fds5` is aliased to its full path name. You may also need to “`chmod + x`” to make the file executable. Once this is done, run FDS from the command line by typing: `fds5 job_name.fds`

The input parameters are read from the file `fireless.fds`, and error statements and other diagnostics are written out to the screen. To run the job in the background: `fds5 fireless.fds >& fireless.err &`

Note that in the latter case, the screen output is stored in the file `fireless.err` and the detailed diagnostics are saved automatically in a file `CHID.out`, where `CHID` is a character string, usually the same as “`fireless`”, designated in the input file. It is preferable to run jobs in the background so as to free the console for other uses.

2- Starting an FDS Calculation (Multiple Processor Version)

Running FDS across a network using multiple processors and multiple banks of memory (RAM) is more difficult than running the single processor version. More is required of the user to make the connections between the machines as seamless as possible. This involves creating accounts for a given user on each machine, sharing directories, increasing the speed of the network, making each machine aware of the others, etc.

FDS uses MPI (Message-Passing Interface) to allow multiple computers to run a single FDS job. The main idea is that you must break up the FDS domain into multiple meshes, and then the flow field in each mesh is computed as a different process. Note the subtle difference between these terms – a process does not have the same meaning as a processor. The process can be thought of as a “task” that you would see in the Windows Task Manager or by executing the “`top`” command on a Linux/Unix machine. The processor refers to the computer hardware. A single processor may run multiple processes, for example. The computation on a given FDS mesh is thought of as an individual process, and MPI handles the transfer of information between these processes. Usually, each mesh is assigned its own process in a parallel calculation although it is also possible assign multiple meshes to a single process. In this way, large meshes can be computed on dedicated processors, while smaller meshes can be clustered together in a single process running on a single processor, without the need for MPI message passing between themselves.

Also note that FDS refers to its meshes by the numbers 1, 2, 3, and so on, whereas MPI refers to its processes by the numbers 0, 1, 2, and so on. Thus, Mesh 1 is assigned to Process 0; Mesh 2 to Process 1, and so on. As a user, you never actually number the meshes or the processes yourself, but error statements from FDS or from MPI might refer to the meshes or processes by number. As an example, if a five mesh FDS case is run in parallel, the first printout (usually to the screen unless otherwise directed) is:

```
Process 4 of 4 is running on fire65
```

```
Process 3 of 4 is running on fire64
```

Process 2 of 4 is running on fire63

Process 0 of 4 is running on fire61

Process 1 of 4 is running on fire62

Mesh 1 is assigned to Process 0

Mesh 2 is assigned to Process 1

Mesh 3 is assigned to Process 2

Mesh 4 is assigned to Process 3

Mesh 5 is assigned to Process 4

This means that 5 processes (numbered 0 to 4) have started on the computers named fire61, fire62, etc., and that each mesh is being computed as an individual process on the individual computers. Each computer has its own memory (RAM), and MPI is the protocol by which information is passed from process to process during the calculation. Note that these computers may have multiple processors, and each processor may have multiple “cores.” You have control over how many processes get assigned to each computer, but you may or may not have control over how the processes are handled by a given computer. That depends on the operating system and the particular version of MPI. For example, fire62 happens to have two quad-core processors, and all five meshes could have been assigned to run as five processes all on fire62.

There are different implementations of MPI, much like there are different Fortran and C compilers. Each implementation is essentially a library of subroutines called from FDS that transfer data from one thread to another across a fast network.

The way FDS is executed in parallel depends on which implementation of MPI has been installed. At NIST, the parallel version of FDS is presently run on Windows PCs connected by the Local Area Network

(LAN, 100 Mbps) or on a cluster of Linux PCs linked together with a dedicated, fast (1000 Mbps) network. The Windows computers use MPICH2, a free implementation of MPI from Argonne National Laboratory, USA.

With MPICH2, a parallel FDS calculation can be invoked either from the command line or by using a Graphical User Interface (GUI). After the MPICH2 libraries are installed on each computer and the necessary directories are shared, FDS is run using the command issued from one of the computers `mpixec -file config.txt` where `config.txt` is a text file containing the

name and location of the FDS executable, name of the FDS input file, the working directory, and the names of the various computers that are to run the job. For example, the config.txt file might look like this for a job run at NIST with computers named fire_1, fire_2, and fire_3:

```
exe \\fire_1.nist.gov\NIST\FDS\fds5_mpi.exe fireless.fdsdir\\fire_1.nist.gov\Projects\ hosts
```

```
fire_1.nist.gov 2
```

```
fire_2.nist.gov 1
```

```
fire_3.nist.gov 2
```

The numbers following the “host” machines represent the number of threads to run on that particular machine.

In this example, 5 threads are run for an FDS calculation that has 5 meshes. The exe and dir directories need to be shared, with the latter having read and write permissions.

All the computers must be able to access the executable and the working directory on fire_1. This is achieved under Windows by “sharing.” Under Unix/Linux and OS X, the process involves cross-mounting the file systems of the various machines.

On the Linux cluster in the Building and Fire Research Lab at NIST, LAM-MPI, a free implementation from Indiana University, is installed. With LAM/MPI, the computers to be used are linked prior to the actual execution of FDS with a separate command called a “lamboot.” FDS is then run using the command `mpirun -np5 fds5_mpi fireless.fds`, where the 5 indicates that 5 processors are to be used. In this case, the executable `fds5_mpi` is located in the working directory. To make the process run in the background `mpirun -np 5 fds5_mpi fireless.fds >& job_name.err &`

The file `job_name.err` contains what is normally printed out to the screen.

3- Monitoring Progress

Diagnostics for a given calculation are written into a file called `CHID.out`. The CPU usage and simulation time are written here, so you can see how far along the program has progressed. At any time during a calculation, `Smokeyview` can be run and the progress can be checked visually. To stop a calculation before its scheduled time, either kill the process, or preferably create a file in the same directory as the output files called `CHID.stop`. The existence of this file stops the program gracefully, causing it to dump out the latest flow

variables for viewing in Smokeview. Since calculations can be hours or days long, there is a restart feature in FDS.

Briefly, specify at the beginning of calculation how often a “restart” file should be saved. Should something happen to disrupt the calculation, like a power outage, the calculation can be restarted from the time the last restart file was saved.

It is also possible to control the stop time and the dumping of restart files by using control functions

4- User Support

FDS is not a typical PC application. It is a serious calculation that pushes your computer’s processor and memory to its limits. In fact, there are no hardwired bounds within FDS that prevent you from starting a calculation that is too much for your hardware. Even if your machine has adequate memory (RAM), you can still easily set up calculations that can require weeks or months to complete. It is difficult to predict at the start of a simulation just how long and how much memory will be required. Learn how to monitor the resource usage of your computer. Start with small calculations and build your way up. FDS is used for practical engineering applications, but also for research in fire and combustion. As you become more familiar with the software, you will inevitably run into areas that are of current research interest. Indeed, burning a roomful of ordinary furniture is one of the most challenging applications of the model.

5- Version Number

If you encounter problems with FDS, it is crucial that you submit, along with a description of the problem, the FDS version number. Each release of FDS comes with a version number like 5.2.6, where the first number is the major release (occurring every few years), the second is the minor release (occurring every few months and may cause minor changes in functionality), and the third is the maintenance release which are just bug fixes, and should not affect code functionality. Release notes can help you decide whether the changes should effect the type of applications that you typically do. To get the version number, just type the executable at the command prompt: `fds5` and the relevant information will appear, along with a date of compilation and a so-called SVN number. The SVN number refers to the Subversion repository number of the source code. It allows us to go back in time and recover the exact source code files that were used to build that executable.

6- Common Error Statements

An FDS calculation may end before the specified time limit. Following is a list of common error statements and how to diagnose the problems:

Input File Errors: The most common errors in FDS are due to mis-typed input statements. These errors result in the immediate halting of the program and a statement like, “ERROR: Problem with the HEAD line.” For these errors, check the line in the input file named in the error statement. Make sure the parameter names are spelled correctly. Make sure that a / (forward slash) is put at the end of each namelist entry and that the right type of information is being provided for each parameter, like whether one real number is expected, or several integers, or whatever. Make sure there are no non-ASCII characters being used, as can sometimes happen when text is cut and pasted from other applications or word-processing software. Make sure zeros are zeros and O’s are O’s and 1’s are not !’s. Make sure apostrophes are used to designate character strings and the text file on a Unix/Linux machine was not created on a DOS machine, and vice versa. All the parameters listed have to be used – new versions of FDS often drop or change parameters to force you to re-examine old input files.

Numerical Instability Errors: It is possible that during an FDS calculation the flow velocity at some location in the domain can increase due to numerical error causing the time step size to decrease to a point where logic in the code decides that the results are unphysical and stops the calculation with an error message in the file CHID.out. In these cases, FDS ends by dumping out one final Plot3D file giving the user some means by which to see where the error is occurring within the computational domain. Usually, a numerical instability can be identified by fictitiously large velocity vectors emanating from a small region within the domain. Common causes of such instabilities are mesh cells that have an aspect ratio larger than 2 to 1, high speed flow through a small opening, a sudden change in the heat release rate, or any number of sudden changes to the flow field. There are various ways to solve the problem, depending on the situation. Try to diagnose and fix the problem before reporting it.

Inadequate Computer Resources: The calculation might be using more RAM than the machine has, or the output files could have used up all the available disk space. In these situations, the computer may or may not produce an intelligible error message. Sometimes it is your responsibility to ensure that the computer has adequate resources to do the calculation.

There is no limit to how big or how long FDS calculations can be – it depends on the resources of the computer. For any new simulation, try running the case with a modest-sized mesh, and gradually make refinements until the computer can no longer handle it. Then back off somewhat on the size of the calculation so that the computer can comfortably run the case. In fact, for a typical 32 bit Windows PC with 4 GB RAM, only 2 GB will be available to FDS, based on user feedback. In case of running bigger cases, a computer with a 64 bit operating system will be needed or one has to break up the calculation into multiple meshes and use parallel processing.

Run-Time Errors: An error occurs either within the computer operating system or the FDS program. An error message is printed out by the operating system of the computer onto the screen or into the diagnostic output file. This message is most often unintelligible to most people, including the programmers, although occasionally one might get a small clue if there is mention of a specific problem, like “stack overflow,” “divide by zero,” or “file write error, unit=...” These errors may be caused by a bug in FDS, for example if a number is divided by zero, or an array is used before it is allocated. Before reporting the error to the Issue Tracker, try to systematically simplify the input file until the error goes away.

File Writing Errors: Occasionally, FDS fails because it is not permitted to write to a file. A typical error statement reads: `fortrl: severe: write to READONLY file, unit 8598, file C:\Users\...\`

The unit, in this case 8598, is just a number that FDS has associated with one of the output files. If this error occurs just after the start of the calculation, you can try adding the phrase `FLUSH_FILE_BUFFERS=.FALSE.` on the DUMP line of the input file. This will prevent FDS from attempting to flush the contents of the internal buffers, something it does to make it possible to view the FDS output in Smokeview during the FDS simulation.

Poisson Initialization: Sometimes at the very start of a calculation, an error appears stating that there is a problem with the “Poisson initialization.” The equation for pressure in FDS is known as the Poisson equation. The Poisson solver consists of large system of linear equations that must be initialized at the start of the calculation. Most often, an error in the initialization step is due to a mesh IJK dimension being less than 4 (except in the case of a two-dimensional calculation). It is also possible that something is fundamentally wrong with the coordinates of the computational domain.

7- Basic Structure of an Input File

7.1- Naming the Job

The input file provides FDS with all of the necessary information to describe the scenario. The input file is saved with a name such as job_name.fds, where job_name is any character string that helps to identify the simulation. If this same string is repeated under the HEAD namelist group within the input file, then all of the output files associated with the calculation will then have this common name.

There should be no blank spaces in the job name. Instead use the underscore character to represent a space and which also applies to the general practice of naming directories on the system. Be aware that FDS will simply overwrite the output files of a given case if its assigned name is the same. This is convenient when developing an input file because you save on disk space. Just be careful not to overwrite a calculation that you want to keep.

7.2- Namelist Formatting

Parameters are specified within the input file by using namelist formatted records. Each namelist record begins with “&” followed immediately by the name of the namelist group, then a comma-delimited list of the input parameters, and finally a forward slash “/”. For example, the line &DUMP NFRAMES=1800, DT_HRR=10., DT_DEVC=10., DT_PROF=30. / sets various values of parameters contained in the DUMP namelist group. The namelist records can span multiple lines in the input file, but just be sure to end the record with a “/” or else the data will not be understood. Do not add anything to a namelist line other than the parameters and values appropriate for that group. Otherwise, FDS will stop immediately upon execution.

Parameters within a namelist record can be separated by either commas, spaces, or line breaks. Comments and notes can be written into the file so long as nothing comes before the & except a space and nothing comes between & and / except appropriate parameters corresponding to that particular namelist group.

The parameters in the input file can be integers (T_END=5400), real numbers (CO_YIELD=0.008), groups of real numbers or integers (XYZ=6.04,0.28,3.65) or (IJK=90,36,38), character strings: CHID='WTC_05_v5' groups of character strings: SURF_IDS='burner','STEEL','BRICK' or logical parameters: POROUS_FLOOR=.FALSE.

A logical parameter is either .TRUE. or .FALSE.

Most of the input parameters are simply real or integer scalars, like $DT=0.02$, but sometimes the inputs are multidimensional arrays. For example, when describing a particular solid surface, you need to express the mass fractions of multiple materials that are to be found in multiple layers. The input array `MATL_MASS_FRACTION(IL,IC)` is intended to convey to FDS the mass fraction of component `IC` of layer `IL`. For example, if the mass fraction of the second material of the third layer is 0.5, then write `MATL_MASS_FRACTION(3,2)=0.5`

To enter more than one mass fraction, use this notation:

`MATL_MASS_FRACTION(1,1:3)=0.5,0.4,0.1` which means that the first three materials of layer 1 have mass fractions of 0.5, 0.4, and 0.1, respectively. The notation `1:3` means array element 1 through 3, inclusive.

Be careful not to create the input file by pasting text from something other than a simple text editor, in which case the punctuation marks may not transfer properly into the text file.

If file reading errors occur and no typographical errors can be found in the input file, try saving the input file using a different encoding.

7.3- Input File Structure:

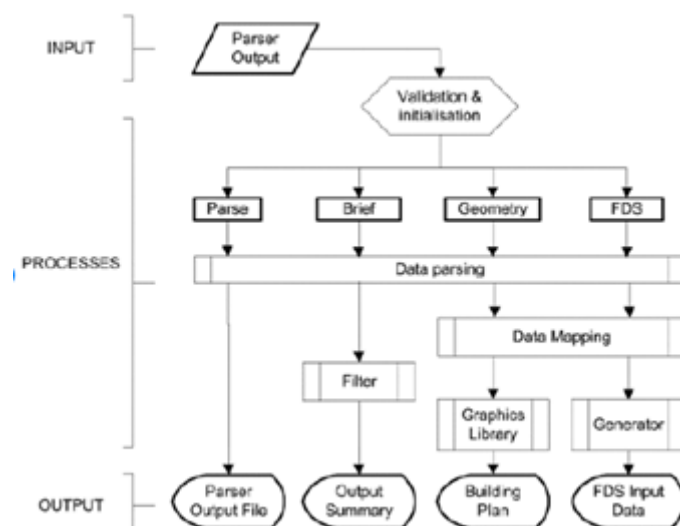


Figure1: FDS input structure

It is a good idea to organize the namelist records in some systematic way. Typically, general information are listed near the top of the input file, and detailed information, like obstructions,

devices, and so on, are listed below. FDS scans the entire input file each time it processes a particular namelist group.

To ensure the reading of the last line of the file, FDS reads the entire input file, add &TAIL / as the last line at the end of the input file. This completes the file from &HEAD to &TAIL. FDS does not even look for this last line. It just forces the “end of file” character past relevant input.

Another general rule of thumb when writing input files is to only add to the file parameters that are to change from their default value. That way, you can more easily distinguish between what you want and what FDS wants.

The general structure of an input file is shown below, with many lines of the original validation input file removed for clarity.

```
&HEAD CHID='WTC_05_v5', TITLE='WTC Phase 1, Test 5, FDS version 5' /
&MESH IJK=100,44,42, XB=-1.5,8.5,-2.2,2.2,0.0,4.2 /
&TIME T_END=1400. /
&MISC SURF_DEFAULT='MARINITE BOARD', TMPA=22.5., POROUS_FLOOR=.FALSE. /
&DUMP NFRAMES=1600, DT_HRR=17., DT_DEVC=12., DT_PROF=34. /
&REAC ID = 'HEPTANE TO CO2'
FYI = 'Heptane, C_7 H_16'
C = 7.
H = 16.
CO_YIELD = 0.0075 /
SOOT_YIELD = 0.015 /
&OBST XB= 3.0, 4.0,-2.0, 2.0, 0.0, 0.0, SURF_ID='STEEL FLANGE' / Fire Pan
...
&SURF ID = 'STEEL FLANGE'
COLOR = 'BLACK'
MATL_ID = 'STEEL'
BACKING = 'EXPOSED'
THICKNESS = 0.0055 /
...
&VENT MB='XMIN',SURF_ID='OPEN' /
...
&SLCF PBY=0.0, QUANTITY='TEMPERATURE', VECTOR=.TRUE. /
...
&BNDF QUANTITY='GAUGE HEAT FLUX' /
...
&DEVC XYZ=6.0,0.4,3.5, QUANTITY='oxygen', ID='EO2_FDS' /
...
&TAIL / End of file.
```

It is strongly recommended that when looking at a new scenario, first select a pre-written input file that resembles the case, make the necessary changes, then run the case at fairly low resolution to determine if the geometry is set up correctly. It is best to start off with a relatively simple file that captures the main features of the problem without getting tied down with too much detail that might mask a fundamental flaw in the calculation. Initial calculations ought to be meshed coarsely so that the run times are less than an hour and

corrections can easily be made without wasting too much time. As you learn how to write input files, you will continually run and re-run your case as you add in complexity.

8- Governing Assumptions

8.1- Hydrodynamic Model FDS

It solves numerically a form of the Navier-Stokes equations appropriate for low-speed, thermally-driven flow with an emphasis on smoke and heat transport from fires. The core algorithm is an explicit predictor-corrector scheme that is second order accurate in space and time.

Turbulence is treated by means of the Smagorinsky form of Large Eddy Simulation (LES). It is possible to perform a Direct Numerical Simulation (DNS) if the underlying numerical grid is fine enough. LES is the default mode of operation.

8.2- Combustion Model For most applications

FDS uses a combustion model based on the mixture fraction concept. The mixture fraction is a conserved scalar quantity that is defined as the fraction of gas at a given point in the flow field that originates as fuel. Unlike versions of FDS prior to 5, the reaction of fuel and oxygen is not necessarily instantaneous and complete, and there are several optional schemes that are designed to predict the extent of combustion in under-ventilated spaces. The mass fractions of all of the major reactants and products can be derived from the mixture fraction by means of “state relations,” expressions arrived at by a combination of simplified analysis and measurement.

8.3- Radiation Transport

Radiative heat transfer is included in the model via the solution of the radiation transport equation for a gray gas. In a limited number of cases, a wide band model can be used in place of the gray gas model to provide a better spectral accuracy. The radiation equation is solved using a technique similar to a finite volume method for convective transport, thus the name given to it is the Finite Volume Method (FVM). Using approximately 100 discrete angles, the finite volume solver requires about 20 % of the total CPU time of a calculation, a modest cost given the complexity of radiation heat transfer. Water droplets can absorb and scatter thermal radiation. This is important in

8 cases involving mist sprinklers, but also plays a role in all sprinkler cases. The absorption and scattering coefficients are based on Mie theory. The scattering from the gaseous species and soot is not included in the model.

8.4- Geometry FDS

It approximates the governing equations on one or more rectilinear grids. The user prescribes rectangular obstructions that are forced to conform with the underlying grid.

8.5- Boundary Conditions

All solid surfaces are assigned thermal boundary conditions, plus information about the burning behavior of the material. Heat and mass transfer to and from solid surfaces is usually handled with empirical correlations, although it is possible to compute directly the heat and mass transfer when performing a Direct Numerical Simulation (DNS).

8.6- Sprinklers and Detectors

The activation of sprinklers and heat and smoke detectors is modeled using fairly simple correlations of thermal inertia for sprinklers and heat detectors, and transport lag for smoke detectors. Sprinkler sprays are modeled by Lagrangian particles that represent a sampling of the water droplets ejected from the sprinkler.

Annex 2: application of LES

1- Filtered (LES) forms of the equations

Of the three main techniques of simulating turbulence, FDS contains only Large Eddy Simulation (LES) and Direct Numerical Simulation (DNS). There is no Reynolds-Averaged Navier-Stokes (RANS) capability in FDS.

LES is a technique used to model the dissipative processes (viscosity, thermal conductivity, material diffusivity) that occur at length scales smaller than those that are explicitly resolved on the numerical grid.

This means that the parameters μ , k and D in the equations above cannot be used directly in most practical simulations. They must be replaced by surrogate expressions that “model” their impact on the approximate form of the governing equations.

There is a small term in the energy equation known as the dissipation rate, ε , the rate at which kinetic energy is converted to thermal energy by viscosity:

$$\varepsilon \equiv \tau_{ij} \cdot \nabla \mathbf{u} = \mu \left(2S_{ij} \cdot S_{ij} - \frac{2}{3} (\nabla \cdot \mathbf{u})^2 \right) = \mu \left[2 \left(\frac{\partial u}{\partial x} \right)^2 + 2 \left(\frac{\partial v}{\partial y} \right)^2 + 2 \left(\frac{\partial w}{\partial z} \right)^2 + \left(\frac{\partial v}{\partial x} + \frac{\partial u}{\partial y} \right)^2 + \left(\frac{\partial w}{\partial y} + \frac{\partial v}{\partial z} \right)^2 + \left(\frac{\partial u}{\partial z} + \frac{\partial w}{\partial x} \right)^2 - \frac{2}{3} \left(\frac{\partial u}{\partial x} + \frac{\partial u}{\partial x} + \frac{\partial u}{\partial x} \right)^2 \right] \quad (1)$$

This term is usually neglected in the energy conservation equation because it is very small relative to the heat release rate of the fire. To understand where this term originates, form an evolution equation for the kinetic energy of the fluid by taking the dot product of the momentum equation (6.3) with the velocity vector1:

$$\rho \frac{D\mathbf{u}}{Dt} \cdot \mathbf{U} = \rho \frac{D\left(\frac{|\mathbf{u}|^2}{2}\right)}{Dt} = \rho \mathbf{f}_b \cdot \mathbf{u} - \nabla p \cdot \mathbf{u} + \nabla \cdot (\tau_{ij} \cdot \mathbf{u}) - \varepsilon \quad (2)$$

As mentioned above ε is a negligible quantity in the energy equation. However, its functional form is useful in representing the dissipation of kinetic energy from the resolved flow field. Following the analysis of Smagorinsky, the viscosity μ is modeled

$$\mu_{LES} = \rho (C_s \Delta)^2 \left(2 \bar{S}_{ij} : \bar{S}_{ij} - \frac{2}{3} (\nabla \cdot \bar{\mathbf{u}})^2 \right)^{\frac{1}{2}} \quad (3)$$

C_s : an empirical constant.

Δ : a length on the order of the size of a grid cell.

The bar above the various quantities denotes that these are the resolved values, meaning that they are computed from the numerical solution sampled on a coarse grid (relative to DNS). The other diffusive parameters, the thermal conductivity and material diffusivity, are related to the turbulent viscosity by

$$k_{LES} = \frac{\mu_{LES} c_p}{Pr_t}; \quad (\rho D)_{i,LES} = \frac{\mu_{LES}}{Sc_t} \quad (4)$$

The turbulent Prandtl number Pr_t and the turbulent Schmidt number Sc_t are assumed to be constant for a given scenario.

The model for the viscosity, μ_{LES} , serves two roles: first, it provides a stabilizing effect in the numerical algorithm, damping out numerical instabilities as they arise in the flow field, especially where vorticity is generated. Second, it has the appropriate mathematical form to describe the dissipation of kinetic energy from the flow.

In the parlance of the turbulence community, the dissipation rate is related to the turbulent kinetic energy (most often denoted by k) by the relation $\varepsilon \approx k^{3/2} / L$, where L is a length scale.

There have been numerous refinements of the original Smagorinsky model, but it is difficult to assess the improvements offered by these newer schemes for fires. There are two reasons for this. First, the structure of the fire plume is so dominated by the large-scale resolvable eddies that even a constant eddy viscosity gives results comparable to those obtained using the Smagorinsky model. Second, the lack of precision in most large-scale fire test data makes it difficult to assess the relative accuracy of each model.

The Smagorinsky model with constant C_s produces satisfactory results for most large-scale applications where boundary layers are not well-resolved. In fact, experience to date using the simple form of LES described above has shown that the best results are obtained when the Smagorinsky constant C_s is set as low as possible to maintain numerical stability. In other words, the most realistic flow simulations are obtained when resolvable eddies are not “damped” by excessive amounts of artificial viscosity.

In the discretized form of the momentum equation, the LES form of the dynamic viscosity is defined at cell centers

$$\mu_{ijk} = \rho_{ijk} (C_s \Delta)^2 |S| \quad (5)$$

C_s : an empirical constant, $\Delta = (\delta x \delta y \delta z)^{1/3}$, and

$$|S|^2 = 2 \left(\frac{\partial u}{\partial x} \right)^2 + 2 \left(\frac{\partial v}{\partial y} \right)^2 + 2 \left(\frac{\partial w}{\partial z} \right)^2 + \left(\frac{\partial v}{\partial x} + \frac{\partial u}{\partial y} \right)^2 + \left(\frac{\partial w}{\partial y} + \frac{\partial v}{\partial z} \right)^2 + \left(\frac{\partial u}{\partial z} + \frac{\partial w}{\partial x} \right)^2 - \frac{2}{3} (\nabla \cdot \mathbf{u})^2 \quad (6)$$

The quantity $|S|$ consists of second order spatial differences averaged at cell centers. For example

$$\frac{\partial u}{\partial x} \approx \frac{u_{ijk} - u_{i-1,jk}}{\delta x i} \quad (7)$$

$$\frac{\partial u}{\partial y} \approx \frac{1}{2} \frac{u_{i,j+1,k} - u_{i,jk}}{\delta y j + \frac{1}{2}} + \frac{u_{ijk} - u_{i,j-1,k}}{\delta y j - \frac{1}{2}} \quad (8)$$

The thermal conductivity and material diffusivity of the fluid are related to the viscosity by

$$k_{ijk} = \frac{c p,0 \mu_{ijk}}{Pr_t} \quad ; \quad (\rho D)_{ijk} = \frac{\mu_{ijk}}{Sc_t} \quad (9)$$

Pr_t : turbulent Prandtl number

Sc_t : the turbulent Schmidt number both assumed constant.

Note that the specific heat $c_{p,0}$ is that of the dominant species of the mixture. Based on simulations of smoke plumes, C_s is 0.20, Pr_t and Sc_t are 0.5.

2- LES governing equation

The governing equations, called the Navier–Stokes equations, are derived from the fundamental conservation laws for mass, momentum and energy. In LES only large eddies (large scale motions) are computed directly and hence a low-pass spatial filter is applied to the instantaneous conservation equations to formulate the 3D unsteady governing equations for large scale motions. It is called explicit filtering and Fig.5 illustrates the difference between the filtered velocity \bar{u}_i and the instantaneous velocity u_x .

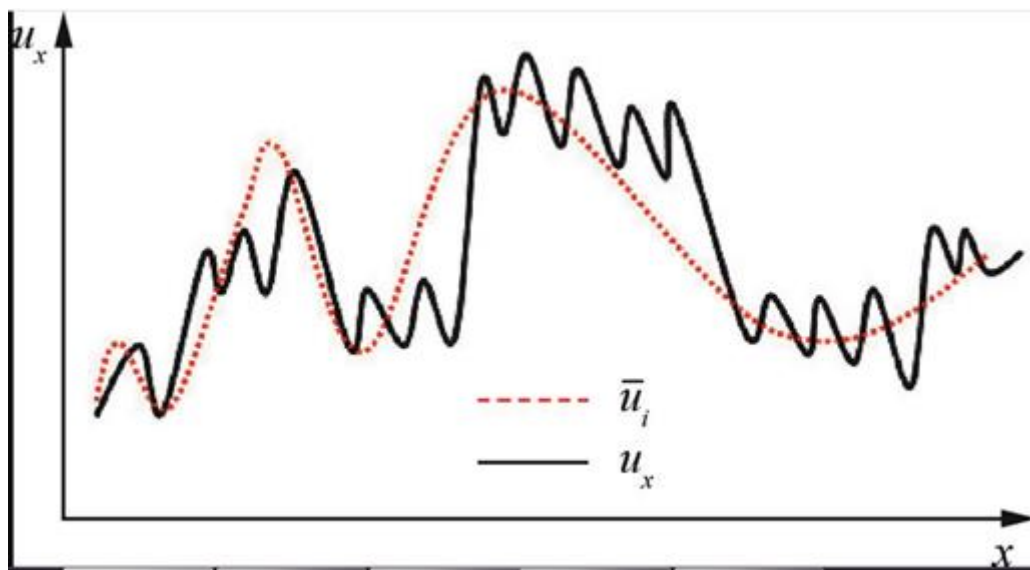


Figure2: Difference between the filtered velocity and the instantaneous velocity.

When the finite volume method is employed to solve the instantaneous governing equations numerically the equations are integrated over control volumes, equivalent to convolution with a top-hat filter, therefore there is no need to apply a filter to the instantaneous equation explicitly and this is called implicit filtering. However, it is worth pointing out that there is potentially a big shortcoming or pitfall in implicit filtering, i.e., a truly mesh independent results can never be achieved as with the refinement of mesh, smaller scale motions are resolved and if one keeps on refining the mesh then eventually a DNS is performed, not an

LES. In other words, when implicit filtering is employed it is almost impossible to distinct between numerical and modelling errors and hence prohibits useful analysis of numerical schemes.

The filtered equations expressing conservation of mass and momentum in a Newtonian incompressible flow can be written in conservative form as

$$\partial_t \bar{u}_i = 0 \quad (10)$$

$$\partial_t (\rho \bar{u}_i) + \partial_j (\rho \bar{u}_i \bar{u}_j) = -\partial_i \bar{p} + 2 \partial_j (\mu \bar{S}_{ij}) - \partial_j (\tau_{ij}) \quad (11)$$

$$\bar{S}_{ij} = \frac{1}{2} (\partial_i \bar{u}_j + \partial_j \bar{u}_i) \quad (12)$$

$$\tau_{ij} = \rho (\overline{u_i u_j} - \bar{u}_i \bar{u}_j) \quad (13)$$

ρ : density

\bar{u}_i : filtered velocity

\bar{p} : filtered pressure

μ : molecular viscosity

\bar{S}_{ij} : the filtered, or resolved scale strain rate tensor

τ_{ij} : the unknown SGS stress tensor, representing the effects of the SGS motions on the resolved fields of the LES, which needs to be modelled using a so-called SGS model so that the above governing equations can be solved.

3- Numerical methods

The finite volume method has become the most popular numerical method for LES and when this numerical method is employed it is not necessary to apply a filter to the instantaneous equation explicitly, hence called implicit filtering as discussed in Section so that filtering will not be discussed anymore in this section.

4- Spatial and temporal discretization

One of the most popular spatial discretization scheme used in LES is the second-order central difference because it is non-dissipative and conservative (not only mass and momentum but also kinetic energy conserving), which are essential for LES. Usually, first- and second-order upwind schemes or any upwind-biased schemes are not used in LES since they produce too much numerical dissipation. While higher-order numerical schemes are desirable and can be applied fairly easily in simple geometries, their use in complex configurations is rather difficult.

Explicit schemes seem to be more suitable for LES than implicit schemes and most researchers in LES use explicit schemes such as the second-order Adams–Bashforth scheme. Since the time steps are usually small in LES, it is not essential to use higher-order temporal schemes either.

5- Inflow boundary conditions

Among all the boundary conditions the most important one is how to specify inlet boundary conditions accurately because the downstream flow development within the domain is largely determined by the inlet behaviour in many cases. Nevertheless, it is an extremely difficult task to generate inlet boundary conditions accurately in LES because, unlike the RANS computations where only time-averaged information is required, in LES three components of instantaneous velocity need to be specified at each time step, which should possess characteristics such as stochastically varying, with scales down to the filter scale (spatially and temporally), compatible with the Navier–Stokes equations, turbulent structures (turbulence intensities, length scales, spectrum etc.). Therefore it is extremely hard, if not impossible, to generate inlet boundary conditions in LES. In particular it is possible to generate a wide range of flow fluctuations around the mean which may have specified spectral properties such as intensity and length scales, and even compatible with the Navier–Stokes equations.

Generally speaking, current inflow boundary condition generation methods in LES can be classified into two basic categories: the so-called “precursor methods” in which an additional simulation (precursor simulation) is performed and the required data are stored as the input for the required simulation, and “synthesis methods” in which some form of random fluctuation is generated/manipulated and combined with the given mean flow at the inlet. Precursor methods can generate the most realistic turbulence information at inflow boundary

but the disadvantage is the necessity to set up and run a separate calculation, leading to usually very high computational cost. One way to save the computational cost is to integrate the precursor calculation into the main domain, with data downstream of the inlet being mapped back into the inlet. It is of course necessary to provide some mechanism for driving the flow towards a pre-specified target such as mean velocity profiles and turbulent stresses etc. by recycling and rescaling. This method, which was first developed for flat-plate boundary layers, consists of taking a plane of data from a location downstream and rescaling the inner and outer layers of velocity profiles separately, to account for the different similarity laws that are observed in these two regions. The rescaled velocity profiles are then reintroduced at the inlet. The main shortcoming is that the inlet must be placed in a region in which the flow is in an equilibrium or very slowly developing, well-known condition (mean velocity and turbulent quantities) and a fairly long domain must be used for the region of interest for the recycling.

Many synthesis generation methods have been developed and the simplest way is to specify the mean flow velocity profile plus some kind of random perturbations, e.g., adding a white-noise random component to the mean velocity at inlet, with an amplitude determined by the turbulent intensity level. This method is very easy to implement but not a good one at all since the white noise component has hardly any of the required characteristics of turbulent flow – in particular it possesses no spatial or temporal correlations at all. Therefore, they decay rapidly and it takes usually a long distance downstream from the inflow boundary for a desired realistic turbulence to develop, and in some cases the use of random noise at the inlet does not develop turbulence downstream at all. Available advanced synthesis generation methods can be broadly classified into four categories: Fourier techniques and related approaches, proper orthogonal decomposition (POD) methods, digital filter generation methods and finally vortex method or synthetic eddy method (SEM).

6- Study of Flow and Mixing in a Generic GT Combustor using LES

Due to careful and deliberate trade-offs between often conflicting design requirements (low emission, high operating pressure and temperatures etc.), development and improvement of gas turbines nowadays relies heavily on advanced simulation methods. While the basic capability of LES has been amply demonstrated on a number of relatively simple academic configurations, there is still a lack of works applying LES to practical systems also performing detailed quantitative comparisons based on experimental data. This is mostly due

to the lack of suitable reference data. Beyond a pure validation, the LES is used to analyze the influence of the processing vortex core present in the studied configuration on the mixing of fuel and oxidizer and possible implications for reacting conditions are discussed.

7- Large Eddy Simulation of Impinging Jets in a Confined Flow

Large Eddy Simulation (LES) has been applied to a representative primary combustion zone in an isothermal constant density simulation. The geometry consists of an annular passage that feeds a row of six port-holes. The resulting radial jets impinge strongly within a confined core cross-flow. Both uncoupled (core only) and coupled (core and annulus) simulations are considered. The uncoupled simulation applies detailed experimental data as port boundary conditions. The findings conclude that the coupled LES can adequately reproduce port characteristics resulting in a good description of the core combustor flow-field, potentially superior to that given by the uncoupled case and far superior to that given by RANS predictions.

8- Current state of LES

During the early period of LES applications it was used successfully to investigate the details of flow problems having relatively simple geometry and at low Reynolds numbers such as homogeneous turbulence, mixing layers, plane channel flows. Although use of LES in such an academic or fundamental setting continues today mainly for model validation and fundamental understanding of flow physics etc. emphasis has shifted to more complex configurations having flow characteristics where the RANS approach has failed. Nevertheless LES has not replaced the RANS approach and will not replace it for the near future to become the main computational analysis tool for practical engineering problems due to two main reasons: firstly, even with the current computing power it is still far too expensive computationally to perform LES on a routine basis for practical engineering flow problems; secondly, LES has not reached such a level of maturity that users can obtain results with the level of solution fidelity that can be expected.

9- Outlook

It is safe to assume that, between the increases in computational power that are still achievable, and the algorithmic developments, LES will be used in more complex configurations, and will yield reliable results for engineering analysis in 2030, if not design.

The most significant advance might be achieved through the development of grid-optimized LES, which will be better able to tackle complex geometries. It will be characterized by a filter width that is some fraction of the integral scale, i.e. is defined by the physics of turbulence. A constant ratio between Δ and the integral scale will ensure that the LES resolve roughly the same percentage of the turbulent kinetic energy (and hence the momentum transport) everywhere. The ratio between filter width and grid size, Δ/h should be large to minimize numerical errors, and, ideally, remain nearly constant throughout the domain (although grid-generation constraints might make this difficult to achieve). The wall layer will, hopefully, be modelled accurately, so that the grid resolution is affordable, even at high Reynolds numbers.

As Reynolds numbers closer to those in real-life applications can be reached, the information gleaned from LES can also be used to develop improved models for engineering applications. This has been always a stated objective of LES and DNS, but its achievement has been, so far, elusive. Most applications of LES to RANS models, for instance have compared model predictions (for each term of interest) to the results of the LES or DNS. This comparison is not always helpful, if the Reynolds numbers at which LES and DNS are performed are much lower than those ideally suited to turbulence models; furthermore, the solution of transport equations in the models includes dynamics that are absent from the kinematic comparisons most often seen in the literature.

In 2030, the full aircraft will still be beyond reach for pure LES; everything considered, that might not be the most useful application of the technique. Smaller problems, in which the turbulence physics are very complex (multiple scales, strong departures from equilibrium, massive separation, etc.) may remain the natural target for LES. The information generated by this method, with its ability to capture the most important turbulent eddies and the flow unsteadiness, can result in more complete understanding of the flow physics, more accurate predictions, and, eventually, the development of better engineering designs.